# A THEORETICAL AND EXPERIMENTAL INVESTIGATION OF ION ACOUSTIC WAVE DISPERSION IN A NON-UNIFORM HIGHLY IONIZED ARGON PLASMA

## RICHARD ROBERT LEVIN

A THEORETICAL AND EXPERIMENTAL INVESTIGATION OF ION ACOUSTIC

WAVE DISPERSION IN A NON-UNIFORM HIGHLY IONIZED ARGON PLASMA

by

Richard Robert Levin
Lieutenant Commander, United States Navy
B.E.P., Cornell University, 1957

Submitted in partial fulfillment
for the degree of

DOCTOR OF PHILOSOPHY

from the

UNITED STATES NAVAL POSTGRADUATE SCHOOL
December 1966

# ABSTRACT

Ion acoustic waves have been artificially excited and detected in
the Steady State Plasma Facility at the Naval Postgraduate School by a
magnetic excitation device and an optical detection system.  The dis-
persion of these waves has been studied as a function of the exciting
frequency and the confining static magnetic field.

Dispersion curves are presented which compare the experimental data
to a new dispersion equation which is derived in the present thesis.
After the validity of this dispersion relation is demonstrated, the
measurements are used as a diagnostic tool, and five operating para-
meters of the plasma facility are deduced from the measurements.

Theories are presented to explain the behavior of the dispersion
curves and three of the five operating parameters.

ACKNOWLEDGEMENT

During the period in which the theoretical and experimental research necessary for the completion of this paper were accomplished, many persons have contributed greatly of their time and effort in solving the problems arising from such an undertaking.  Principal thanks go to the author's thesis director, Professor Norman L. Oleson for his invaluable assistance in all phases of the work and for providing much of the experimental equipment necessary.  Professors Kai Woehler, Alfred Cooper, and Elmo Stewart contributed generously of their time and provided many hours of useful discussions.

The author is also indebted to Mr. Hal Herreman for his generous assistance in the laboratory and to Mr. Peter Wisler and Mr. Michaél O'Dea for the manufacture of much of the equipment necessary for the experiment.

Deepest appreciation also goes to Mr. Roger Hilleary for giving so generously of his time and ability in the preparation of the computer programs so vitally necessary for the reduction and analysis of the experimental data.

# TABLE OF CONTENTS

# LIST OF TABLES AND ILLUSTRATIONS

TABLE OF SYMBOLS

$\omega$      angular frequency of wave

$\ell$      wavenumber = $\alpha + i\beta$

$\kappa$      Boltzmann constant

$\Upsilon$      electron temperature

$T$      ion temperature

$M$      ion mass

$m$      electron mass

$\lambda_0$      Debye length = $\left(\dfrac{\epsilon_0 \kappa \Upsilon}{Ne^2}\right)^{\frac{1}{2}}$

$N$      equilibrium plasma density of charged particles

$\overline{W}$      ion drift velocity

$\overline{B}_0$      static magnetic field strength

$\nu$      effective ion-neutral collision frequency for momentum loss

$P$      equilibrium electron pressure

$\Pi$      equilibrium ion pressure

$p$      electron pressure perturbation

$\pi$      ion pressure perturbation

$\overline{V}$      ion velocity induced by wave

$n$      plasma density perturbation of charged particles

$\Omega$      ion cyclotron frequency = $\dfrac{eB_0}{M}$

$e$      electron charge

$\ell$      radial distance at which density perturbations vanish

$\delta$      radial density profile parameter of unperturbed plasma

$\epsilon_0$      permittivity of free space

$r,\theta,z$      cylindrical coordinates

$\mathcal{N}$      electron-neutral collision frequency

$$c \equiv (\frac{KT}{M})^{\frac{1}{2}}$$

$$C \equiv (\frac{KT}{M})^{\frac{1}{2}}$$

$$x \equiv \frac{\omega}{\Omega}$$

$$y \equiv \frac{\alpha c}{\Omega}$$

$$z \equiv \frac{\beta c}{\Omega}$$

$$\eta \equiv \frac{W}{c}$$

$$J \equiv \frac{\nu}{\Omega}$$

$$\sigma \equiv \frac{C}{c}$$

$$\mathcal{E} \equiv \frac{c}{\Omega \ell}$$

$$\epsilon \equiv \frac{\delta c}{\Omega}$$

INTRODUCTION

For the purposes of the present thesis a plasma may be defined as a quasi-neutral electrically conducting mixture of positive ions and electrons plus a number of neutral background gas atoms. Due to the particular plasma production mechanism employed in the Steady State Plasma Facility of the Naval Postgraduate School, the electrons are at a relatively high temperature (22 electron volts) on the cylindrical beam axis, while the ions have thermal energies of the order of .09 ev and the neutral gas atom energies are approximately .01 ev.

Due to the high electrostatic restoring forces created by even a small internal charge imbalance, a plasma has the ability to maintain overall internal charge neutrality. If a charge imbalance should develop due to the random thermal motion of the electrons and ions, the particles will rearrange themselves to shield the remainder of the plasma from the resulting electric field. Thus beyond a certain average distance from the imbalance the electric field so created will not be felt. This distance is called the Debye length and is, of course, a function of the plasma parameters. In a true plasma the Debye length must be much less than the smallest dimension of the plasma system. The Debye length is given by: [1]

$$\lambda_D = \left(\frac{\epsilon_o K T}{N e^2}\right)^{\frac{1}{2}}$$

where

$\epsilon_o$   is the permittivity of free space

$K$   is the Boltzmann constant

$T$   is the electron temperature

N is the equilibrium plasma density

e is the electron charge

Ion acoustic waves are longitudinal plasma density oscillations occurring at frequencies well below those of the electron plasma oscillations. The plasma ions and electrons move exactly in phase only at $\omega = 0$; for $\omega \neq 0$ in-phase motion is only approximately realized. For the frequencies employed in the present investigation, however, the approximation is an excellent one. The ion oscillations are slightly larger in amplitude than those of the electrons. The ratio of ion perturbation velocity to electron perturbation velocity can be shown to be $1 + (\frac{\lambda_D k}{2\pi})^2$ [2], where $k$ is the wavenumber. In Section 2 it will be shown that $(\frac{\lambda_D k}{2\pi})^2 \lesssim 10^{-14}$, so it may be neglected compared to 1.

Due to their small mass and high mobility the electrons see these low frequency waves as quasi-static perturbations. Ion acoustic waves are similar to ordinary sound waves in a neutral gas, except that the propagation mechanism is the Coulomb interaction between charged particles rather than the short range collision forces between molecules. Their existence was first predicted by Tonks and Langmúir in 1929 based on the fluid analysis of a two component plasma. [3]

Before proceeding to an account of previous work, the Tonks-Langmuir dispersion relation for ion acoustic waves will be derived. The following assumptions are made:

1) The plasma electrons have negligible momentum compared to the plasma ions.

2) The plasma ions have zero temperature and are singly charged. Thus there is no ion pressure.

3) There is always 100% ionization within the plasma.

4) There is no electric field associated with the wave.

5) The Debye length is much smaller than the wavelength, that is $\lambda_D \ll \frac{2\pi}{\mathcal{L}}$ .

6) The drift velocity of the ions is zero.

7) The unperturbed plasma has uniform density.

Under these assumptions the momentum transfer equation for the ions can be written as:

$$\frac{-1}{M}\nabla(P + p) = \left[\frac{\partial}{\partial t} + \bar{v}\cdot\nabla\right]\left[(N + n)\bar{v}\right] - \frac{eB_o}{M}(N + n)\bar{v}\times\hat{z}$$

where

M is the ion mass

p is the electron pressure perturbation

P is the equilibrium electron pressure

$\bar{V}$ is the ion velocity inducted by the wave

N is the equilibrium plasma density of charged particles

n is the plasma density perturbation of charged particles

e is the electron charge

$B_o$ is the static magnetic field strength

$\hat{z}$ is a unit vector parallel to the direction of $\bar{B}_o$.

Subtracting the momentum transfer equation for the ions in the unperturbed system from the above equation and linearizing to the limit of small perturbations gives:

$$\frac{-1}{M}\nabla p = \frac{\partial}{\partial t}(N\bar{v}) - \Omega NV_\theta\hat{r} + \Omega NV_r\hat{\theta} \tag{1}$$

where $\Omega$ is the ion cyclotron frequency $= \frac{eB_o}{M}$ .

Now for perturbations of the form $e^{i(\mathcal{L}z - \omega t)}$, equation (1) can be solved to give:

11

$$NV_r = \frac{i\omega}{M} \frac{\partial p}{\partial r} \left(\frac{1}{\Omega^2 - \omega^2}\right)$$

and

$$NV_\theta = \frac{\Omega}{M} \frac{\partial p}{\partial r} \left(\frac{1}{\Omega^2 - \omega^2}\right)$$

Therefore

$$\nabla \cdot (NV_\theta \hat{r} - NV_r \hat{\theta}) = \frac{\Omega}{M} \left(\frac{\partial^2 p}{\partial r^2} + \frac{1}{r} \frac{\partial p}{\partial r}\right) \left(\frac{1}{\Omega^2 - \omega^2}\right)$$

Taking the divergence of equation (1) gives:

$$\frac{-1}{M} \nabla^2 p = -i\omega \nabla \cdot (N\bar{v}) - \Omega \nabla \cdot (NV_\theta \hat{r} - NV_r \hat{\theta}),$$

or

$$\frac{-1}{M} \nabla^2 p = -i\omega \nabla \cdot (N\bar{v}) - \frac{\Omega^2}{M} \left(\frac{\partial^2 p}{\partial r^2} + \frac{1}{r} \frac{\partial p}{\partial r}\right) \left(\frac{1}{\Omega^2 - \omega^2}\right) \quad (2)$$

But by the linearized equation of continuity,

$$\nabla \cdot (N\bar{v}) = -\frac{\partial n}{\partial t} = i\omega n$$

Therefore equation (2) becomes:

$$\nabla^2 p = -\omega^2 n_{,} + \frac{\Omega^2}{M} \left(\frac{\partial^2 p}{\partial r^2} + \frac{1}{r} \frac{\partial p}{\partial r}\right) \left(\frac{1}{\Omega^2 - \omega^2}\right).$$

Assuming there is no radial electron temperature variation,

$$\nabla^2 p = \kappa T \nabla^2 n, \quad \frac{\partial^2 p}{\partial r^2} = \kappa T \frac{\partial^2 n}{\partial r^2}, \quad \frac{\partial p}{\partial r} = \kappa T \frac{\partial n}{\partial r},$$

and

$$c^2 \left(\frac{\partial^2 n}{\partial r^2} + \frac{1}{r} \frac{\partial n}{\partial r} - \ell^2 n\right) = -\omega^2 n + \frac{\Omega^2 c^2}{\Omega^2 - \omega^2} \left(\frac{\partial^2 n}{\partial r^2} + \frac{1}{r} \frac{\partial n}{\partial r}\right)$$

where

$$c^2 \equiv \frac{\kappa T}{M} \qquad \text{(definition)}$$

and $T$ is the electron temperature.

12

Rearranging and defining

$$x \equiv r \left[ (\frac{\Omega^2}{\omega^2} - 1)(\beta^2 - \frac{\omega^2}{c^2}) \right]^{\frac{1}{2}}$$

this equation becomes:

$$x^2 n'' + x n' + x^2 n = 0$$

Its solution is:

$$n = n_o e^{i(\beta z - \omega t)} J_o(x)$$

where $J_o$ is the zero order Bessel function.

Therefore it must be true that

$$\ell^2 (\frac{\Omega^2}{\omega^2} - 1)(\beta^2 - \frac{\omega^2}{c^2}) = (2.405\ldots)^2$$

where the boundary condition that the perturbations vanish at the position $r = \ell$ is used. (The use of this type of boundary condition will be more fully discussed in Section 2.) This can be rewritten as:

$$\beta^2 = \frac{5.79}{\ell^2 (\frac{\Omega^2}{\omega^2} - 1)} + \frac{\omega^2}{c^2} \; .$$

Now for an infinite medium $\ell \rightarrow \infty$ and $\beta^2 = \frac{\omega^2}{c^2}$ or $\beta = \frac{\pm \omega}{c}$  (3)

Thus for an infinite medium the application of a static magnetic field has no effect. Equation (3) is the well known Tonks-Langmuir dispersion relation for ion acoustic waves.

From an elementary acoustic analogy the "hot" electrons provide the perturbing and restoring pressure gradients, while the massive ions provide the inertia. This dispersion relation predicts a phase velocity of $\frac{\omega}{\beta} = c = (\frac{\kappa T}{M})^{\frac{1}{2}}$. Also, since $\frac{\omega}{\beta} = \frac{\partial \omega}{\partial \beta}$, the group velocity equals the phase velocity and, there is no dispersion.

A similar dispersion relation will be derived in greater detail

13

including additional effects in Section 2.

Ion acoustic waves can be self-excited or externally excited both in gaseous discharges of low percentage ionization and in highly ionized plasmas. The existence of self-excited waves in low density gaseous discharges has been observed by Alexeff and Neidigh [4] and by Little and Jones [5] in the form of standing waves in the discharge tubes employed. The present investigation deals exclusively with propagating waves. Two earlier experiments (one on standing waves and one on propagating waves) will be described.

Ion acoustic waves have been excited by electrostatic methods (grids [6] and probes [7]) and by magnetic perturbations of the local electron diffusion coefficient [5]. The magnetic perturbation method was used in this experiment. Its theory of operation appears in Section 3.

Once the ion acoustic waves have been excited, they can be detected by grids, probes, and light sensitive detectors. In this experiment both probe detection and photomultiplier detection were used, although only the photomultiplier detection system was used to make quantitative measurements. Detector theory and operation are also covered in Section 3.

Wavelength and attenuation measurements were made as functions of exciting frequency for various static magnetic field strengths. The validity of the dispersion relation is demonstrated, the data are analyzed and the results presented as dispersion and attenuation curves.

The new dispersion and attenuation theories derived in Section 2 contain 5 adjustable parameters. Comparison of the experimental data with theory allows computation of these 5 parameters, whose values are presented as functions of the static magnetic field strength. The ion acoustic waves are thus employed as a diagnostic tool. Physical inter-

14

pretations of the experimental results (dispersion curves, attenuation curves, and parameter behavior) are also given in Section 5.

Wong, Motley, and D'Angelo have carried out experiments on the dispersion of ion acoustic waves in cesium and potassium plasmas in strong magnetic fields. [6]

Fried and Gould [8] have shown that the Vlasov equation predicts ion acoustic wave propagation even in the absence of collisions in the plasma. Under this condition, however, the analysis predicts that the waves will be strongly damped due to a "trapping" of ions moving with velocities close to the wave phase velocity. This can occur if there are ions whose temperatures are close to the electron temperature $(T \doteq \Upsilon)$. From equation (3) the wave phase velocity is $c = (\frac{k\Upsilon}{M})^{\frac{1}{2}}$, and if $T \doteq \Upsilon$ there will be ions meeting this condition.

This type of collisionless damping was first predicted by Landau. [9] It was observed by Wong, Motley, and D'Angelo, and their work provided the first experimental proof of its existence. The conditions of their experiment were such that ion-neutral collisions were negligible (the percentage ionization varied between 40% and 90%). Their plasma was produced by surface ionization of cesium and potassium atoms on a hot tungsten plate. This method guaranteed that electron and ion temperatures were approximately equal. The damping was so strong that standing waves were not observed.

The Q-3 Machine (Princeton) was used for the experiment. The features essential to the experiment appear in Fig. 1. The plasma was produced at one end of the machine, allowed to drift longitudinally, and terminated approximately 90 cm away by a similar tungsten plate. Radial confinement was achieved by adjusting the longitudinal magnetic field to

FIG. I

SCHEMATIC DIAGRAM OF Q-3 MACHINE

16
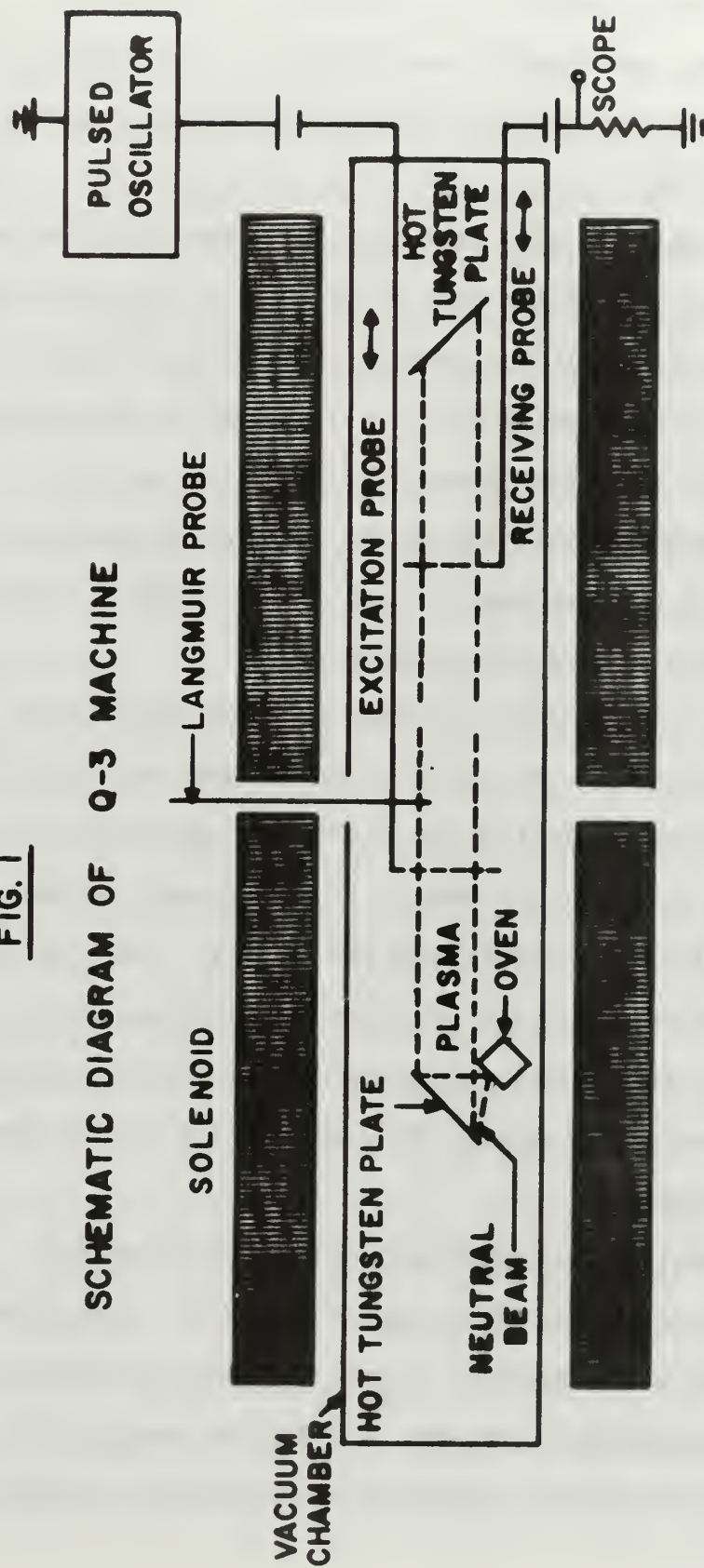
12,000 gauss for cesium and 6000 gauss for potassium (these values were chosen to avoid possible ion cyclotron resonance).

In the Princeton experiment an electrostatic excitation method was used, in constrast to the magnetic excitation method employed in the present investigation. The perturbing signal was applied to the excitation grid and modulated the percentage ion transmission through the grid. The movable receiving grid detected the density perturbations.

Phase velocity calculations were made by measuring the slope of the curve of phase delay vs. receiving grid position (the movable grid) for the propagating wave. One result of the experiment was that the phase velocity was found to be independent of frequency for the range from 15 kc to 100 kc (ion cyclotron frequency was 140 kc for cesium and 240 kc for potassium). This conforms to the predictions of the dispersion relation derived in the present thesis, although the frequency range relative to the ion cyclotron frequency is different.

The damping observed by Wong, Motley, and D'Angelo was found to be in excellent agreement with the theory of Landau damping. In Section 2 the criteria necessary for the presence of Landau damping will be discussed, and it will be shown that it can be ignored in the present investigation.

Figs. 2 and 3 show phase velocities for the ion acoustic waves in the Q-3 experiment for propagation parallel and anti-parallel to the plasma drift velocity.

The drift velocity of the plasma was estimated from the difference between the phase velocities of the waves for parallel and anti-parallel propagation. In the present investigation the plasma drift velocity is one of the 5 adjustable parameters. The magnitude of the drift velocity
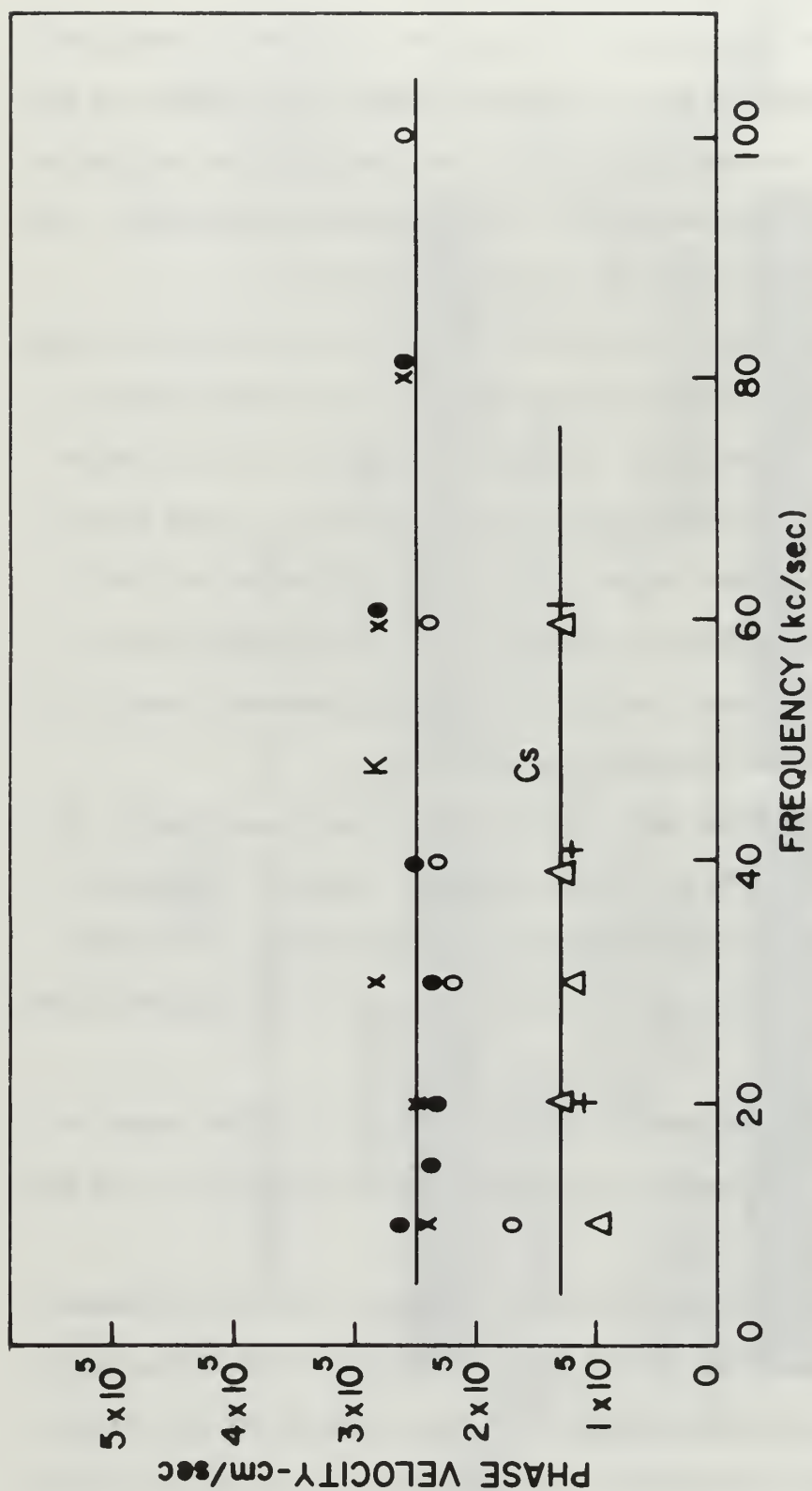
17

PHASE VELOCITY OF THE DOWNSTREAM WAVES IN CESIUM AND POTASSIUM PLASMAS AS A FUNCTION OF FREQUENCY. THE DIFFERENT SYMBOLS REFER TO DATA TAKEN AT DIFFERENT ION DENSITIES: $X = 1.8 \times 10^{10}$ cm$^{-3}$; $\bullet = 6.0 \times 10^{10}$ cm$^{-3}$; $o = 15 \times 10^{10}$ cm$^{-3}$; $+ = 6.0 \times 10^{10}$ cm$^{-3}$; $\triangle = 30 \times 10^{10}$ cm$^{-3}$.
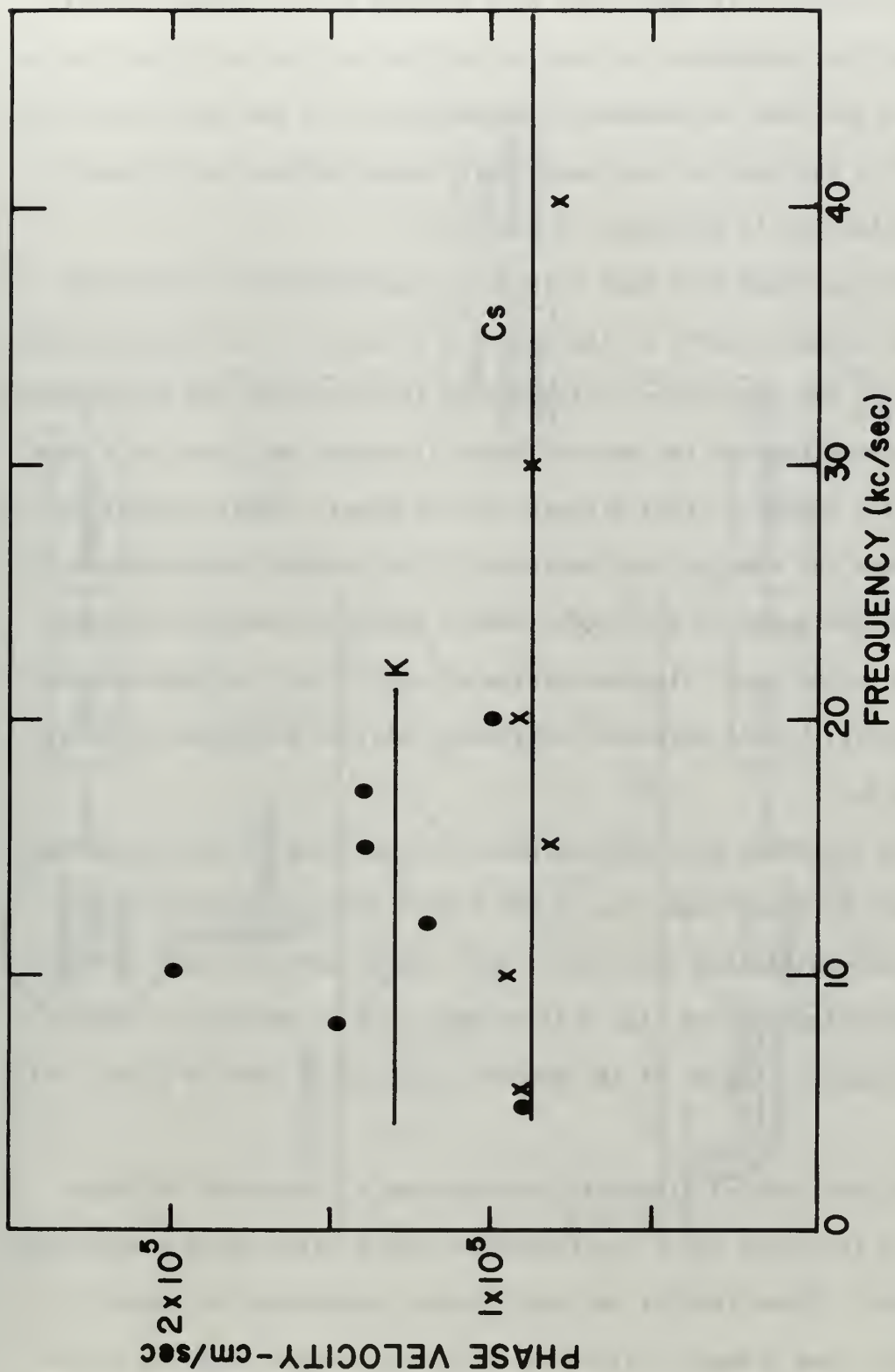
FIG. 2

PHASE VELOCITY OF THE UPSTREAM WAVES IN CESIUM AND POTASSIUM PLASMAS AS A FUNCITION OF FREQUENCY. PLASMA DENSITY IS $2 \times 10^{11}$ cm$^{-3}$.

is machine calculated from the dispersion data. Both parallel and anti-parallel propagation at 1000 gauss were studied in the present investigation, and the difference in phase velocities for the two directions of propagation provided an independent determination of the drift velocity. The method is the same as that employed by Wong, Motley, and D'Angelo. This determination is discussed in Section 5.

Little and Jones have made dispersion measurements on externally excited ion acoustic waves in the positive column of a low pressure mercury arc. [5] The percentage ionization in the discharge was approximately 1%, the current through the mercury vapor discharge was fixed at 9 amps, and the axial magnetic field strength was 45 gauss. Their excitation mechanism was the same as that employed in the present investigation. Essentially the magnetic excitation device employed created sufficient variations in the local electron diffusion coefficient to modulate the plasma density. (This method of excitation will be explained in detail in Section 3.)

Little and Jones detected the waves by observing variations in the light output of the plasma (due to the plasma density variations) by means of photomultiplier detection. This method was also used in the present investigation and also will be explained in Section 3. Fig. 4 shows a schematic diagram of the detection apparatus used by Little and Jones.

Their experimental dispersion curves show a dependence of phase velocity on frequency and a low frequency cutoff below which propagation cannot occur. These results are not directly comparable to those of Wong, Motley, and D'Angelo, since the frequency ranges relative to the ion cyclotron frequency are entirely different. Fig. 5 shows a plot of
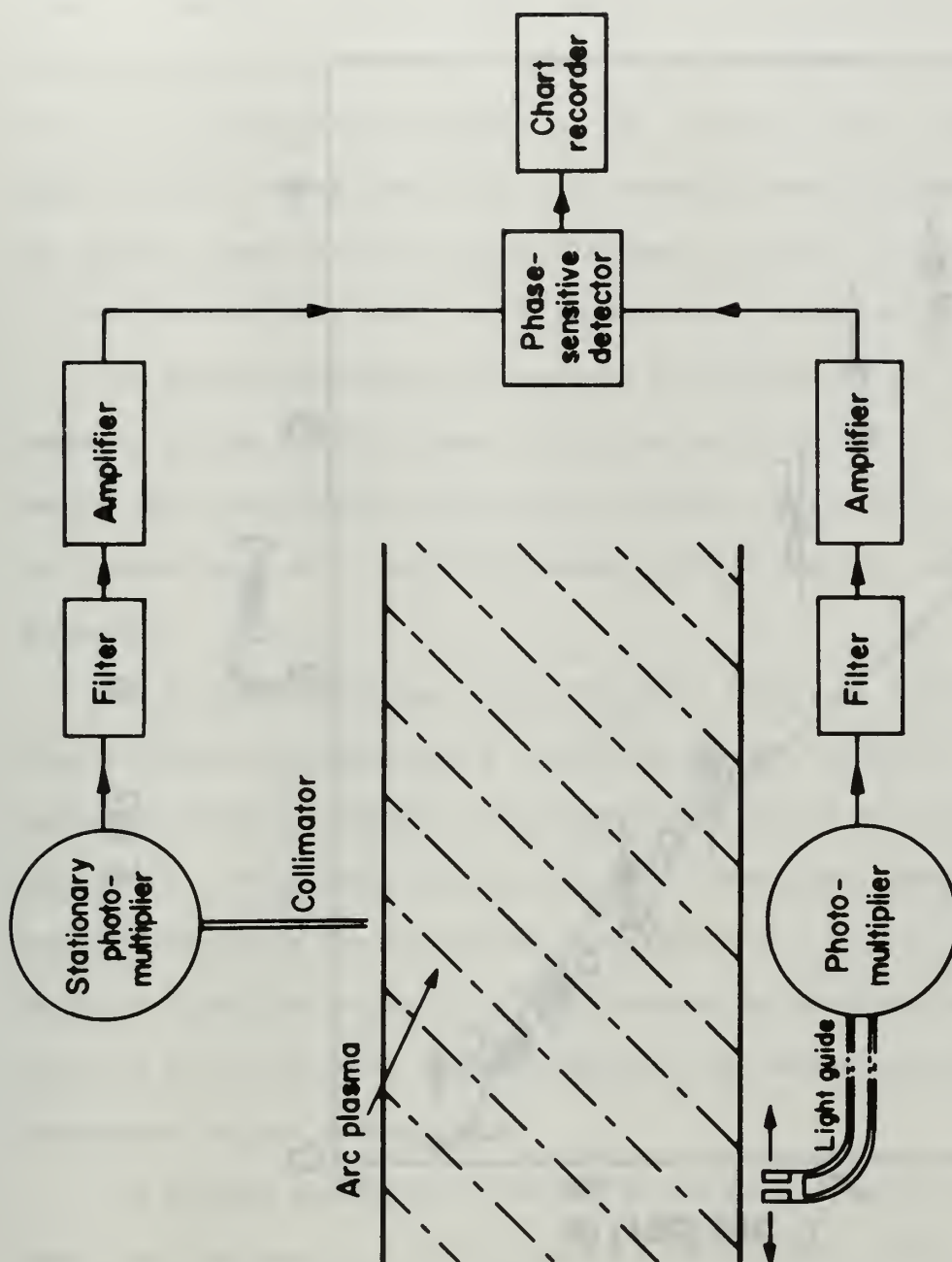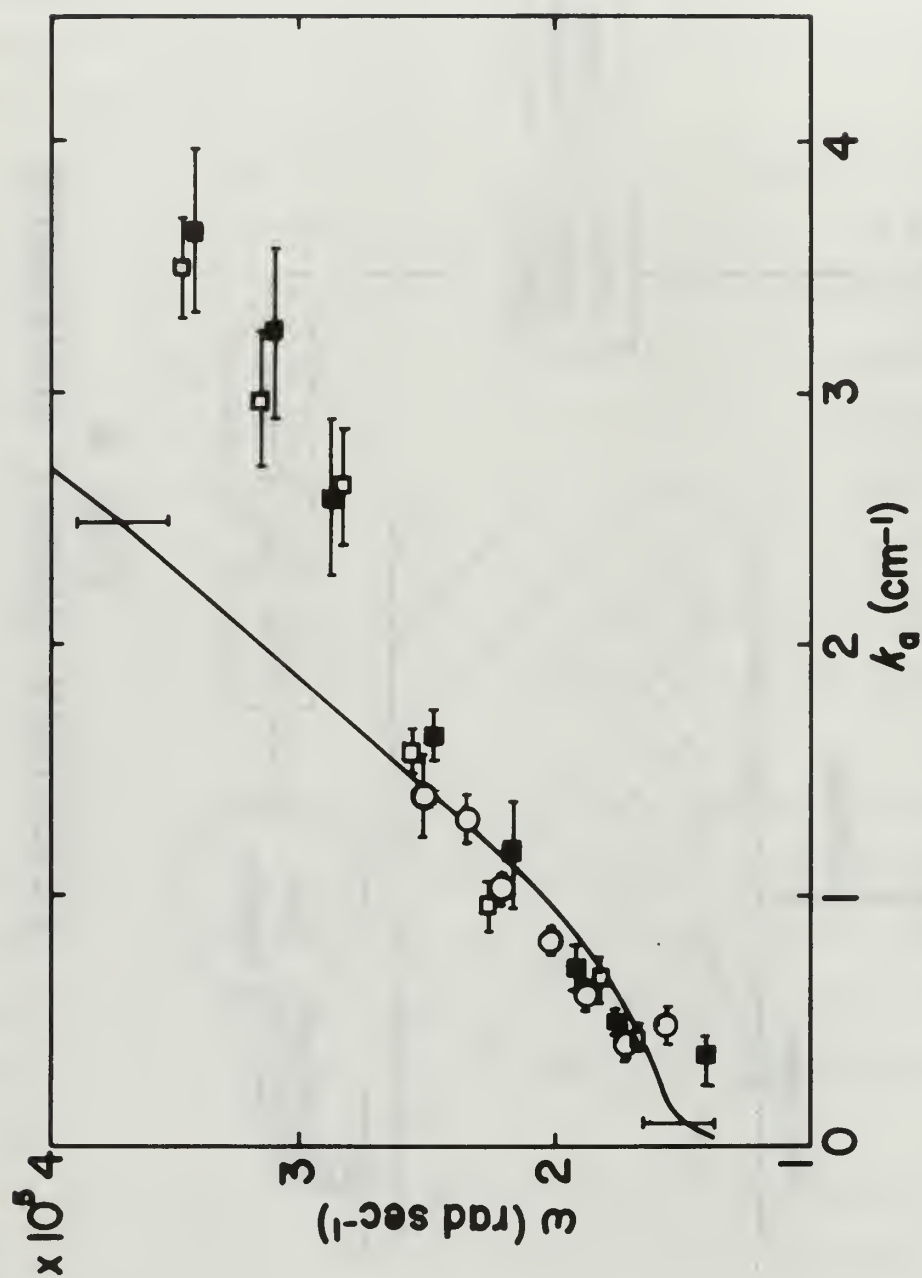
FIG. 4
DETECTION CIRCUIT SCHEMATIC

21

FIG. 5

$\omega$ versus $k$ for 45 gauss external field. The frequency cutoff condition can be seen.

The results reported by Little and Jones conform to the theory derived in Section 2, although their agreement with their theory is not as good as in the present thesis. This is probably due to the unclear nature of the boundary conditions in the discharge tube of their experiment (as they have pointed out). The boundary conditions applicable to the present investigation will be discussed in detail in Section 2, and it will be shown that they can be unambiguously specified.

The present investigation examines the dispersion of ion acoustic waves in a high density plasma of high degree of ionization (approximately 90%) and considers the combined effects of ion drift, damping, ion temperature, and a confining magnetic field together with finite beam geometry.

The present thesis has three purposes. First, an improved dispersion relation is derived for a cylindrical plasma including the aforementioned effects  Second, this dispersion relation is tested against experiment. Third, from the comparison of theory with experiment, the above 5 parameters for the Steady State Plasma Facility at the Naval Postgraduate School are computed by least squares computer search to give the best fit to the data. The validity of the deduced values of the parameters is also demonstrated.

The derived theoretical solution to the wave equation is a complex equation. The real part of the solution predicts the dispersion relation, that is wave number as a function of frequency. The imaginary part predicts the damping as a function of frequency.

The solution to the wave equation is derived by assuming the ion and

electron pressures are scalars. This allows truncation of the set of moments of the Boltzmann equation after the first 2 moments, which are the equation of continuity and the momentum transfer equation respectively. These equations are combined with the plasma equation of state. Assumption of the azimuthal and longitudinal forms of the wave behavior allows the resulting partial differential equation to be reduced to an ordinary differential equation involving only the radial behavior. This is solved in series form and yields the solution to the dispersion problem when the boundary condition is inserted.

Experimentally the waves are excited by perturbing the local electron diffusion coefficient perpendicular to the confining static magnetic field. Increasing the local electron cross-field diffusion coefficient decreased the local electron density. Since the ions and electrons move in phase, this creates a deficiency in the local plasma density of ions and electrons. This density perturbation propagates parallel to the static magnetic field. In the present investigation the frequency of the applied perturbations was varied from 187 kc to 352 kc.

The wavelength and amplitude of the ion acoustic waves are measured as functions of frequency. The results are reduced by machine computation and fitted against theory. As has been previously mentioned the 5 adjustable parameters in the theory are ion drift velocity, the effective ion collision frequency for momentum loss, ion thermal energy, plasma beam diameter, and the e-folding distance for the radial density profile. The first 3 are characteristics of the plasma facility, while the last 2 are functions of the applied static magnetic field. Independent determinations of 4 of these 5 quantities have been made, and these values are compared to the results of the least squares adjusted values obtained in

24

the present investigation.  The results are presented as functions of the static magnetic field, and theories are presented to explain their behavior.

## Section 2

## BASIC THEORY AND DERIVATION OF THE DISPERSION RELATION

If Landau damping is to be a factor in wave propagation, the dispersion analysis must begin with the consideration of the particle distribution functions, since the mechanism involved is the resonant or near-resonant transfer of energy between the wave and those particles having thermal speeds approximating the wave phase velocity. If there are more particles whose thermal speeds are slightly less the wave phase velocity than there are particles whose thermal speeds are slightly greater than the wave phase velocity, there will be more particles taking energy from the wave than there are giving up energy to it. Then there will be a net loss of wave energy, and Landau damping will exist. In any system having a Maxwellian distribution there will be some particles having thermal speeds approximating the wave phase velocity, but for the particular plasma under consideration this is a negligible fraction of the total number of particles.

As will be shown later, the phase velocity of these waves is greater than or equal to $(\frac{KT}{M})^{\frac{1}{2}}$. Spectroscopic measurements by R. Booth and R. L. Kelly of this laboratory have established that ion energies are less than 0.5 ev when argon is used in the plasma facility. [10] Probe measurements made by D. M. Gall have established that electron energies along the cylindrical beam axis are 22 ev. [11] Thus it may be safely assumed that the electron temperature greatly exceeds the ion temperature. (This assumption is also consistent with the results of the data reduction presented in Section 4.) Thus there will be an insignificant number of positive ions capable of causing Landau damping.

An estimate of the Landau damping may be made by examining a dis-

persion relation derived by Fried for the case $\tau \gg T.$ [12]

$$\omega = k(\frac{2\kappa\tau}{m})^{\frac{1}{2}} \left[\frac{m}{2M(1 + \frac{k^2\lambda_D^2}{4\pi^2})^2}\right]^{\frac{1}{2}} \left[1 - \frac{i(\pi\frac{m}{M})^{\frac{1}{2}}}{\left[2(1 + \frac{k^2\lambda_D^2}{4\pi^2})\right]^{3/2}}\right],$$

where

        m is the electron mass

and

        M is the ion mass.

For the plasma studied the Debye length is of the order of 0.02 mm, whereas typical wavelengths varied from 5 cm to 20 cm. Thus $\frac{k^2\lambda_D^2}{4\pi^2} \lesssim 10^{-14}$ and may be neglected compared to 1. Making this approximation,

$$\omega = k(\frac{\kappa\tau}{M})^{\frac{1}{2}} \left[1 - i(\frac{\pi m}{8M})^{\frac{1}{2}}\right].$$

Thus it can be seen that an upper limit on the Landau damping term (the imaginary term in brackets) is $(\frac{\pi m}{8M})^{\frac{1}{2}} \doteq 2.3 \times 10^{-3}$. This is sufficiently small that it may be ignored compared to the damping arising from ion-neutral collisions. This neglect of Landau damping is even more fully justified if ion-ion collisions (ion fluid viscosity) are considered. The effect would be to introduce disruptive collisions which would destroy the phase relationship between the resonant ions and the wave. This critical phase relationship could also be destroyed by ion-neutral collisions, but not appreciably by ion-electron collisions due to the negligible electron-to-ion momentum transfer. It should also be noted that the thermal speeds of the electrons are much higher than the wave phase velocities encountered in the present investigation. Thus the electrons see these waves as quasi-static and do not contribute any Landau damping. The process of Landau damping therefore need not be considered for the purposes of this thesis. The derivation will neglect moments of the

27

Boltzmann equation higher than the second.

For the conditions in this experiment under which ion acoustic waves propagate, ions and electrons move in phase due to the strong electrostatic restoring forces, so the instantaneous ion and electron densities are equal. Although the Coulomb interaction is the mechanism by which these waves propagate, there is no macroscopic electric field associated with the waves. This assumption is justified at any frequency if the magnetic pressure, $(\frac{B_o^2}{2\mu_o})$, is much greater than the plasma pressure (essentially $N\kappa T$). [13] In this experiment $(\frac{B_o^2}{2\mu_o}) \gg 4000$ joules/m$^3$, while $N\kappa T \doteq 10$ joules/m$^3$. The following derivation will therefore omit consideration of any electric field associated with the waves.

In the following derivation the quantities $\overline{W}$, $\overline{B}_o$, $\tau$, T are assumed to be functions neither of position nor of time.

$\overline{W}$ is the equilibrium ion drift velocity

$\nu$ is the effective ion collision frequency for momentum loss due to ion-neutral collisions

These assumptions are justified in the cases of $B_o$ and $\tau$. They are probably approximately true in the case of T as well. Since $\overline{W}$ is defined as an equilibrium drift velocity, it must be independent of time, and for simplicity it is assumed to be independent of position as well.

The momentum transfer equation for ions is first linearized and then combined with the linearized equation of continuity and the plasma equation of state. The usual form is assumed for the azimuthal and longitudinal forms of the wave solutions, and a series solution of the resulting ordinary differential equation of the ion density perturbations is obtained. Insertion of the radial boundary condition yields the dispersion relation which is then compared to the experimental data.

Assuming the electron and ion pressures are scalar quantities, the momentum transfer equation for the ions under the influence of the perturbation is:

$$\frac{-1}{M} \nabla(P + \Pi + p + \pi) = \left[\frac{\partial}{\partial t} + (\overline{V} + \overline{W}) \cdot \nabla\right]\left[(N + n)(\overline{V} + \overline{W})\right] \qquad (4)$$

$$+ (N + n)(\overline{V} + \overline{W})\nu - \Omega(N + n)(\overline{V} + \overline{W}) \times \hat{z}$$

where

$P$ is the equilibrium electron pressure

$\Pi$ is the equilibrium ion pressure

$p$ is the electron pressure perturbation

$\pi$ is the ion pressure perturbation

$\overline{V}$ is the ion velocity induced by the wave

$n$ is the ion density perturbation

and the positive $\hat{z}$ direction is taken in the direction of $\overline{B}_o$.

The momentum transfer equation for the ions in the unperturbed plasma column is:

$$\frac{-1}{M} \nabla(P + \Pi) = \left[\frac{\partial}{\partial t} + \overline{W} \cdot \nabla\right]\left[N\overline{W}\right] + N\overline{W}\nu - \Omega N\overline{W} \times \hat{z} \qquad (5)$$

Expanding equations (4) and (5), subtracting (5) from (4), and assuming the density perturbation is small compared to the unperturbed density allows the resulting equation to be partially linearized to the first order in small quantities.

$$\frac{-1}{M} \nabla(p + \pi) = N \frac{\partial \overline{V}}{\partial t} + \overline{V} \frac{\partial n}{\partial t} + \overline{W} \frac{\partial n}{\partial t}$$

$$+ \overline{V} \cdot \nabla (N + n)(\overline{V} + \overline{W}) \qquad (6)$$

$$+ W \cdot \nabla (N\overline{V} + n\overline{V} + n\overline{W})$$

$$+ \nu (N\overline{V} + n\overline{W}) - \Omega N\overline{V} \times \hat{z}$$

Since solutions of the form $e^{i(\mu\theta + \ell z - \omega t)}$ are sought, the following operators may be replaced by the listed variables:

$$\frac{\partial}{\partial t} \longrightarrow -i\omega \quad (\omega \text{ assumed real})$$

$$\frac{\partial}{\partial z} \longrightarrow i\ell \quad (\ell \text{ complex longitudinal wavenumber})$$

$$\frac{\partial}{\partial \theta} \longrightarrow i\mu \quad (\mu \text{ complex azimuthal wavenumber})$$

Also since $\overline{W}$ is assumed to be in the $\hat{z}$ direction, $\overline{W} = W\hat{z}$ and

$$W \cdot \nabla \longrightarrow W \frac{\partial}{\partial z} .$$

The radial form of the density perturbations is left unspecified for the present.

Linearizing the expression $\overline{V} \cdot \nabla (N + n)(\overline{V} + \overline{W})$ to the first order in small quantities gives:

$$\overline{V} \cdot \nabla (N + n)(\overline{V} + \overline{W}) \doteq \overline{W} \left(V_r \frac{\partial N}{\partial r} + \frac{i\mu}{r} nV_\theta + i\ell nV_z\right),$$

where

$$\overline{V} \equiv V_r\hat{r} + V_\theta\hat{\theta} + V_z\hat{z}.$$

Thus (6) becomes:

$$\frac{-1}{M} \nabla(p + \pi) = -i\omega N\overline{V} - i\omega n\overline{W} + WV_r \frac{\partial N}{\partial r} \hat{z} \tag{7}$$

$$+ i\ell W(N\overline{V} + n\overline{W}) + \nabla N(\overline{V} + \overline{W}) - \Omega NV_\theta\hat{r} + \Omega NV_r\hat{\theta}$$

From (7) are immediately obtained:

$$MNV_\theta = \frac{\frac{i\mu}{r}(p + \pi)(i\omega - i\ell W - \nu) + \Omega\left(\frac{\partial p}{\partial r} + \frac{\partial \pi}{\partial r}\right)}{(i\omega - i\ell W - \nu)^2 + \Omega^2} \tag{7a}$$

$$MNV_r = \frac{\left(\frac{\partial p}{\partial r} + \frac{\partial \pi}{\partial r}\right)(i\omega - i\ell W - \nu) - \frac{i\mu}{r}\Omega(p + \pi)}{(i\omega - i\ell W - \nu)^2 + \Omega^2} \tag{7b}$$

30

$$NV_z = \frac{\frac{ik}{M}(p + \pi) - i\omega wn + ikw^2 n + \nu wN + wV_r \frac{\partial N}{\partial r}}{(i\omega - ikW - \nu)} \qquad (7c)$$

Forming the vector difference of equations (7a) and (7b) and taking the divergence of the resulting quantity gives:

$$\nabla \cdot (NV_\theta \hat{r} - NV_r \hat{\theta}) = \frac{\Omega}{M} \left[ \frac{(\frac{\partial^2 p}{\partial r^2} + \frac{\partial^2 \pi}{\partial r^2}) + \frac{1}{r}(\frac{\partial p}{\partial r} + \frac{\partial \pi}{\partial r}) - \frac{M^2}{r^2}(p + \pi)}{(i\omega - ikW - \nu)^2 + \Omega^2} \right] \qquad (8)$$

Neglecting volume ionization and recombination the equation of continuity for the ions is:

$$\nabla \cdot (N + n)(\overline{V} + \overline{W}) = -\frac{\partial}{\partial t}(N + n) = i\omega n \qquad (9)$$

Taking the divergence of equation (7) gives:

$$\frac{-1}{M}\nabla^2(p + \pi) = -i\omega \left[ \nabla \cdot N\overline{V} + \nabla \cdot n\overline{W} \right] + W\frac{\partial}{\partial z}\left[ V_r \frac{\partial N}{\partial r} \right]$$

$$+ ikW\left[ \nabla \cdot N\overline{V} + \nabla \cdot n\overline{W} \right] + \nu\left[ \nabla \cdot N\overline{V} + \nabla \cdot n\overline{W} \right]$$

$$- \Omega\nabla \cdot \left[ NV_\theta \hat{r} - NV_r \hat{\theta} \right] \qquad (10)$$

Linearizing equation (9) gives:

$$\nabla \cdot (N + n)(\overline{V} + \overline{W}) \doteq \nabla \cdot N\overline{V} + \nabla \cdot n\overline{W} \qquad (11)$$

Using equation (11) to evaluate $\nabla \cdot (N\overline{V}) + \nabla \cdot (N\overline{W})$

and using equation (8) to evaluate $\nabla \cdot (NV_\theta \hat{r} - NV_r \hat{\theta})$,

equation (10) becomes:

$$\frac{1}{M} \nabla^2 (p + \pi) = -\omega^2 n + \omega k Wn - i\omega \gamma n$$

$$+ \frac{\Omega^2}{M} \left[ \frac{(\nabla^2 - \frac{\partial^2}{\partial z^2})(p + \pi)}{(i\omega - ikW - \gamma)^2 + \Omega^2} \right] \quad (12)$$

$$- \frac{W}{MN} \frac{\partial N}{\partial r} \left\{ \frac{\left[ ik(i\omega - ikW - \gamma)\frac{\partial}{\partial r} - \frac{i\mu}{r}\Omega\frac{\partial}{\partial z} \right](p + \pi)}{(i\omega - ikW - \gamma)^2 + \Omega^2} \right\}$$

Under the assumption of the spatial invariance of $\gamma$ and T equation
(12) becomes:

$$(c^2 + C^2) \left\{ \left[ \frac{\partial^2 n}{\partial r^2} + \frac{1}{r}\frac{\partial n}{\partial r} - \frac{\mu^2}{r^2}n \right] \left[ \frac{(i\omega - ikW - \gamma)^2}{(i\omega - ikW - \gamma)^2 + \Omega^2} \right] - k^2 n \right\}$$

$$+ (c^2 + C^2) \frac{W}{N} \frac{\partial N}{\partial r} \left\{ \frac{ik\frac{\partial n}{\partial r}(i\omega - ikW - \gamma) + \frac{\mu}{r}\Omega k n}{(i\omega - ikW - \gamma)^2 + \Omega^2} \right\} \quad (13)$$

$$+ \omega^2 n - \omega k Wn - i\omega \gamma n = 0$$

where $c^2 \equiv \frac{\kappa T}{M}$ (definition)

and $C^2 \equiv \frac{\kappa T}{M}$ (definition).

The differential equation (13) would be directly reducible to
Bessel's equation of order $\mu$ if $\frac{\partial N}{\partial r}$ were equal to zero (that is if the
unperturbed column had a uniform radial density distribution). This,
however, is not the case in the present investigation.

The mean free path for the ion-neutral collision process is greater
than 1 m, while the ion gyro radius is less than $10^{-3}$ m. Up to several
ion gyro radii away from the beam axis the analysis of Pfirsch and
Biermann predicts that for a Maxwellian velocity distribution and a
Gaussian distribution of the guiding centers of the charged particles

32

there will be a Gaussian density profile. [14] Previous probe analysis by Gall and Oleson has fitted a Gaussian radial density profile to N, at least to a good approximation. [15] Thus $N = N_o e^{-\delta^2 r^2}$, so that $\frac{1}{N} \frac{\partial N}{\partial r} = -2\delta^2 r$, and equation (13) becomes:

$$(c^2 + C^2)\left\{\left[\frac{\partial^2 n}{\partial r^2} + \frac{1}{r}\frac{\partial n}{\partial r} - \frac{\mu^2}{r^2} n\right]\left[\frac{(i\omega - ikW - \gamma)^2}{(i\omega - ikW - \gamma)^2 + \Omega^2}\right] - k^2 n\right\}$$

$$- (c^2 + C^2)(2Wr\delta^2)\left\{\frac{ik\frac{\partial n}{\partial r}(i\omega - ikW - \gamma) + \frac{\mu}{r}\Omega kn}{(i\omega - ikW - \gamma)^2 + \Omega^2}\right\} \qquad (14)$$

$$+ \omega^2 n - \omega kWn - i\omega\gamma n = 0$$

Defining $s \equiv \lambda r$

and $\quad \lambda^2 \equiv \left[\frac{\Omega^2}{(\omega - kW + i\gamma)^2} - 1\right]\left[k^2 - \frac{\omega(\omega - kW + i\gamma)}{c^2 + C^2}\right]$

$$+ \frac{2\mu\delta^2 \Omega W k}{(\omega - kW + i\gamma)^2}$$

equation (14) becomes:

$$s^2 \frac{\partial^2 n}{\partial s^2} + \frac{\partial n}{\partial s}\left[s - \frac{2s^3\delta^2 kW}{(\omega - kW + i\gamma)^2}\right] + n\left(s^2 - \mu^2\right) = 0 \qquad (15)$$

Assuming a solution of the form

$$n = n_o s^{\rho} \sum_{j=0}^{\infty} a_j s^j \quad (a_o \neq 0)$$

and inserting this into equation (15) leads to the recursion relation

$$a_{2j} = \frac{g^j \Gamma(j + \frac{|\mu|}{2} - \frac{1}{2g})}{2^{|\mu|} 2^j j! (j + |\mu|)! \Gamma(\frac{|\mu|}{2} - \frac{1}{2g})} \quad \text{and} \quad \rho = |\mu|$$

(where $a_o$ has been chosen as $\frac{1}{2^{|\mu|}|\mu|!}$).

33

Thus the solution of equation (15) is:

$$n(s) = \underline{n} \sum_{j=o}^{\infty} \frac{g^j \; \Gamma \; (j + b) s^{|\mu| + 2j}}{2^{|\mu|} \; 2^j \; j! \; (j + |\mu|)! \; \Gamma \; (b)} \tag{16}$$

where

$$\underline{n} \equiv n_o e^{i(\mu\theta + k z - \omega t)}$$

$$b \equiv \frac{|\mu| g - 1}{2g}$$

and

$$g \equiv \frac{2\delta^2 k W}{(\omega - k W + i \nu)\lambda^2} \quad .$$

Equation (16) reduces to the Bessel function $J_\mu$ for the case $g = 0$ (uniform density in the unperturbed column). For this case the dispersion relation would assume the simple form $\lambda \ell = 2.405$ where the boundary condition has been imposed that $r = \ell$ is the radial position at which the perturbation vanishes. The validity of this type of boundary condition was confirmed by the probe measurement discussed in detail in Section 3. Independent confirmation that this type of boundary condition is appropriate can be obtained from an examination of the radial electron temperature profile as obtained by Gall and Oleson. [15] This curve is reproduced as Fig. 18 in Section 5. It is evident from an examination of Fig. 18 that the electron temperature drops sharply (or at least becomes small compared to the value at $r = 0$) at the position $r = 7,8$ mm. An examination of equation (14) under the condition that both c and C become small reveals that the magnitude of the density perturbation, n, must also approach zero. The use of this type of boundary condition is particularly convenient, since no assumption need be made concerning the existence of either a pressure node or a velocity node at the plasma

34

boundary. This problem has plagued investigators working with low ion-
ization gaseous discharges. [5]

For the case $g \neq 0$ the dispersion relation for $\mu = 0$ is:

$$\sum_{j=o}^{\infty} \frac{g^j \, \Gamma(j - \frac{1}{2g})(\lambda^2 \ell^2)^j}{2^j j! \; j! \; \Gamma(-\frac{1}{2g})} = 0 \qquad (17)$$

where now

$$g \equiv \frac{2\delta^2 \, \ell W}{(\omega - \ell W + i\gamma)\lambda^2}$$

and

$$\lambda^2 \equiv \left[\frac{\Omega^2}{(\omega - \ell W + i\gamma)^2} - 1\right]\left[\ell^2 - \frac{\omega(\omega - \ell W + i\gamma)}{c^2 + C^2}\right]$$

Equation (17), or more accurately the recursion relation between
the coefficients, is compared to the experimental data by a least
squares direct search computer program on a CDC 1604.

EXPERIMENTAL ARRANGEMENT

A schematic illustration of the Steady State Plasma Facility at the Naval Postgraduate School appears in Fig. 6. The plasma is produced by a hollow cathode discharge, which has been investigated by Lidsky et. al. [16] The details of its construction appear in Fig. 7. The facility is capable of operation on helium, neon, and argon, although only argon was employed in the present experiment. The neutral argon gas is supplied through a micrometer valve assembly to the hollow cathode. An r-f voltage is supplied between the cathode and the first anode in order to ignite the arc. Once the arc has been struck, the discharge is self-sustaining, and the r-f voltage is turned off.

The plasma so produced drifts through the hole in the first anode and into the experimental tube. This section is a 3 meter pyrex tube of inside diameter 10 cm. It is axially aligned with the confining magnetic channel to within 1 mm throughout the length of the experimental region.

The optimum operating conditions for the facility are an arc current of 100 amps and a voltage of 90 volts between the cathode and first anode. This condition is most conveniently achieved by regulation of the argon gas pressure through the micrometer valve assembly.

Differential pumping of neutral gas atoms by the diffusion pumps maintains a neutral gas pressure of approximately $3 \times 10^{-5}$ mm Hg throughout the experimental region.

The strength of the confining magnetic field is continuously variable from 500 gauss to 10,000 gauss. Some experimental data were taken at a field strength of 600 gauss, but the agreement with theory was quite poor. It was suspected that some drift occurred in the current supplying the field coils, so that the confining magnetic field was not constant with
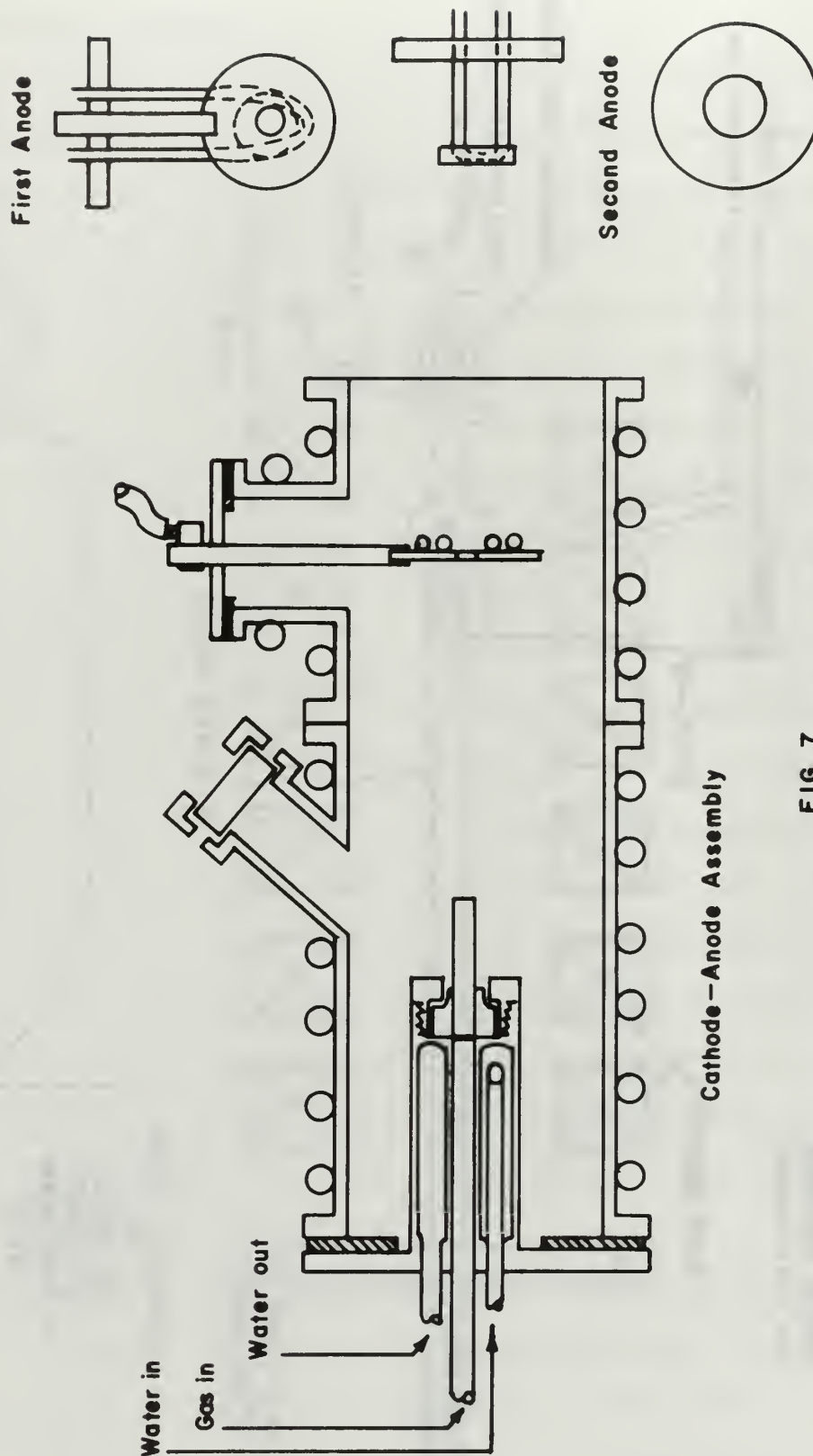
FIG.6

SCHEMATIC DIAGRAM OF PLASMA FACILITY

37

First Anode

Second Anode

Cathode—Anode Assembly

Water in
Gas in
Water out
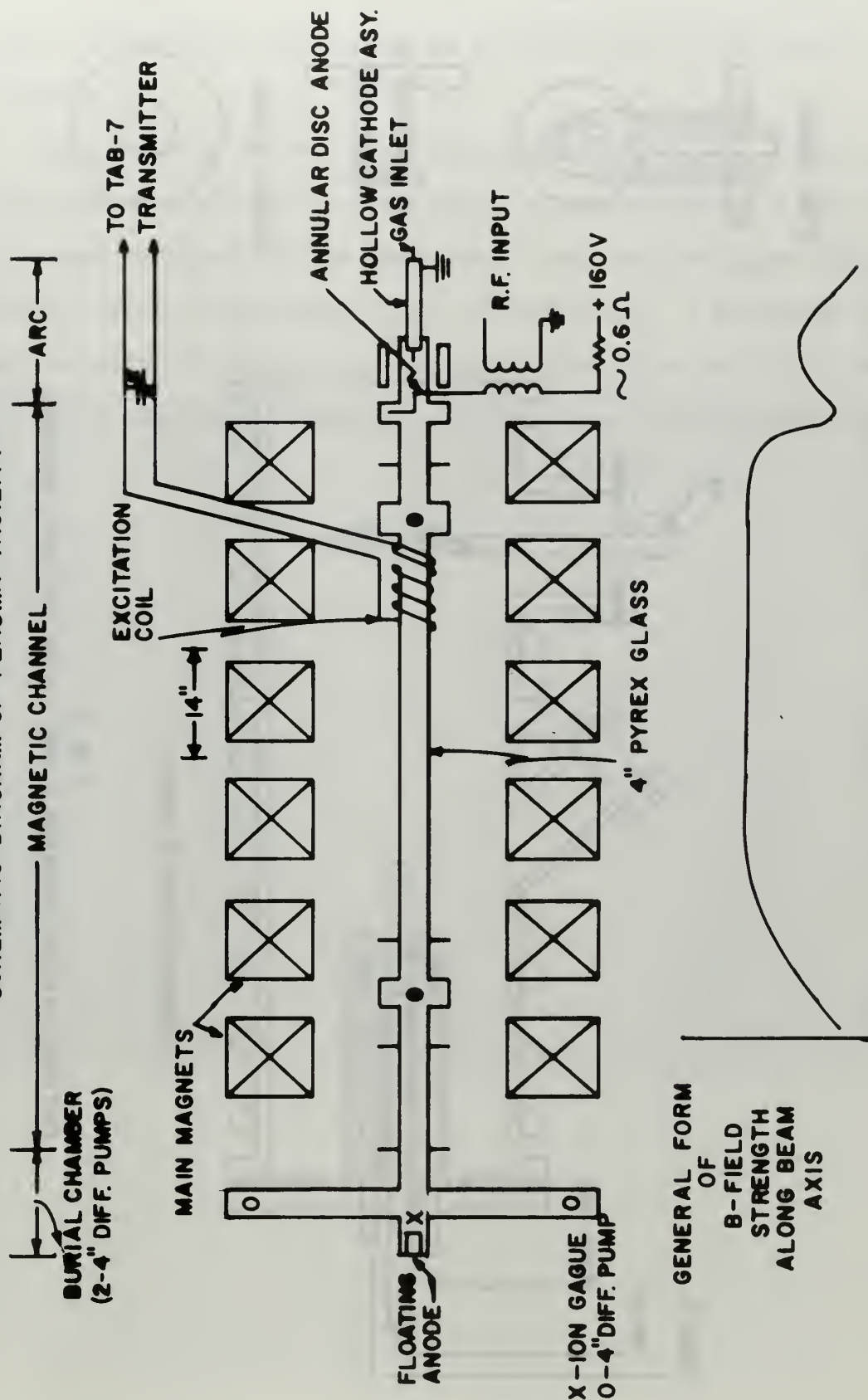
FIG. 7
CATHODE—ANODE ASSEMBLY AND VIEWS OF BOTH ANODES

38

time (a necessary condition for taking a complete set of dispersion data).
These data are not reported, and the minimum field strength employed was
800 gauss.

Upon reaching the end of the experimental region, the plasma ions
and electrons strike the floating anode (so-called because its potential
is allowed to float) and are recombined. They are then pumped away as
neutrals by the vacuum pumps in the burial chamber. A photograph of this
section appears in Fig. 8. A side view of the entire facility appears
in Fig. 9, and a view of the cathode-first anode region appears in Fig.
10.
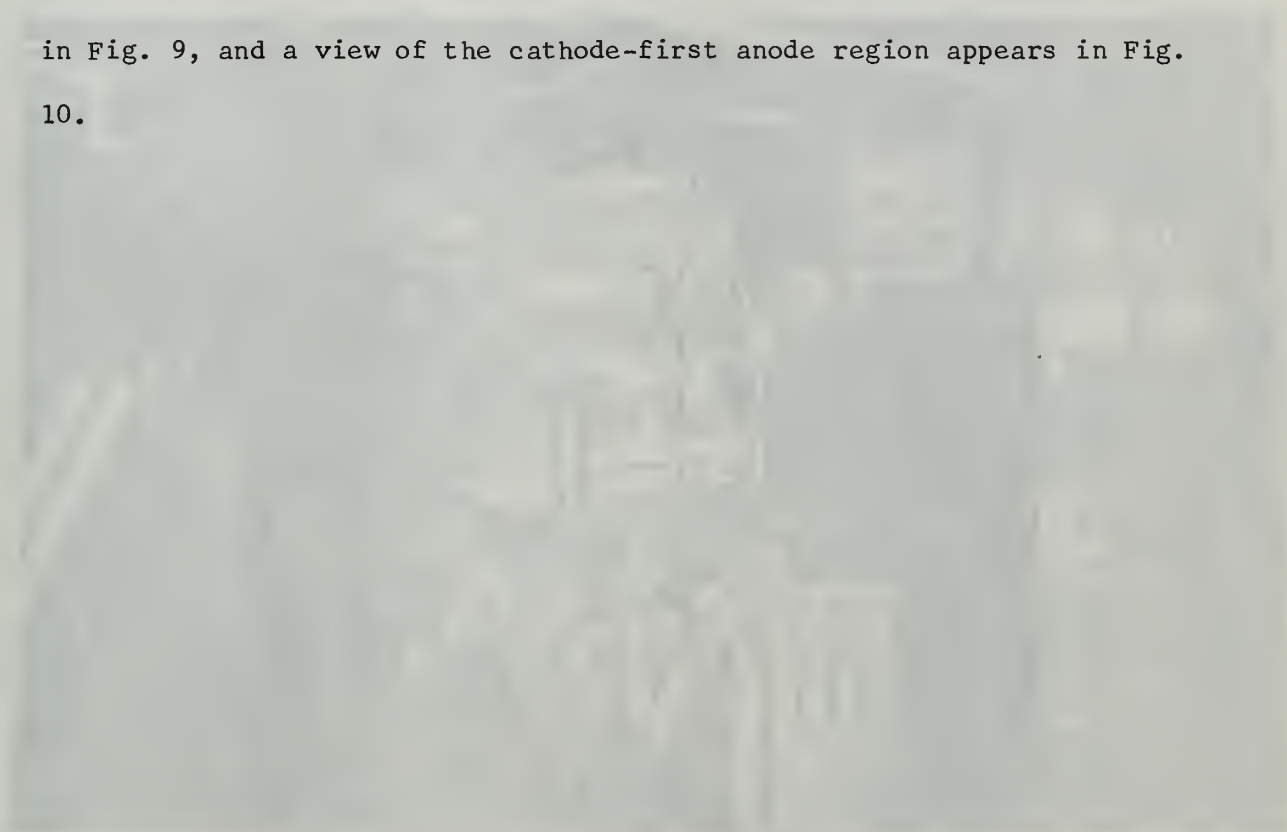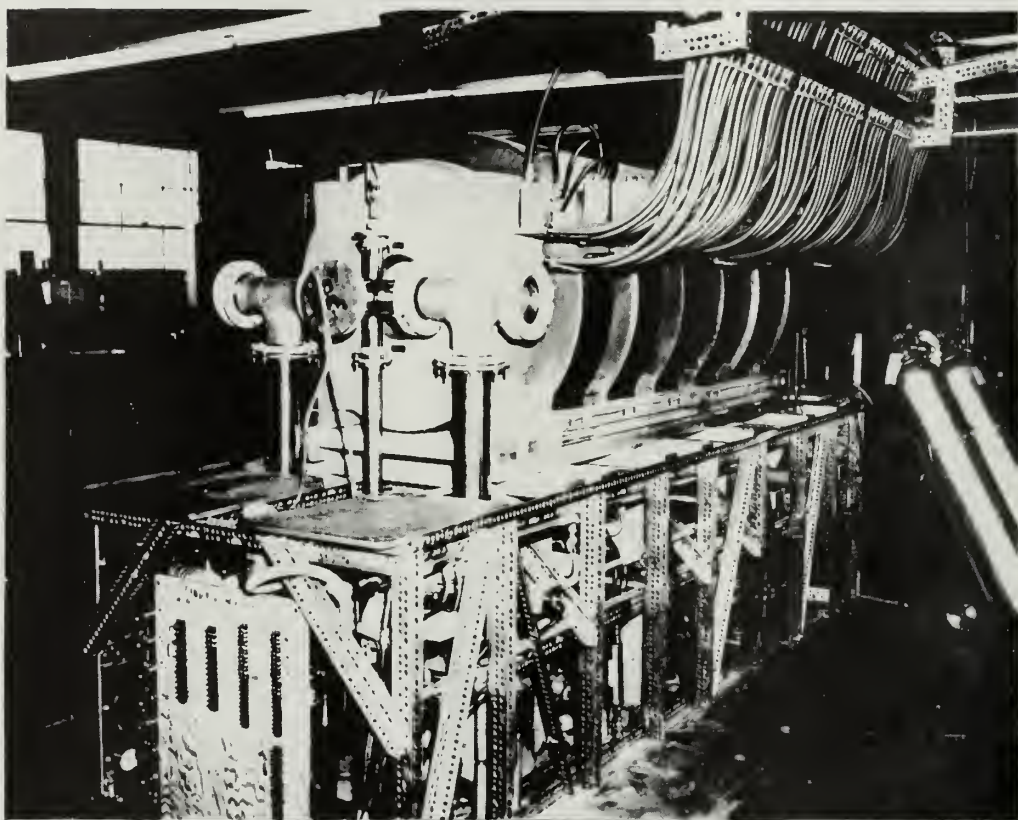
FIG. 8
END VIEW OF PLASMA FACILITY SHOWING FLOATING ANODE

40
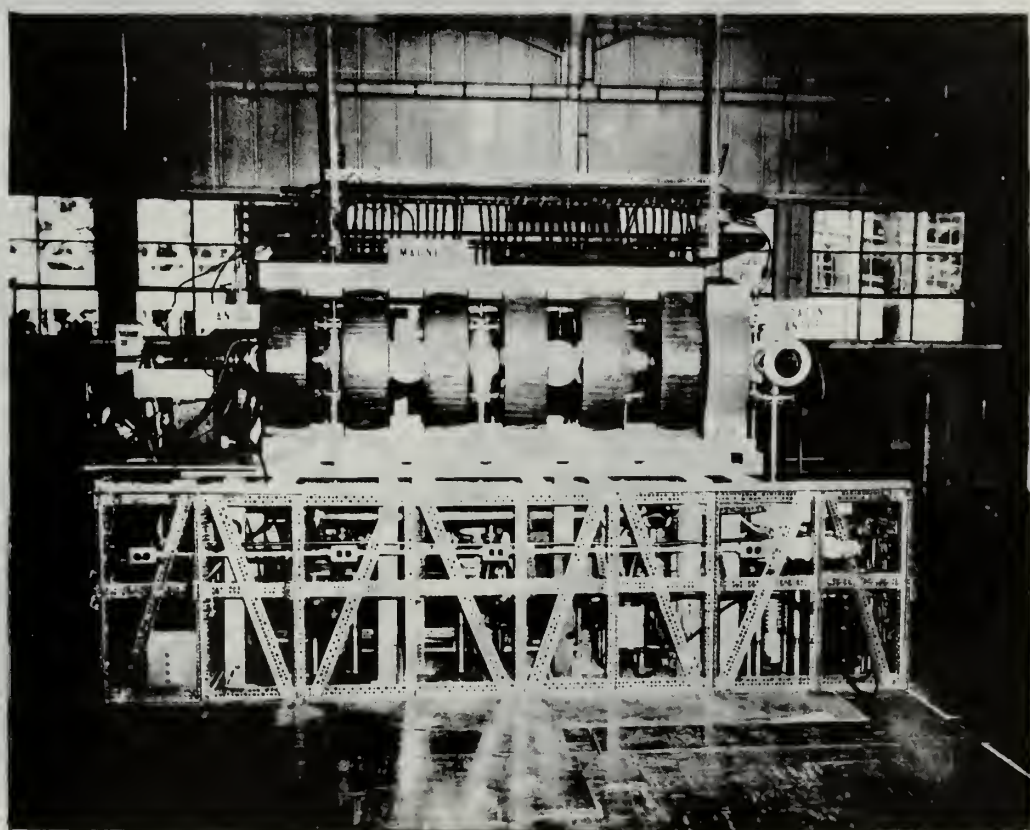
FIG. 9
SIDE VIEW OF PLASMA FACILITY

41
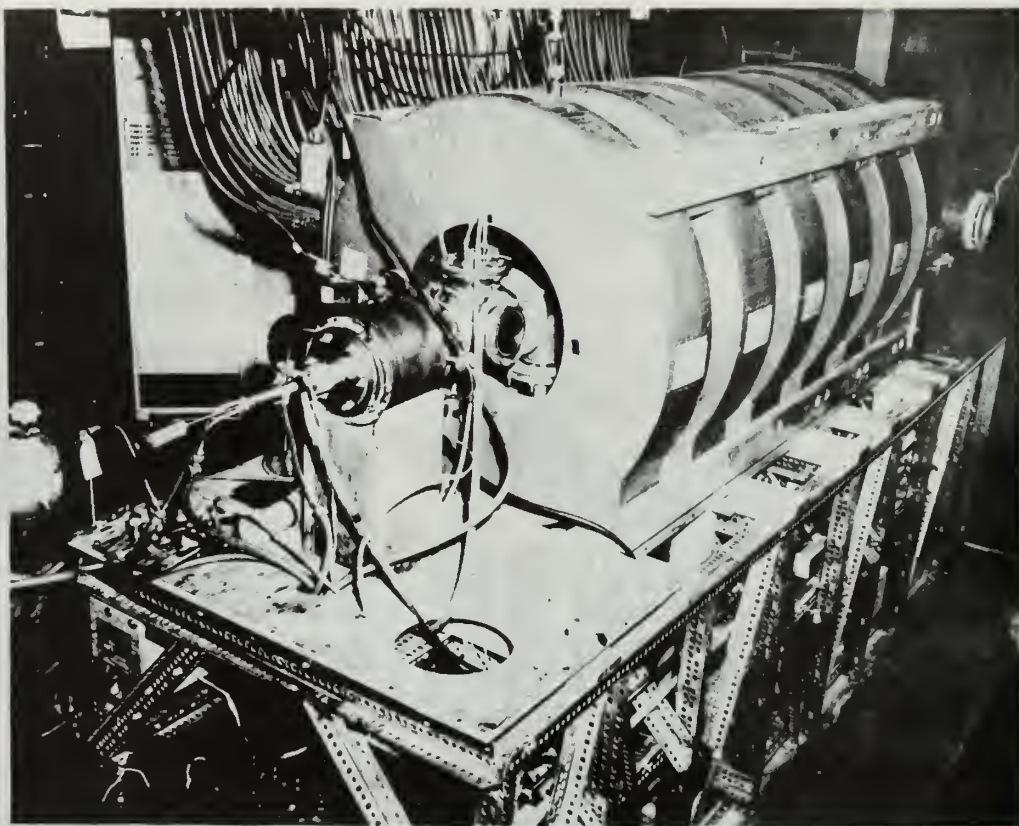
FIG. 10
END VIEW OF PLASMA MACHINE SHOWING CATHODE REGION

42

In order to excite the wave, a short r-f coil was tightly wrapped around the pyrex tube as shown in Fig. 6. It was designed for optimum coupling to the plasma at the center of the band of exciting frequencies employed. This coupling effectiveness was determined by the length of the coil, which was approximately that of the wavelengths excited. Experimentally it was found that the r-f field strength dropped appreciably in the last $\frac{1}{4}$ of the coil at each end, so that these outer regions were ineffective in producing a perturbing field. The coil itself was approximately 15 cm long, leaving approximately 7 cm for the effective field-producing region. This was in the center of the band of wavelengths excited.

The coil was the inductive arm of a parallel "almost resonant" tank circuit, which was tuned (with approximately 1500 $\mu\mu$f excess capacity) to resonance at the applied transmitter frequency. This slight departure from the resonance condition was necessary so that the transmitter would see a load impedance similar to that of the radio transmission antenna which it was designed to feed.

The transmitter used to power the tank circuit was a U.S. Navy type TAB-7 manufactured by the Westinghouse Corp. It is capable of producing a peak r-f power level of 2 kw over the frequency range of 100 kc to 500 kc. This full power condition was not used due to the inability of the r-f exciting coil to dissipate the heat generated at this condition. Typical operating conditions were a transmitter output current of 3-4 amps. The Q value of the tank circuit was estimated to be about 10 at the frequencies used. Thus the actual exciting current in the coil was approximately 30-40 amps. Direct measurement of the r-f magnetic fields produced yielded values of from 125 to 195 gauss,

43

depending on transmitter power. As previously mentioned, this perturbing magnetic field produced variations in the local electron diffusion co-efficient, creating plasma density variations.

Assuming the magnetic perturbation, B, is of the form $B = B_1 \sin \omega T$ and that $\omega > \Omega$ (which was true in all cases), only the influence of the perturbing field on the electrons need be considered, since the massive ions are unable to respond directly to the rapidly varying magnetic field, while the electrons can instantaneously follow its variations. The diffusion rate of electrons perpendicular to the magnetic field is:

$$D_B = \frac{D}{1 + \left[\dfrac{e(B + B_o)}{m \, N}\right]^2}$$

where   $D_B$ is the local electron diffusion coefficient with both B and

$B_o$ applied

D   is the local electron diffusion coefficient with zero applied

magnetic field

e   is the electron charge

m   is the electron mass

$N$   is the electron-neutral collision frequency

Now under the conditions of the experiment, $\left(\dfrac{eB_o}{m \, N}\right) \gg 1$. Therefore

$D_B \doteq D \left[\dfrac{m \, N}{e(B + B_o)}\right]^2$ or $D_B \propto \dfrac{1}{(B + B_o)^2}$ .

Now for the general diffusion problem $D_B \dfrac{\partial^2 N}{\partial r^2} = Q$ (source) (under conditions of steady state). Replacing $\dfrac{\partial^2 N}{\partial r^2}$ by $\dfrac{N}{a^2}$ , where a is an average effective diffusion mean free path, there results $\dfrac{D_B N}{a^2} \doteq Q$ or $N = \dfrac{Q a^2}{D_B}$ . Thus $N \propto \dfrac{1}{D_B}$ and $(N + n) \propto (B + B_o)^2$ or

$(N + n) \propto (B_1 \sin \omega t + B_o)^2$. Since $B_1 \ll B_o$, $(N + n) = N(1 + \frac{B_1 \sin \omega t}{B_o})^2$ $\doteq N(1 + \frac{2B_1 \sin \omega t}{B_o})$. Therefore $n \doteq 2N \frac{B_1}{B_o} \sin \omega t$, and the plasma density is modulated at the applied frequency, the strength of the perturbation being proportional to that of the r-f magnetic field. These perturbations were studied over the frequency range of 187 kc to 352 kc and for static magnetic fields from 800 to 2200 gauss.

Once the waves have been generated, they propagate parallel to the static magnetic field in both directions. Only propagation anti-parallel to the static magnetic field was investigated in detail. (One set of parallel propagation measurements was made; this allowed an independent determination of the ion drift velocity, $\overline{w}$.)

Previous spectroscopic measurements have established that virtually all the light emitted by the plasma is from excited neutral atoms. [10] Therefore the emitted light intensity at any point along the plasma column is directly dependent on the local electron density. (An ion-electron light production mechanism would produce a light intensity which was proportional to the square of the local charged particle density.) Thus a photomultiplier tube can be used to detect the presence of the waves. The detection circuit schematic is given in Fig. 11. The photomultiplier tube was housed in a light-tight electrostatic and magnetic shield manufactured by the Quanta Corp. A 1P21 photomultiplier tube was mounted inside this shield and dynode voltages were supplied by batteries. The entire assembly was located in a region of minimum magnetic field (less than 25 gauss). The optical signal was fed to the phototube through a 10 ft flexible unaligned optical fiber bundle manufactured by Optics Technology, Inc. This fiber bundle caused a 67% loss in light intensity, but the signal strength was large enough that this caused no

FIG. II

DETECTION CIRCUIT SCHEMATIC
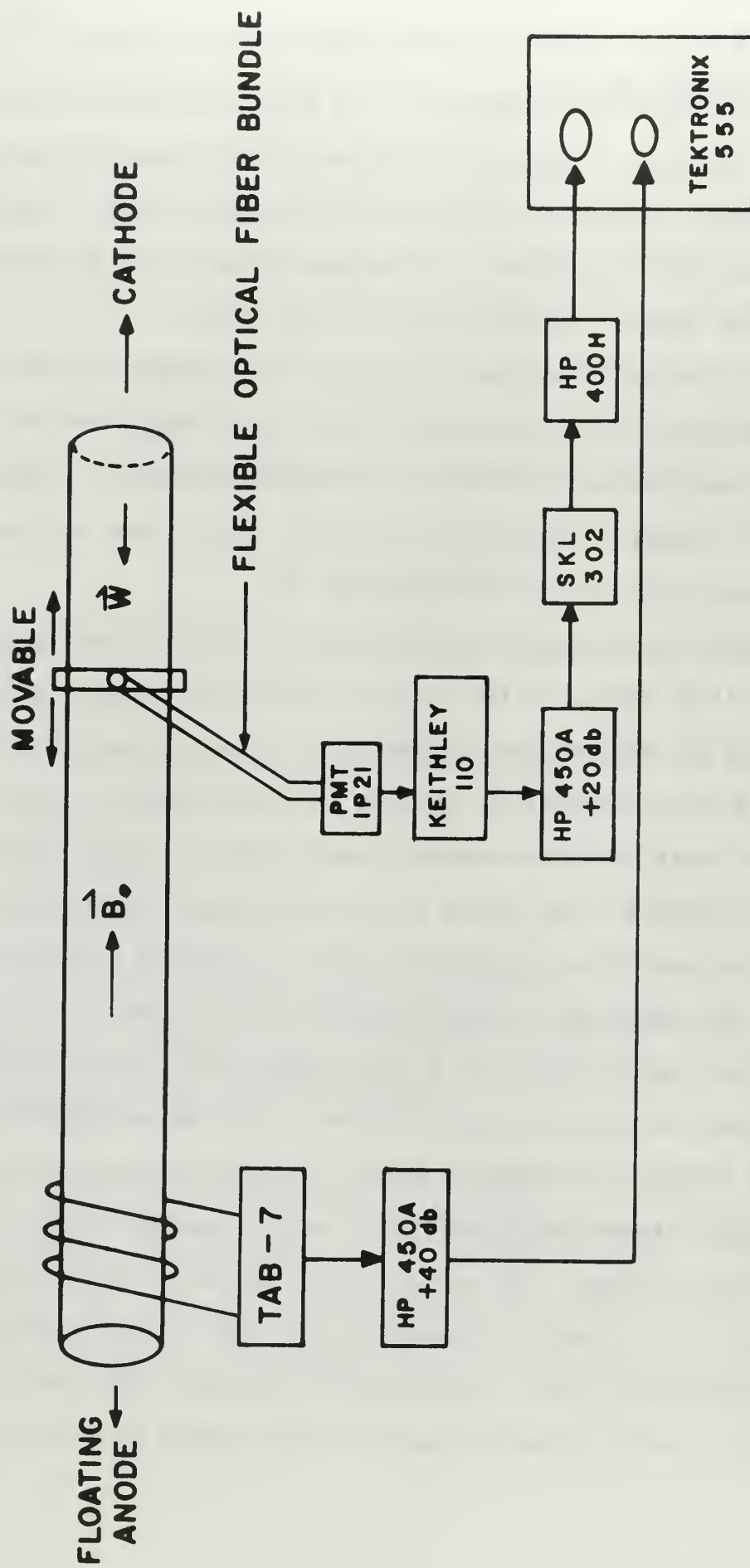
problem.

A Keithley Model 110 Wideband Amplifier with an overall gain of unity was used as an impedance matching device between the phototube and the Hewlett-Packard Model 450A Wideband Amplifier (which was set to a 20 db gain). In order to improve discrimination against noise the signal was then fed into a Spencer-Kennedy Electronic Filter Model 302, which served as a band pass filter centered at the transmitter frequency.

The next element in the detector circuit was a Hewlett-Packard Model 400H Vacuum Tube Voltmeter which was used to make amplitude (attenuation) measurements. Finally a Tektronix Dual Beam Oscilloscope Type 555 was used to display the detected signal and compare it with a monitor signal taken directly from the TAB-7 transmitter. Both signals were subject to various phase delays (due to coupling into and out of the plasma, elements in the detector circuit, etc.), but comparison of the phases of the two signals appearing on the oscilloscope gave the relative phase delay of the arriving signal. Moving the optical fiber bundle along the plasma column until the phase of the arriving signal was the same as before allowed a direct determination of the wavelength of the propagating signal.

Signal strength after amplification and filtering was of the order of 100 mv (depending on dynode voltages and transmitter power). Signal-to-noise ratios varied widely depending primarily on the electronic filter settings and on the transmitter power. Individual filter settings at each frequency employed were necessary in order to discriminate against the noise background in the plasma. The frequencies selected for study were chosen in the quieter regions of the plasma noise spectrum. There was a marked variation in the location of these regions depending on the static magnetic field strength. A trial and error

approach proved to be the most productive method for finding their location.

A typical oscilloscope photograph is shown in Fig. 12. The upper trace shows the detected signal (after amplification and filtering). Part of its amplitude is due to an unavoidable inductive pickup condition. This part was, of course, subtracted from the raw data before analysis. Some plasma noise can be clearly seen within the signal envelope. The signal-to-noise ratio here is slightly greater than 1. The lower trace is a comparison signal taken from the TAB-7 transmitter. This photograph was taken for a 250 kc signal. Deflection sensitivity of both traces was 100 mv/cm, and sweep speed was 5 $\mu$sec/cm.

Wavelength and amplitude measurements were taken as functions of frequency for various magnetic field strengths. The results provide the raw data from which the dispersion and attenuation curves presented in the next section were derived.
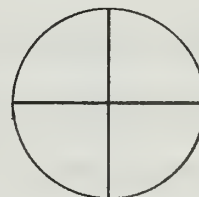
To insure that modes other than the $\mu$= 0 were not excited, probe measurements were made in an attempt to detect the presence of the $\mu$ = 1, 2, 3 modes. (The form of these modes is sketched below.)
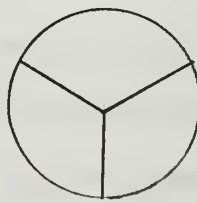


$\mu$=1      $\mu$=2      $\mu$=3

At maximum detection sensitivity no such waves were detected. Since the excitation mechanism had azimuthal symmetry, modes other than $\mu$= 0 should not be present. Actual confirmation that the detected wave was actually the $\mu$ = 0 mode was made by probe measurement. The perturbation

Figure 12. Typical Oscilloscope Trace

49

was observed to have a maximum at r = 0 (on the beam axis) and was ob-
served to decrease as the probe was moved out from the axis. This be-
havior would only be possible for the $\mu$ = 0 mode. All other modes would
exhibit a null at r = 0. This probe measurement also forms the basis for
the comparison theory for the cutoff distance (that is $\ell$). These mea-
surements showed no detectable perturbations beyond a distance of 15 mm
from the beam axis.

No standing waves were observed to exist. This was probably due
to the effect of the burial chamber surrounding the floating anode. In
the burial chamber ions and electrons are recombined and the resulting
neutral gas pumped away. Thus the plasma charge density is low, and
the neutral gas density is high. Both of these conditions would tend
to preclude the establishment of a standing wave pattern. Reflection
of the waves from the floating anode could produce a standing wave pat-
tern, but this effect has never been observed. [17]

EXPERIMENTAL RESULTS

Given a fixed static magnetic field strength, a set of data consists of $\alpha$ and $\beta$ as functions of $\omega$. The raw data are reduced in the following way. Assuming $\omega$ is real, let $k = \alpha + i\beta$ ($\alpha$ and $\beta$ both real). First the measured wavelengths are reduced to dimensionless variables by defining $y \equiv \frac{\alpha c}{\Omega}$. Knowing the wavelength allows direct calculation of the damping decrement, $\beta$. If two intensity measurements are made one wavelength apart, $\frac{I_1}{I_0} = e^{-\beta|z_1 - z_0|}$ where $|z_1 - z_0| = \frac{2\pi}{\alpha}$. Thus $\frac{I_1}{I_0} = e^{-\frac{2\pi\beta}{\alpha}}$, from which $\beta$ can be calculated directly. The damping decrement is then reduced to a dimensionless variable by defining $z \equiv \frac{\beta c}{\Omega}$. The frequency is reduced to a dimensionless variable by defining $x \equiv \frac{\omega}{\Omega}$. For a given magnetic field strength the entire set of data (that is y and z vs. x) are read into a direct search computation program. The 5 adjustable parameters $W, \nu$, C, $\ell$, and $\delta$ are reduced to dimensionless variables by defining

$$\eta \equiv \frac{W}{c} \qquad \mathcal{J} \equiv \frac{\nu}{\Omega} \qquad \sigma \equiv \frac{C}{c} \qquad \xi \equiv \frac{c}{\Omega\ell} \qquad \epsilon \equiv \frac{\delta c}{\Omega} \; .$$

The computation program simultaneously adjusts these parameters to find the dispersion function yielding the least square error when compared to the data. In addition to performing this calculation, graphical displays are also presented for y vs. x and z vs. x. The plotted squares represent the data points, and the continuous curve represents the dispersion relation using the 5 parameters just computed. Results are presented from 800 to 2200 gauss in the following curves, the parameter being $B_0$ (web/m$^2$).
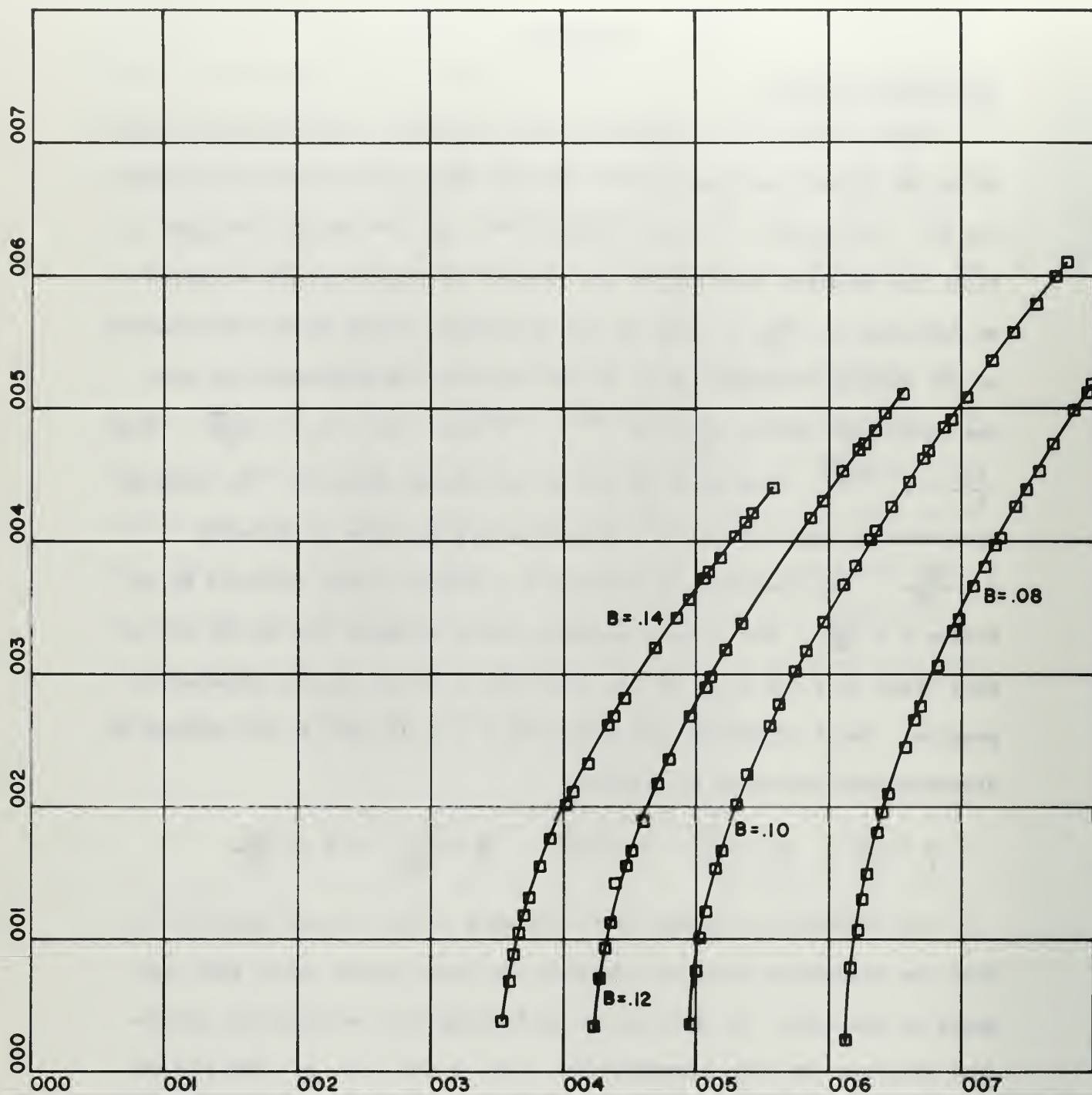
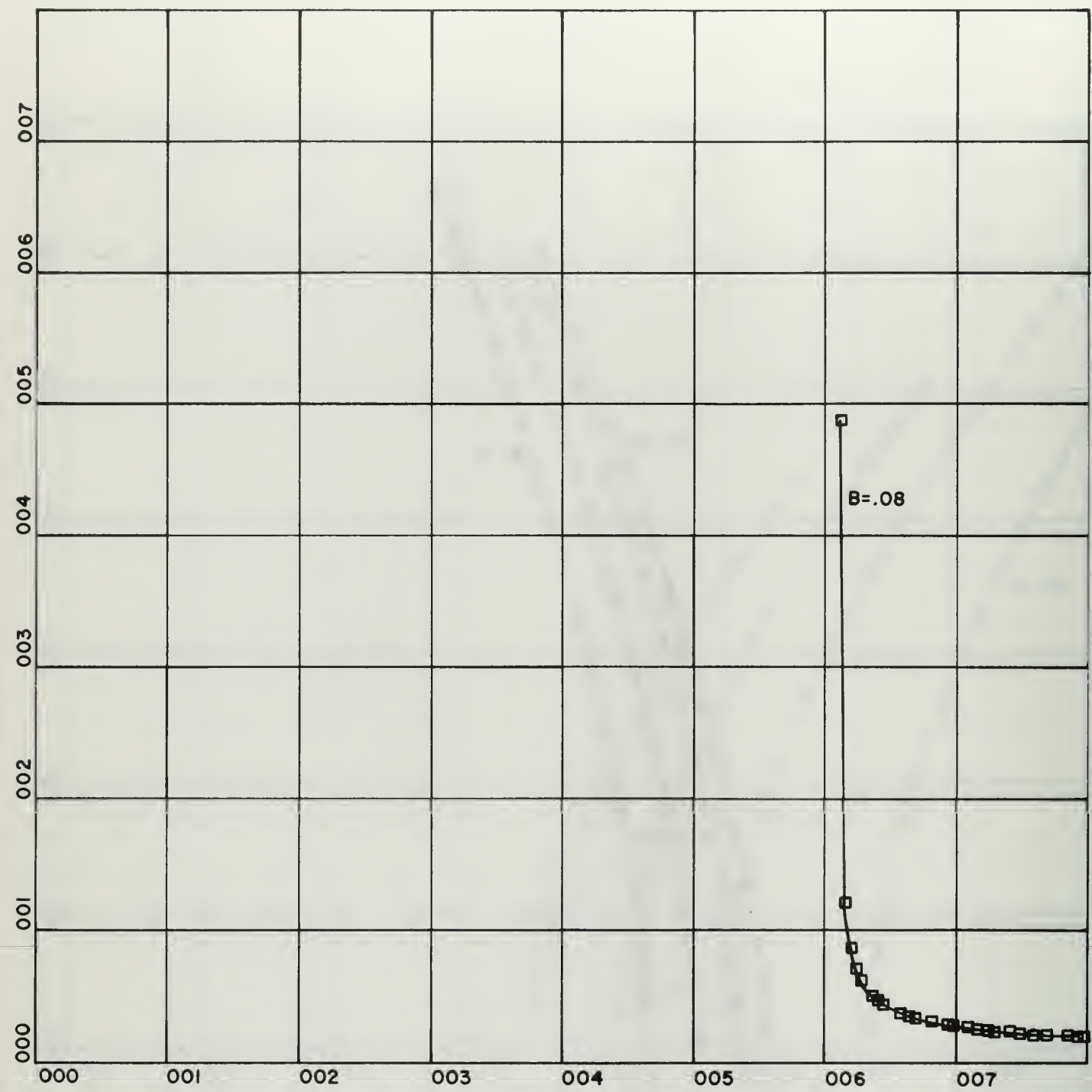X-SCALE= 1.00E+00 UNITS/INCH.
Y-SCALE= 1.00E+00 UNITS/INCH.

PROPAGATION CONSTANT VS FREQUENCY

52
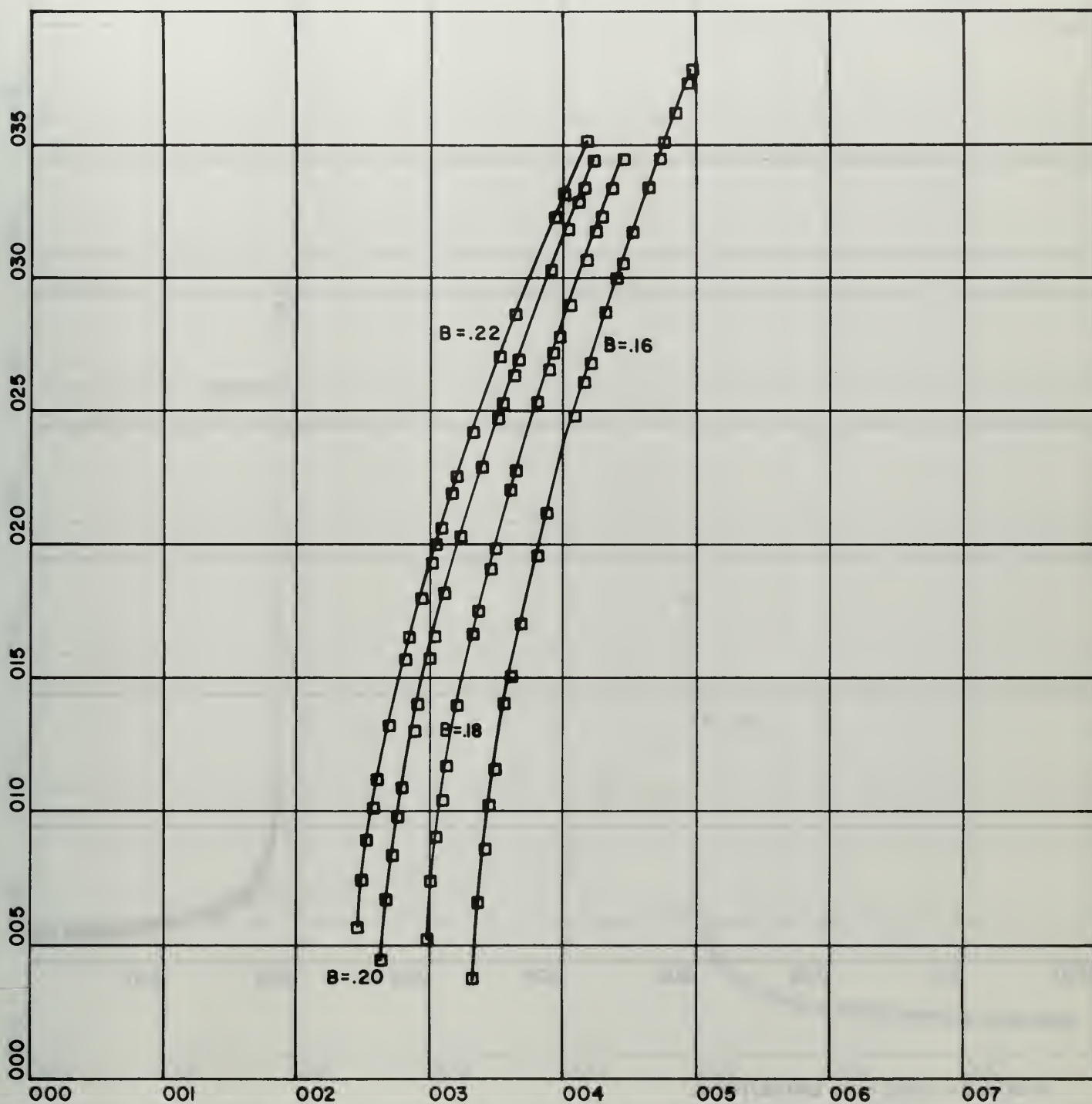
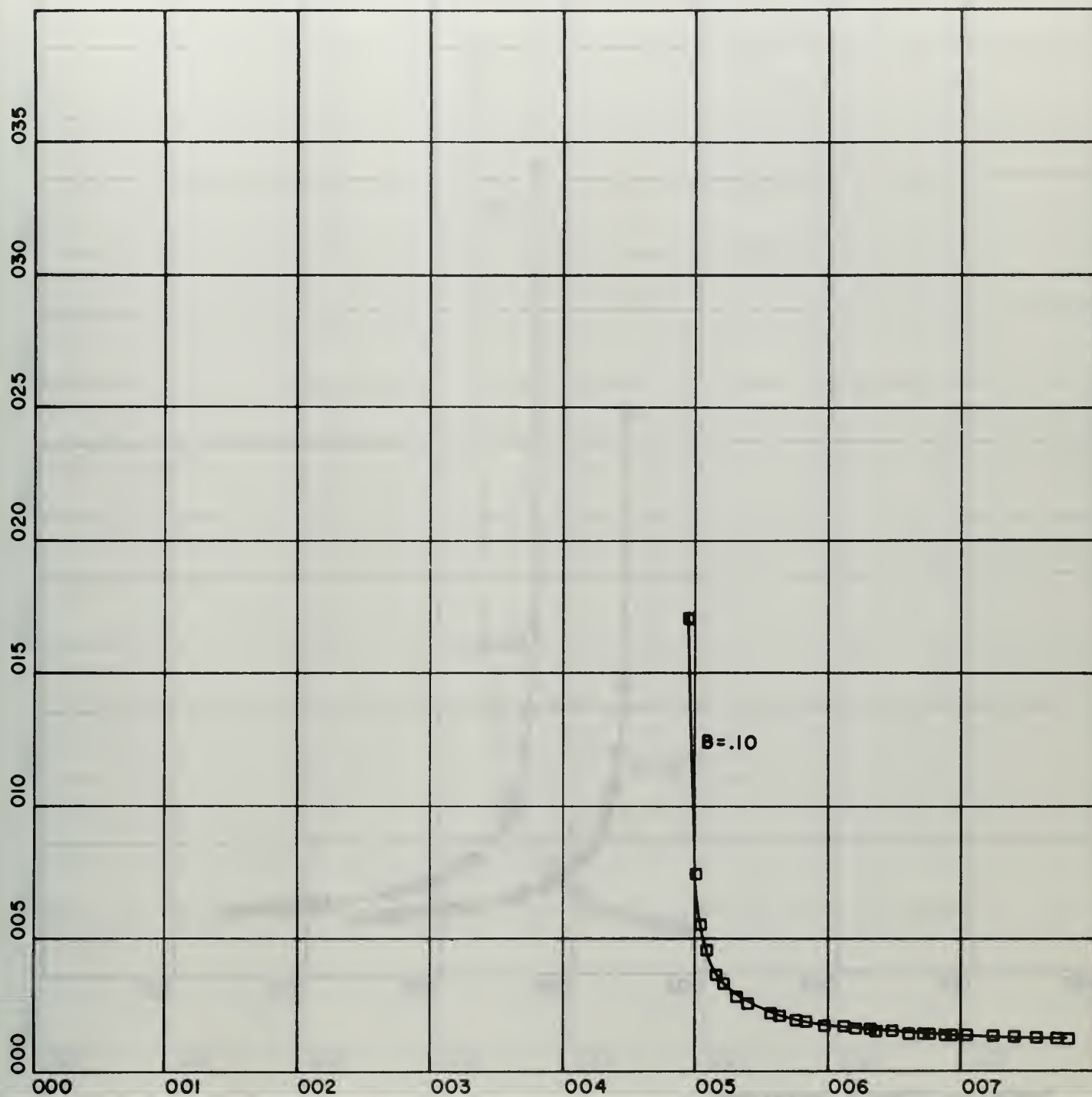X-SCALE=1.00E+00 UNITS/INCH.
Y-SCALE=5.00E-01 UNITS/INCH.

PROPAGATION CONSTANT VS FREQUENCY

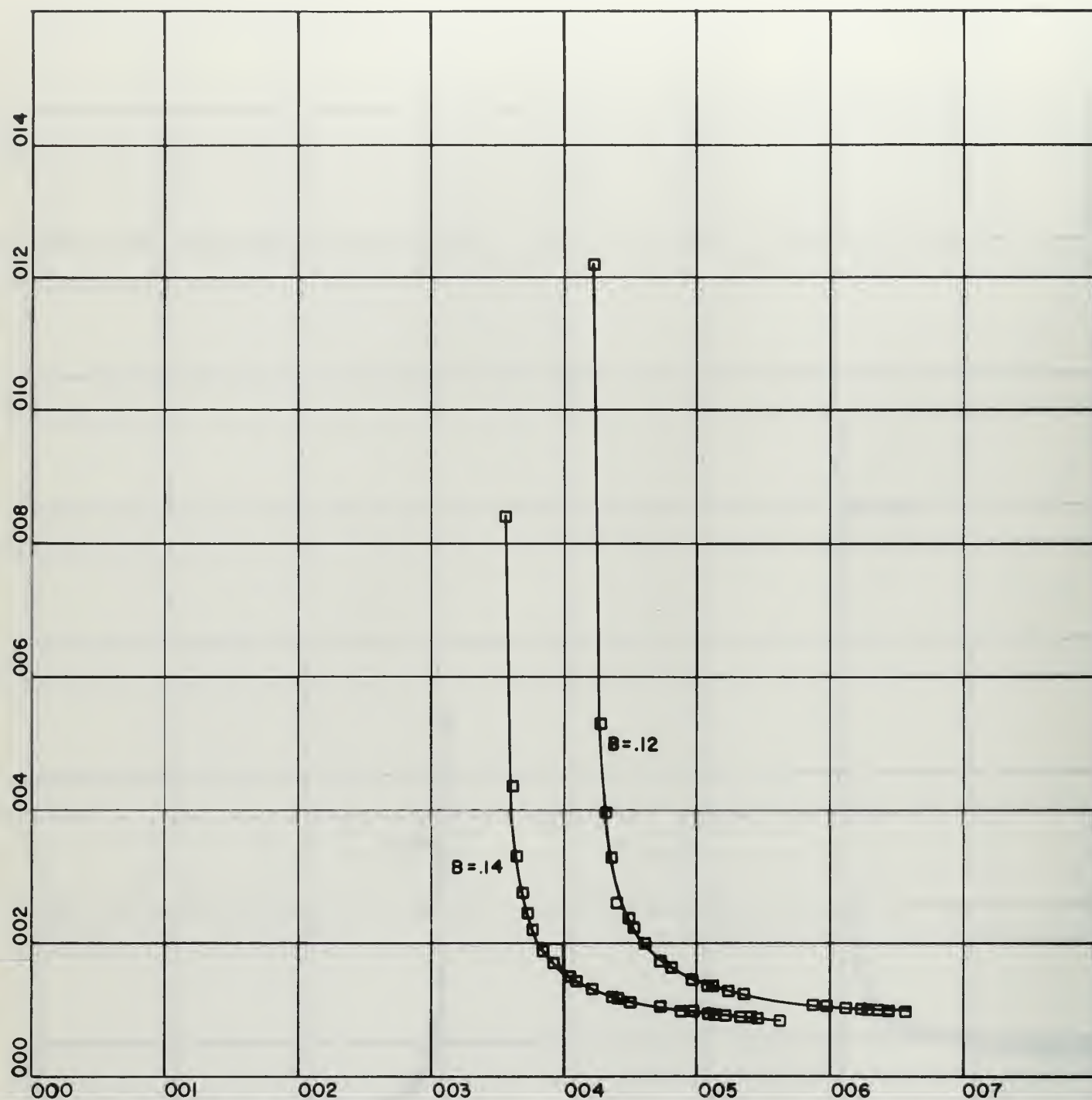X-SCALE= 1.00E+00 UNITS/INCH.
Y-SCALE= 1.00E-02 UNITS/INCH.
ATTENUATION CONSTANT VS FREQUENCY

B=.10

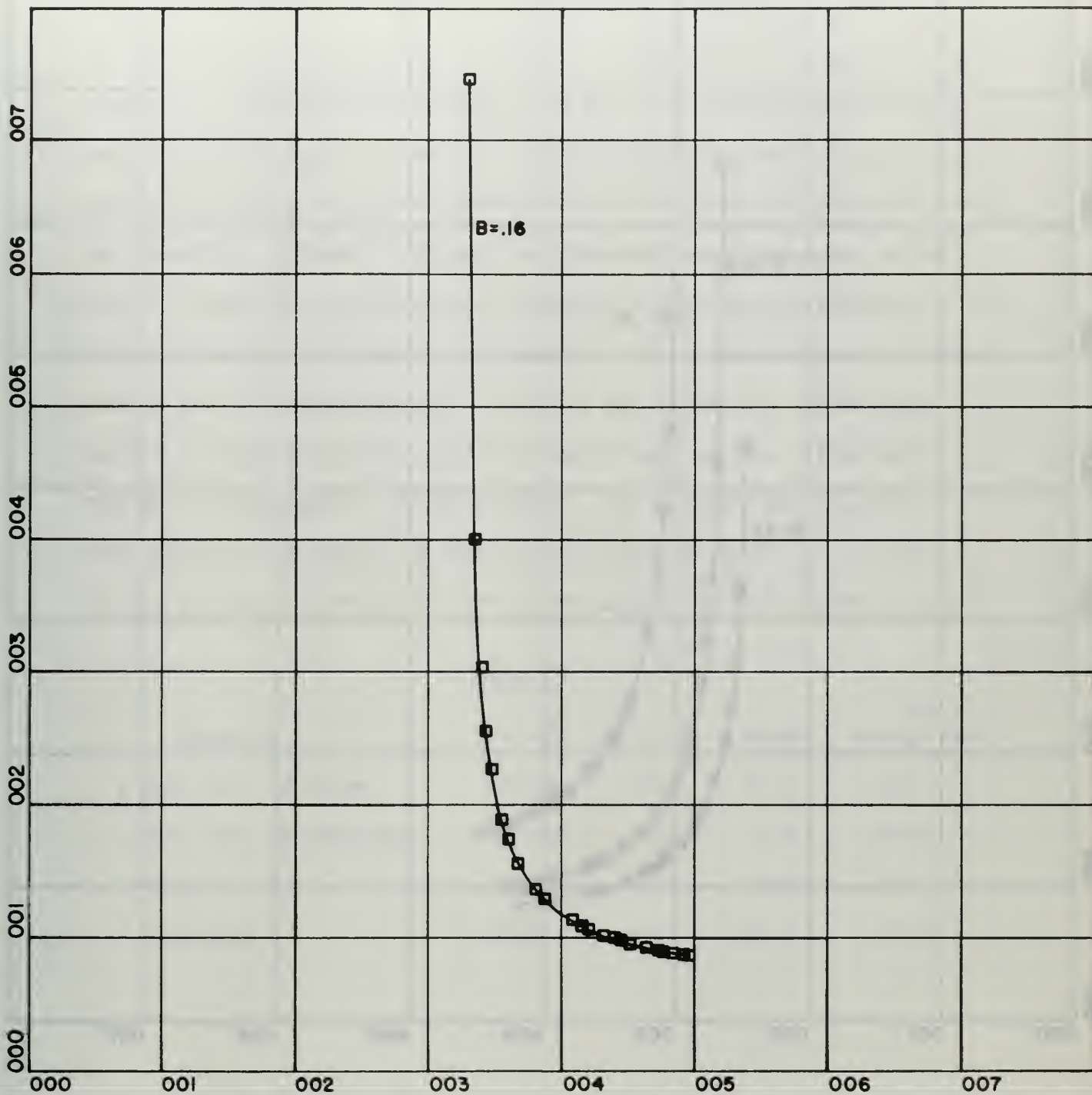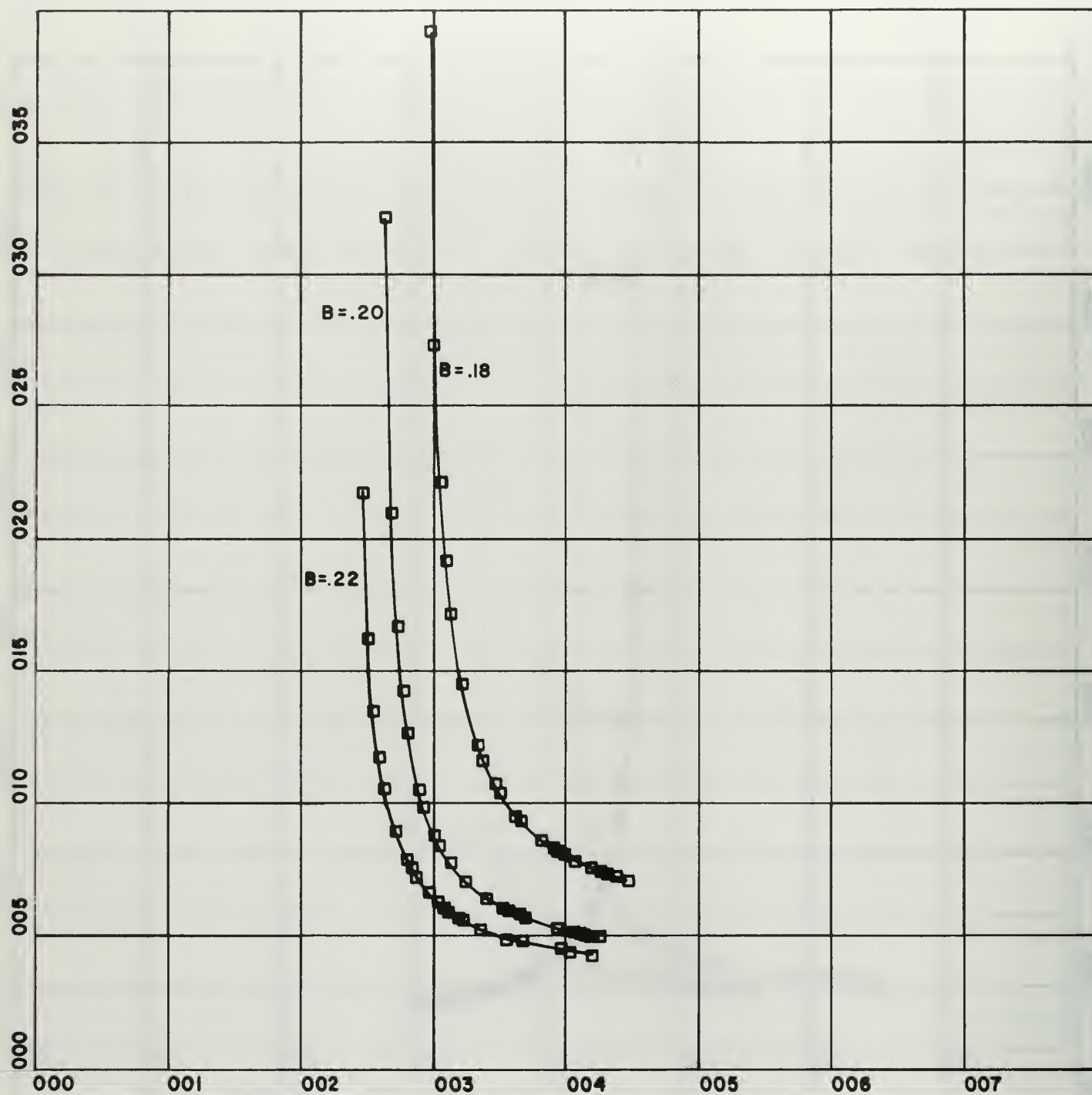X-SCALE = 1.00E+00 UNITS/INCH.
Y-SCALE = 5.00E-03 UNITS/INCH.

ATTENUATION CONSTANT VS FREQUENCY

B=.12

B=.14

X-SCALE= 1.00E+00 UNITS/INCH.
Y-SCALE= 2.00E-03 UNITS/INCH.

ATTENUATION CONSTANT VS FREQUENCY

56

B=.16

X-SCALE=1.00E+00 UNITS/INCH.
Y-SCALE=1.00E-03 UNITS/INCH.
ATTENUATION CONSTANT VS FREQUENCY

B=.20

B=.18

B=.22

X-SCALE= 1.00E+00 UNITS/INCH.
Y-SCALE= 5.00E-04 UNITS/INCH.

ATTENUATION CONSTANT VS FREQUENCY

The following 4 curves present the behavior of $\eta$ (the dimensionless drift velocity) and $\sigma$ (the dimensionless ion thermal speed) plus the non-normalized parameters W and C as functions of the magnetic field strength. Independent measurement of W was made at 1000 gauss by studying parallel propagation, and the results of the data reduction for that set of dispersion data gave a value within 12% of that obtained from the anti-parallel analysis. This will be discussed more thoroughly in Section 5. However, no theories are presented to explain the behavior of either parameter. A program was prepared to fit a least squares straight line to the deduced parameters as a first approximation. These lines are the continuous curves, and the squares represent the fitted parameters for each magnetic field strength. The standard deviations of both slope and intercept for these plots appear in Table 1. The units of each of the non-normalized quantities appear on the individual curves.
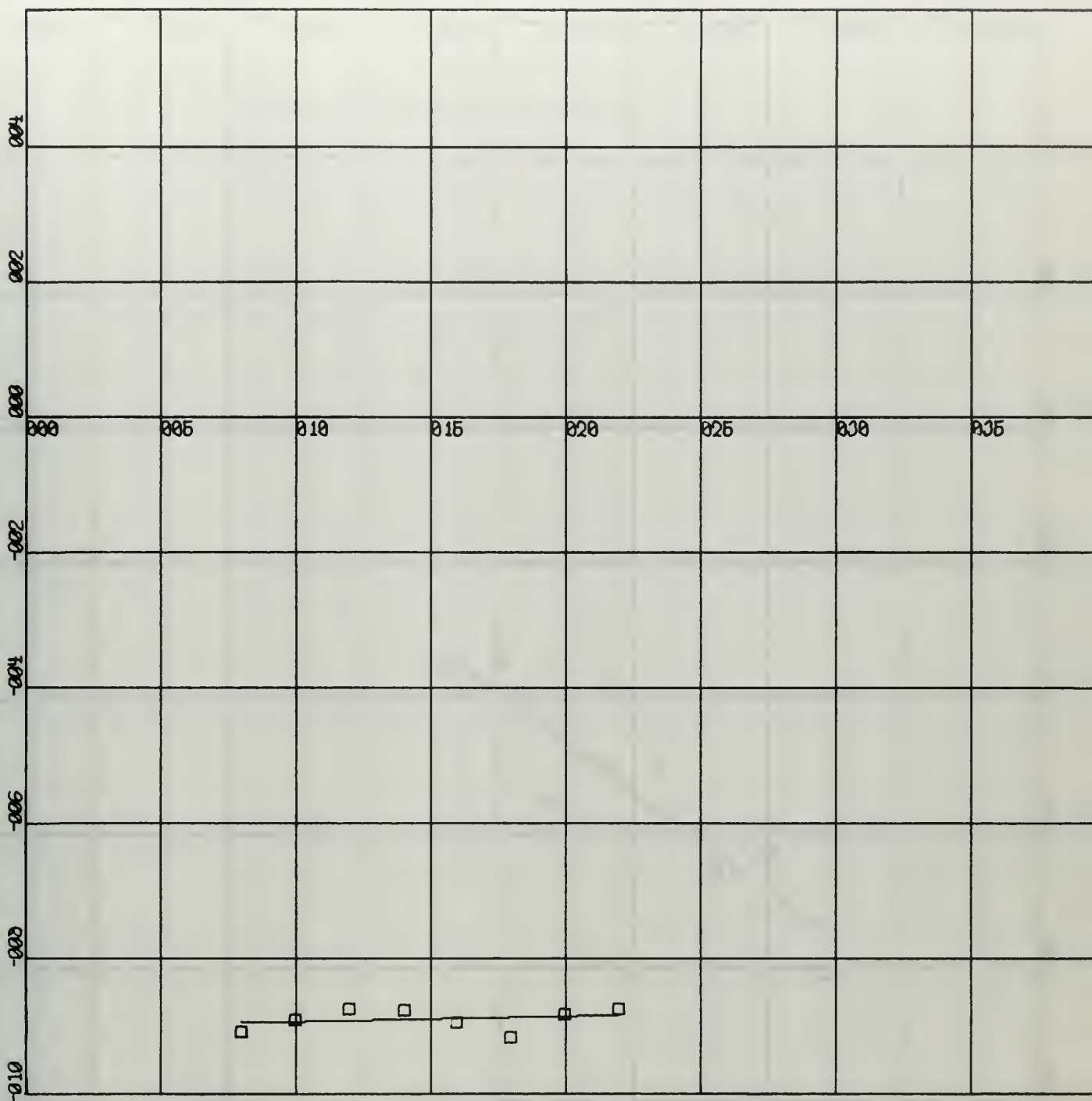
### Table 1

| Quantity | $\eta = \dfrac{W}{c}$ | $\sigma = \dfrac{C}{c}$ | W(m/s) | ion energy (ev) |
|---|---|---|---|---|
| std. dev. of slope | .00168 | .0741 | 12.2 | .120 |
| std. dev. of intercept | .000264 | .0116 | 1.9 | .0188 |
| slope | .00109 | .415 | 7.92 | .727 |
| intercept | -.0124 | .0614 | -90.0 | .00635 |
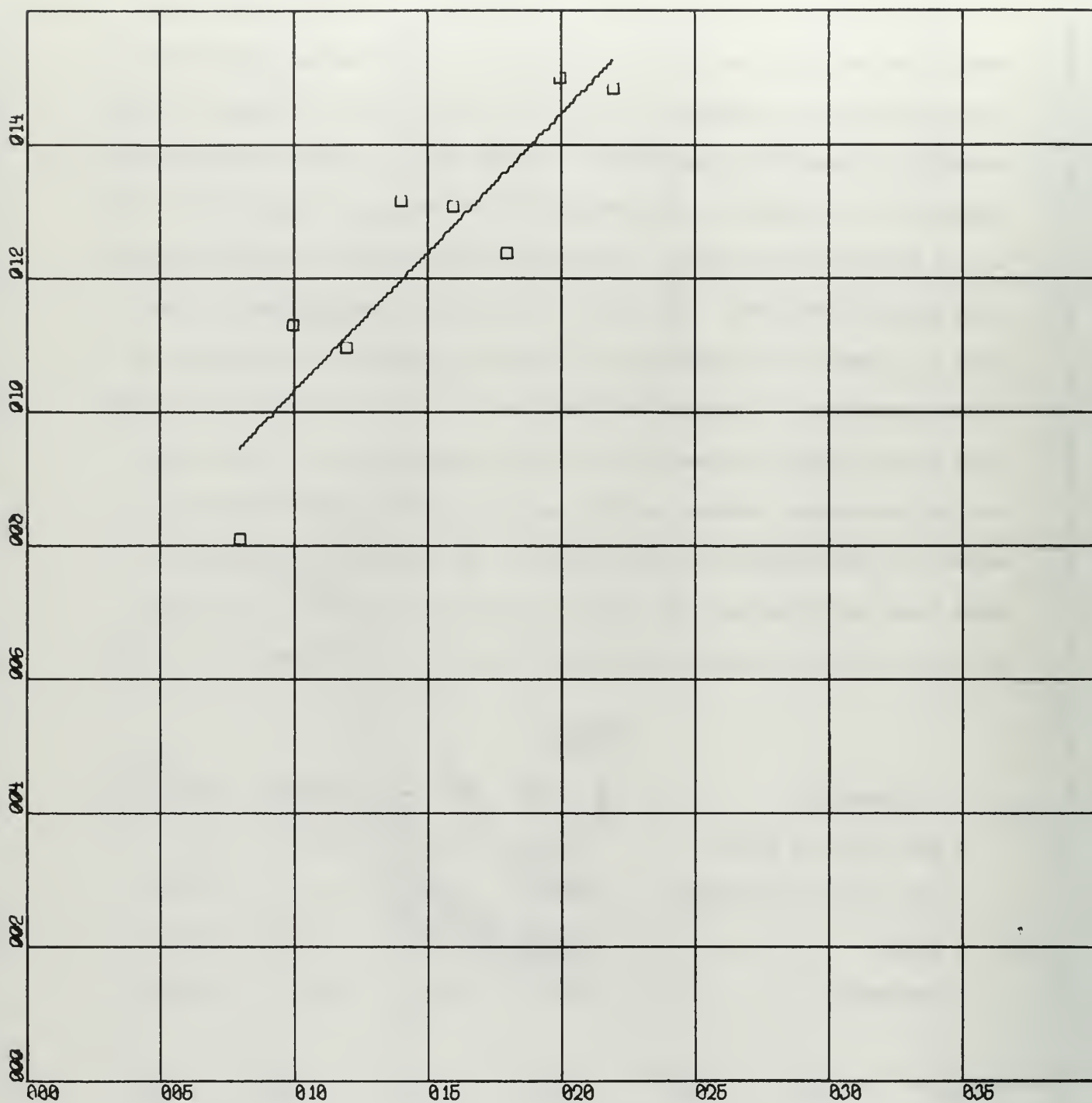
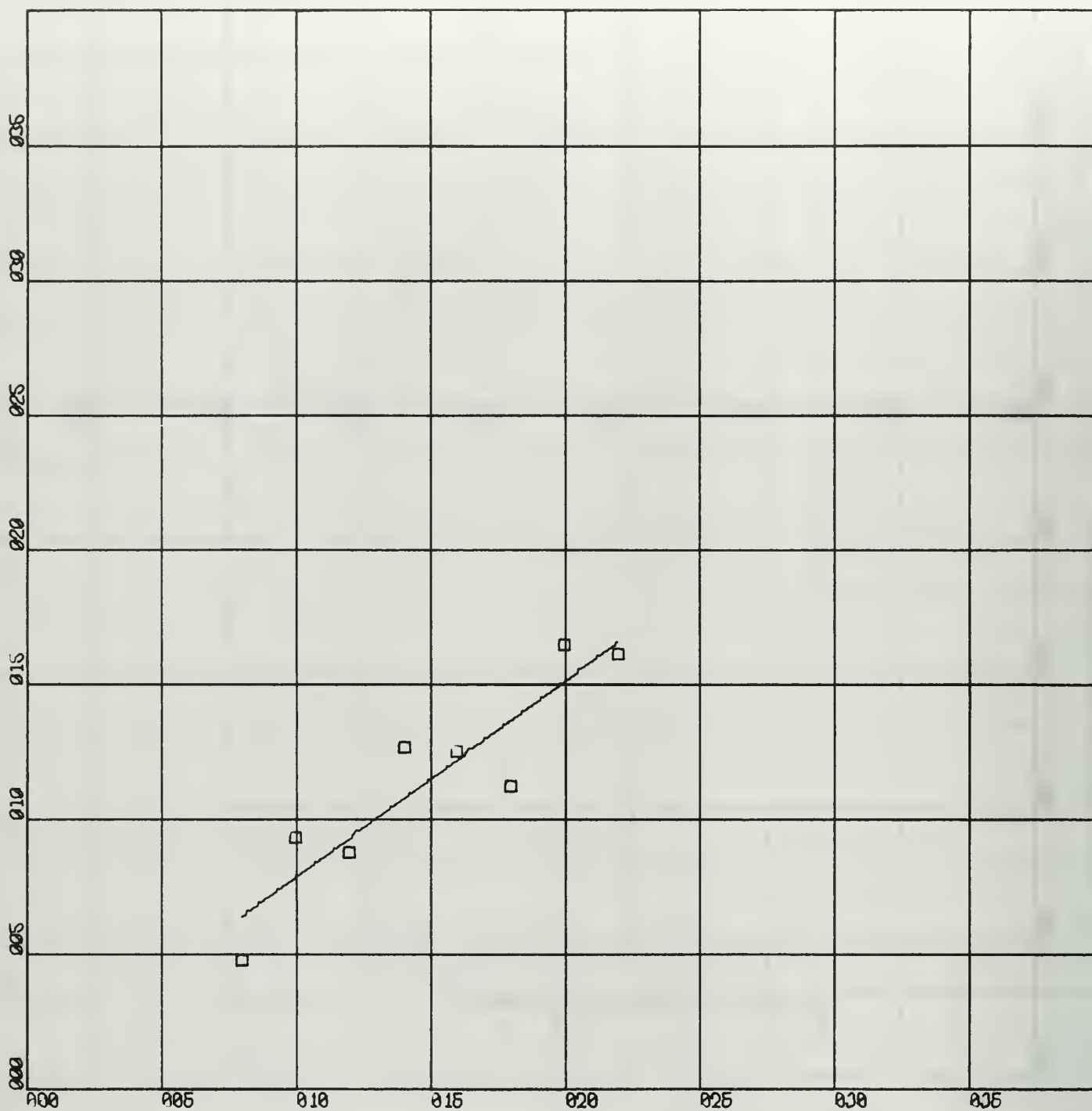Y-SCALE = 5.00E-02 UNITS/INCH.
Y-SCALE = 2.00E-02 UNITS/INCH.
SIGMA U STATIC MAGNETIC FIELD (WEBR/SQ MET)

X-SCALE = 5.00E-02 UNITS/INCH.
Y-SCALE = 2.00E+01 UNITS/INCH.
ION DRIFT VELOCITY (MET/SEC) V
STATIC MAGNETIC FIELD (WEB/SQ MET)
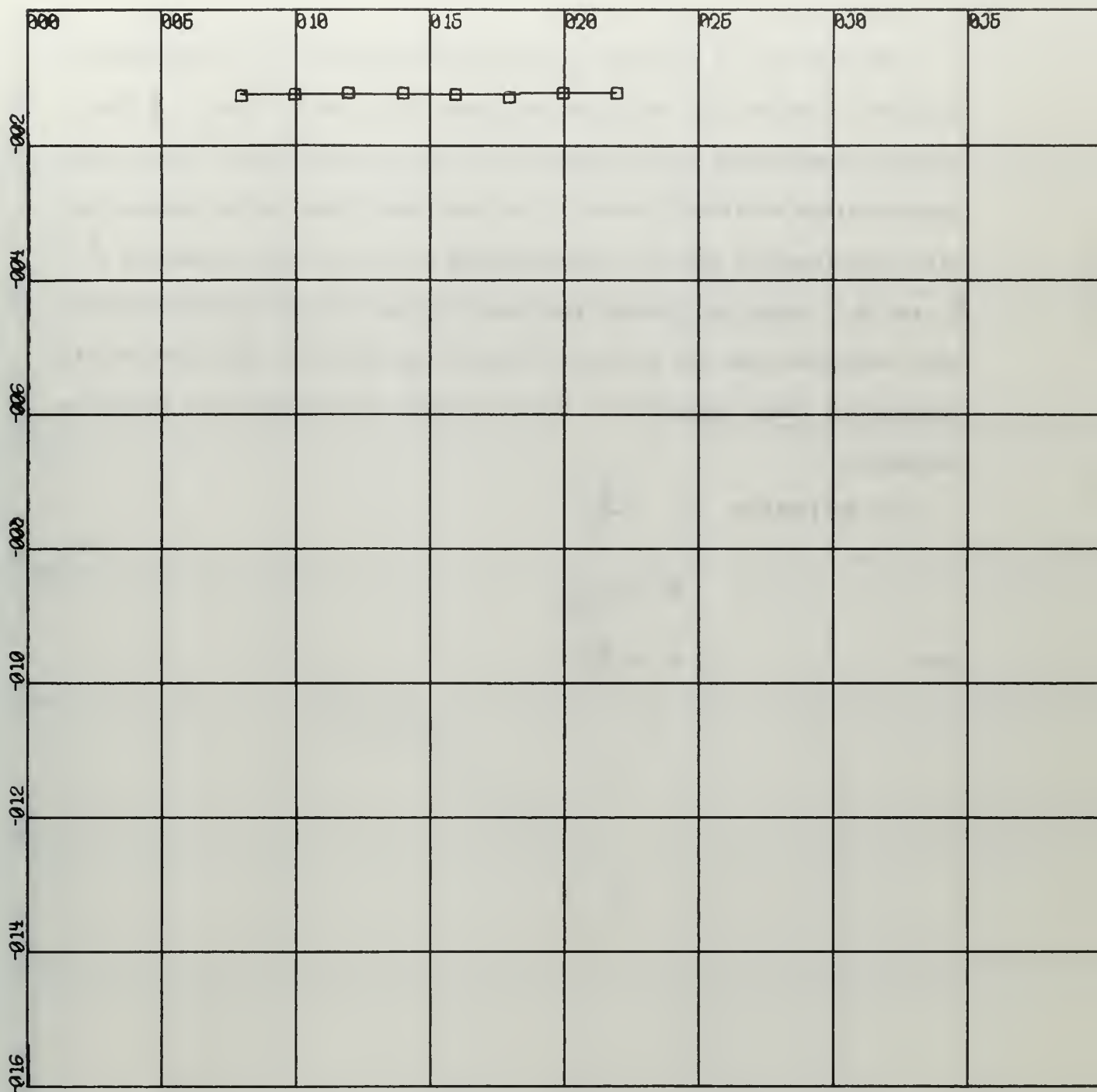
X-SCALE = 5.00E-02 UNITS/INCH.
Y-SCALE = 5.00E-02 UNITS/INCH.
ION THERMAL ENERGY (EV) V
STATIC MAGNETIC FIELD (WEB/SQ MET)

62

X-SCALE = 5.00E-02 UNITS/INCH.
Y-SCALE = 2.00E-02 UNITS/INCH.

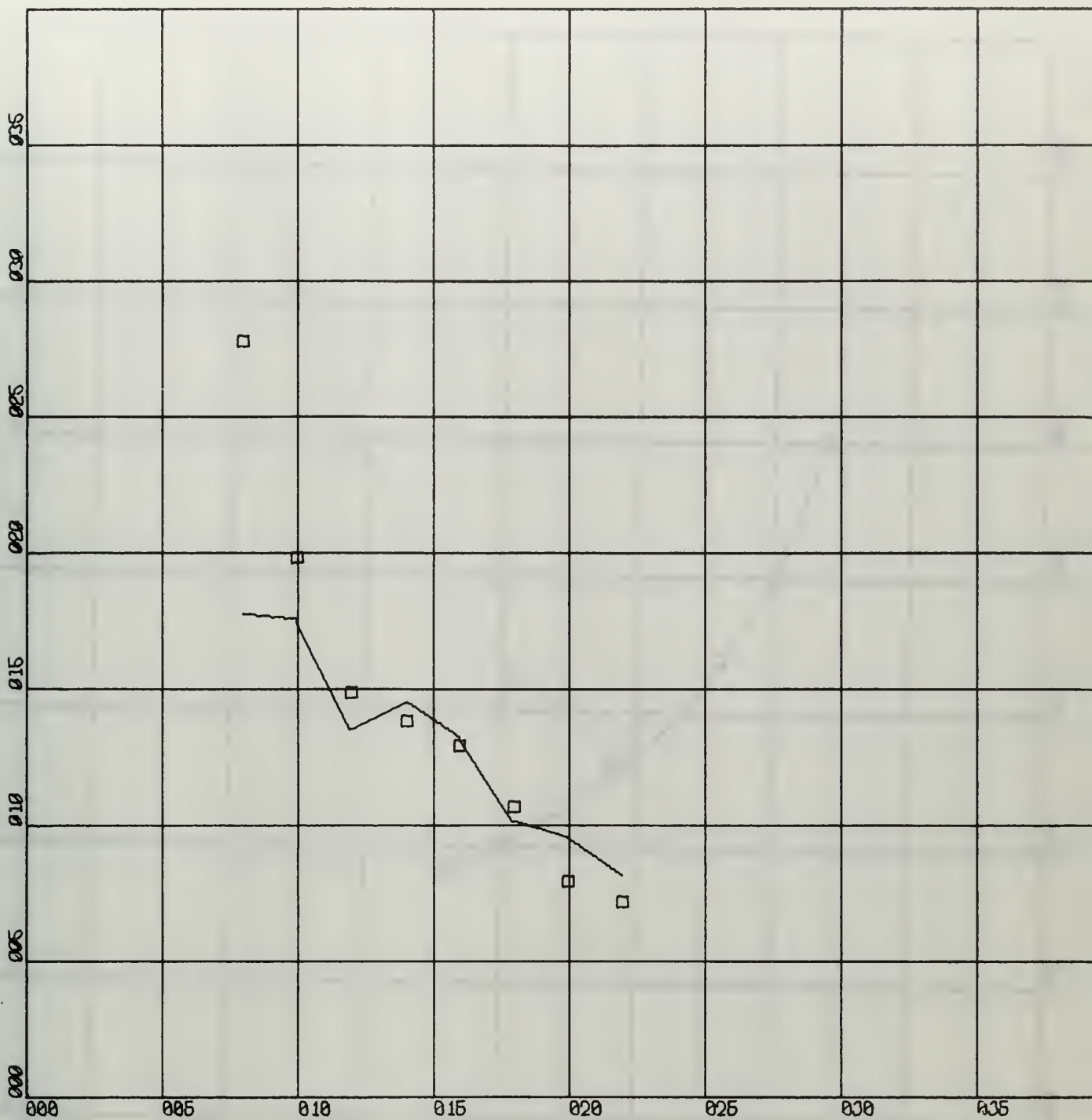ETA V STATIC MAGNETIC FIELD (WEB/SQ MET)   63

The next set of 6 curves represents the behavior of $\mathcal{J}$ (the dimensionless effective ion collision frequency for momentum loss), $\mathcal{E}$ (the dimensionless radial cutoff distance for the perturbations), and $\epsilon$ (the dimensionless e-folding parameter for the unperturbed radial plasma density distribution) plus the corresponding non-normalized parameters $\nu$, $\ell$, and $\delta$. Again the squares represent the data points deduced from the data reduction, and the continuous curves represent the theories for the behavior of these parameters. These theories are presented in detail in Section 5.

By definition

$$\mathcal{J} \equiv \frac{\nu}{\Omega}$$

$$\mathcal{E} \equiv \frac{c}{\Omega \ell}$$

and

$$\epsilon \equiv \frac{\delta c}{\Omega} \quad .$$

64

X-SCALE = E.00E-02 UNITS/INCH.
Y-SCALE = 5.00E-04 UNITS/INCH.

ZETA V STATIC MAGNETIC FIELD (WEB/SQ MET)   65
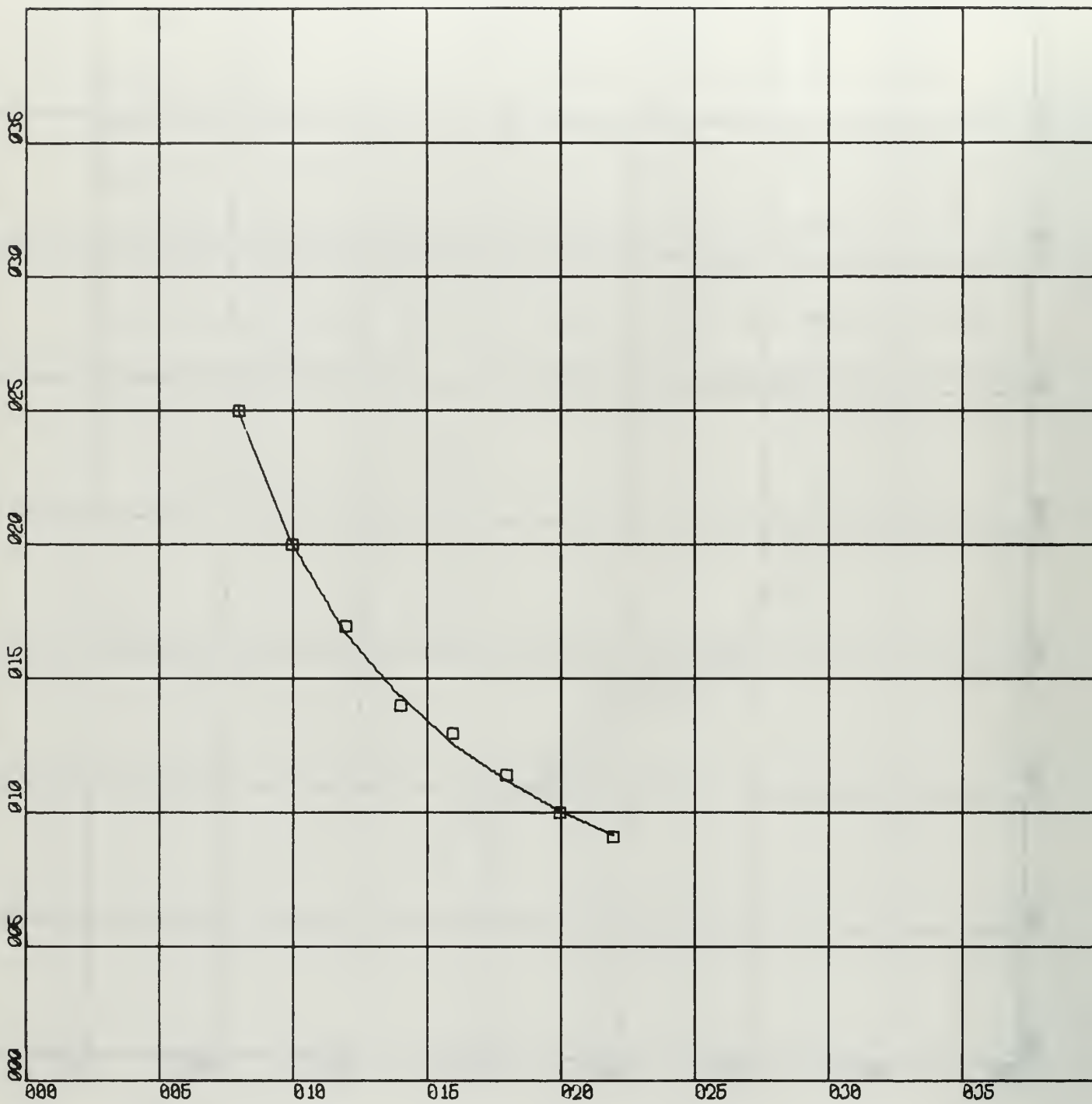
X-SCALE = 5.00E-02 UNITS/INCH.
Y-SCALE = 5.00E-01 UNITS/INCH.
XI V STATIC MAGNETIC FIELD (WEB/SQ MET)
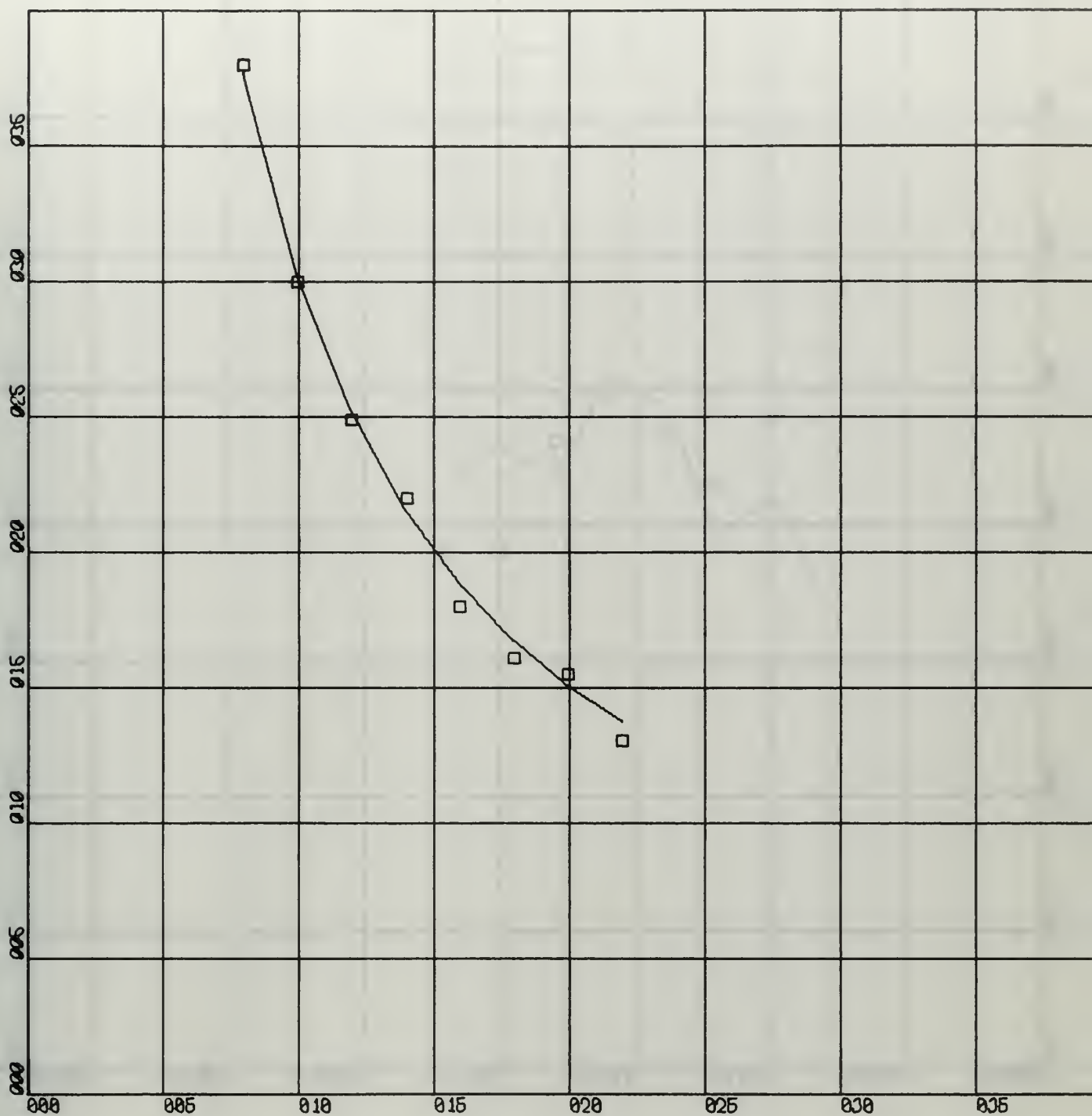
X-SCALE - 5.00E-02 UNITS/INCH.
Y-SCALE - 5.00E-01 UNITS/INCH.
EPSILON V STATIC MAGNETIC FIELD (WEB/SQ MET) 67
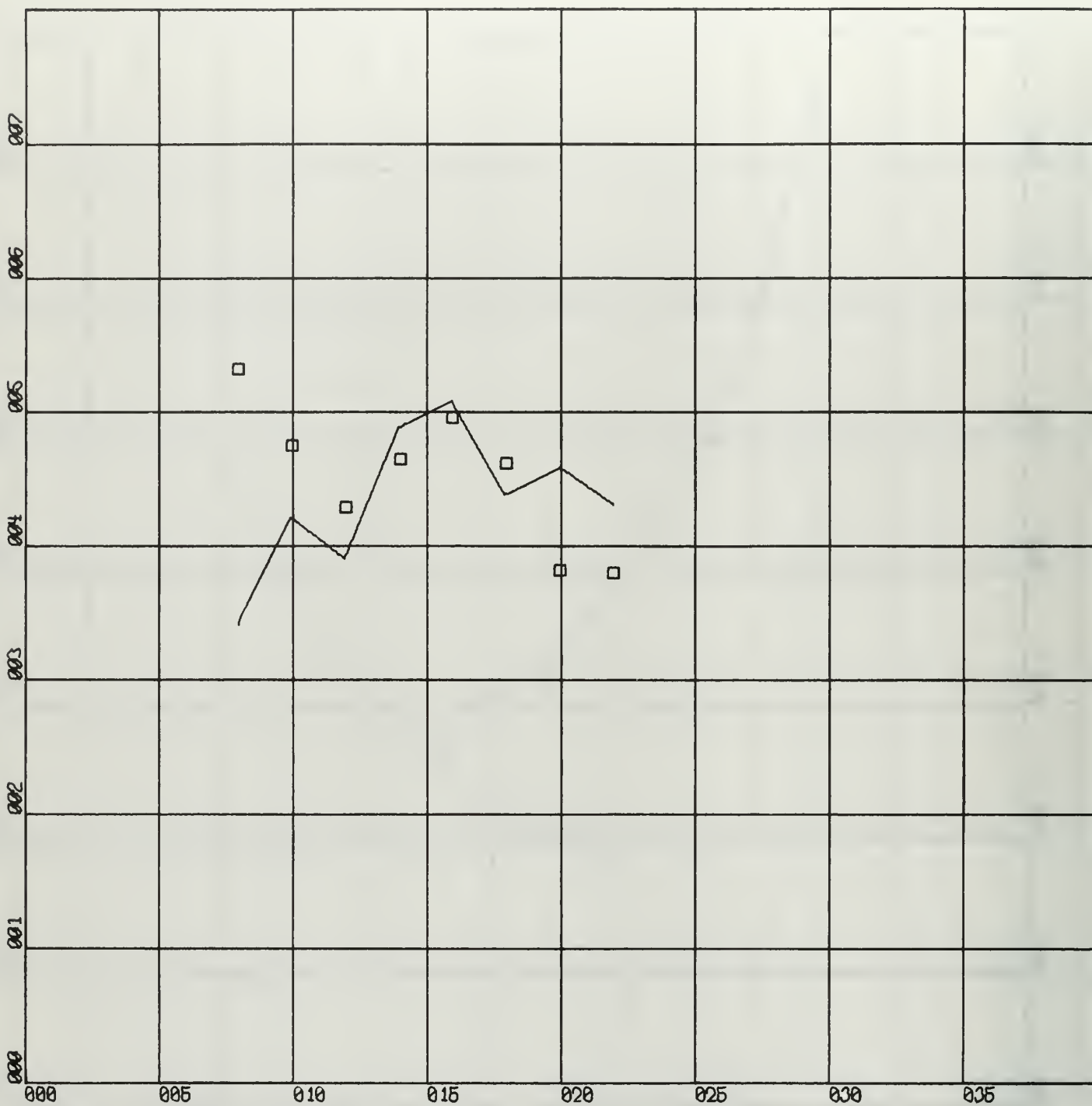
Y-SCALE = 5.00E-02 UNITS/INCH.
Y-SCALE = 1.00E+02 UNITS/INCH.
EFFECTIVE ION COLLISION FREQUENCY (PER SEC) V
STATIC MAGNETIC FIELD (WEB/SQ MET)

68
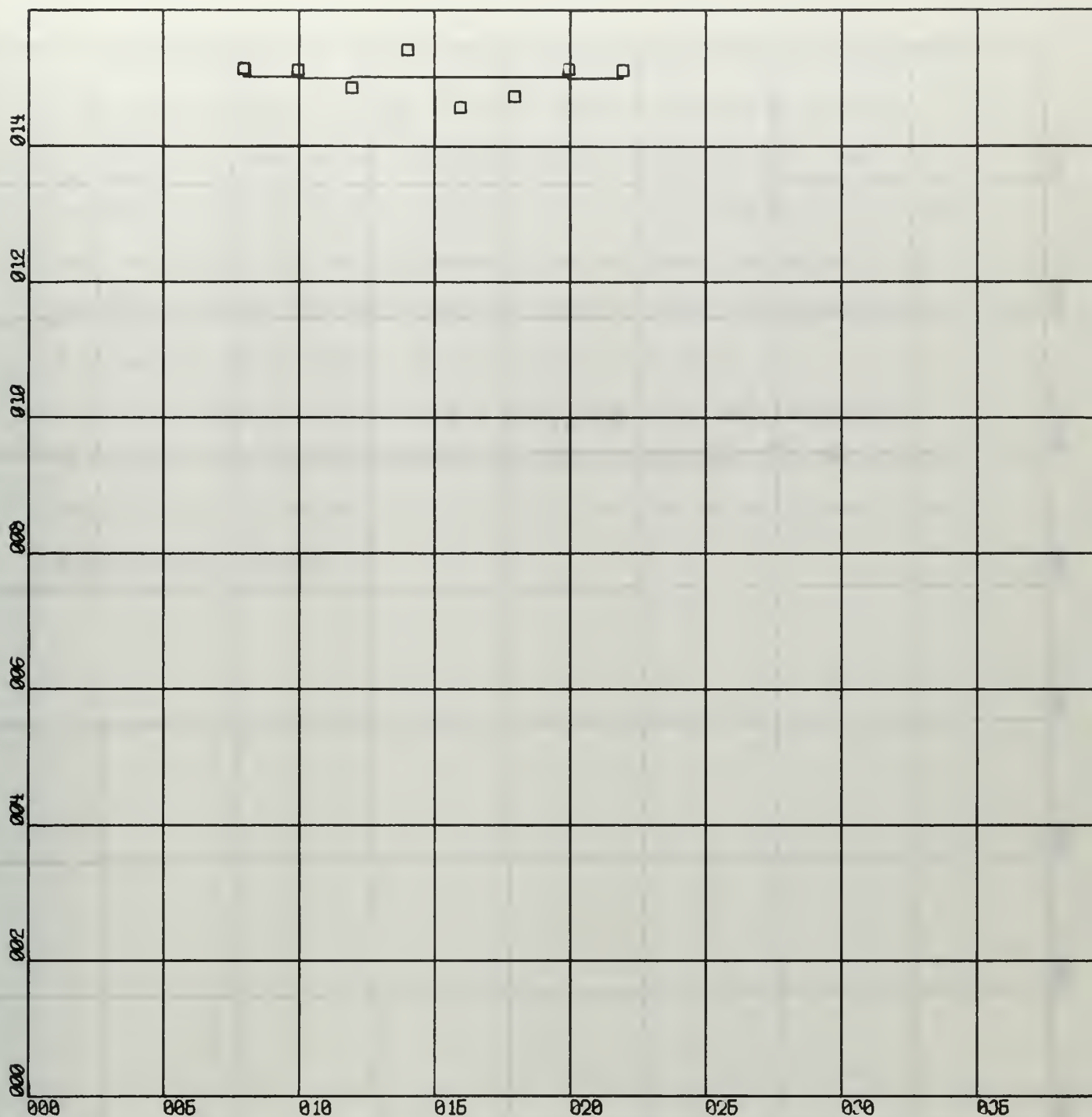
X-SCALE = 5.00E-02 UNITS/INCH.
Y-SCALE = 2.00E-03 UNITS/INCH.
RADIAL CUTOFF DISTANCE (MET) V
STATIC MAGNETIC FIELD (WEB/SQ MET)

69

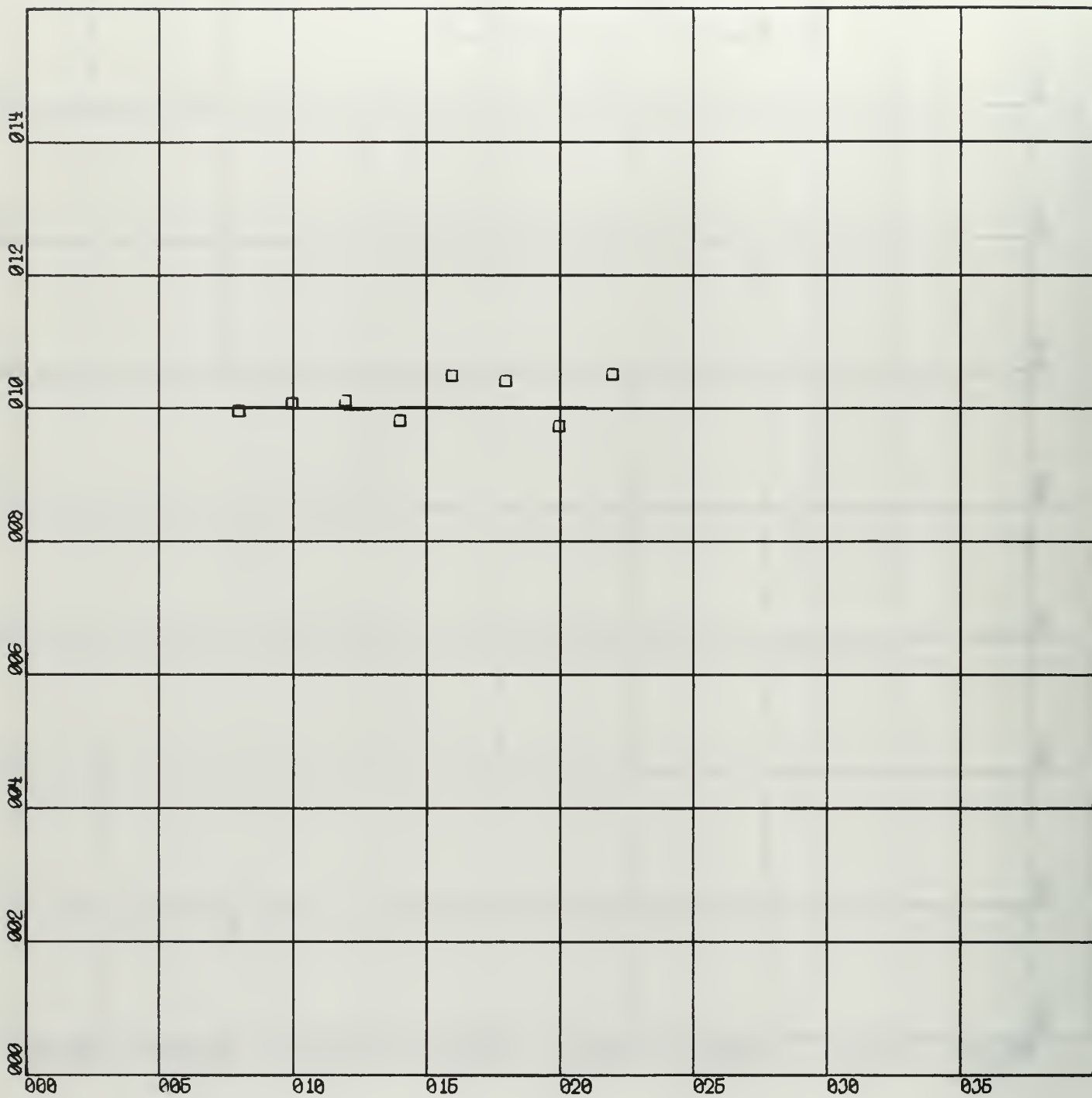X-SCALE = 5.00E-02 UNITS/INCH.
Y-SCALE = 2.00E-03 UNITS/INCH.

UNPERTURBED RADIAL E-FOLDING PROFILE DISTANCE
(MET)'V STATIC MAGNETIC FIELD (WEB/SQ MET)

The following set of curves depects the behavior of the dimension-less phase velocity, $\frac{1}{c}\frac{\omega}{k}$, and the dimensionless group velocity, $\frac{1}{c}\frac{\partial\omega}{\partial k}$, for each value of static magnetic field strength. Again the parameter is the value of $B_0$ (web/m$^2$). The squares represent the normal-ized data points and the continuous curves represent the values of $\frac{\omega}{k}$ and $\frac{\partial\omega}{\partial k}$ as taken from the dispersion relation using the values of the 5 parameters appropriate to the particular value of $B_0$.

The modulation feature of the TAB-7 transmitter was inoperative, so no group velocity measurements were made, and there is no data with which to test the theory. For this reason no data points appear on the group velocity curves.

B=.08
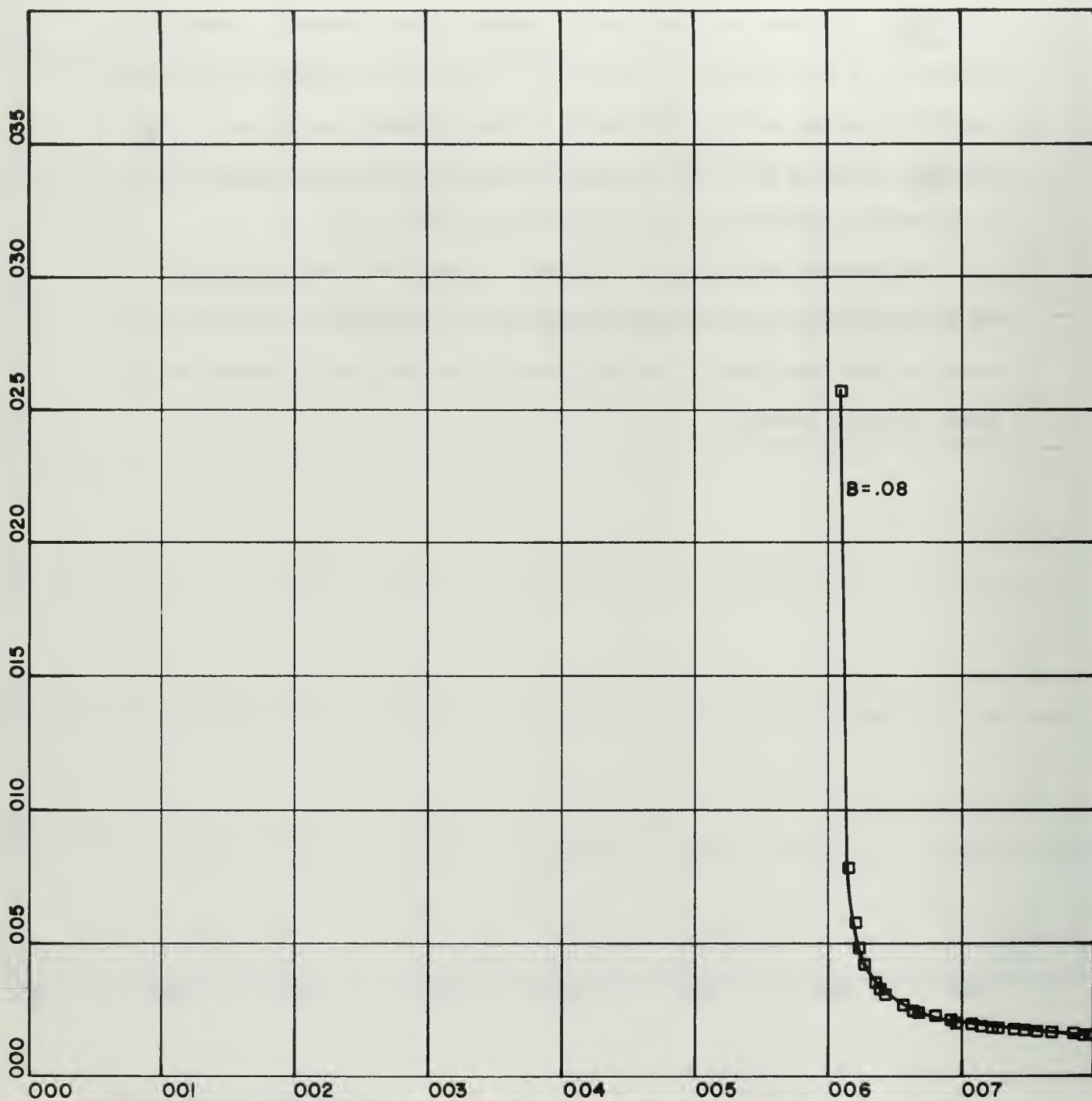
X-SCALE= 1.00E+00 UNITS/INCH.
Y-SCALE= 5.00E+00 UNITS/INCH.

PHASE VELOCITY VS FREQUENCY
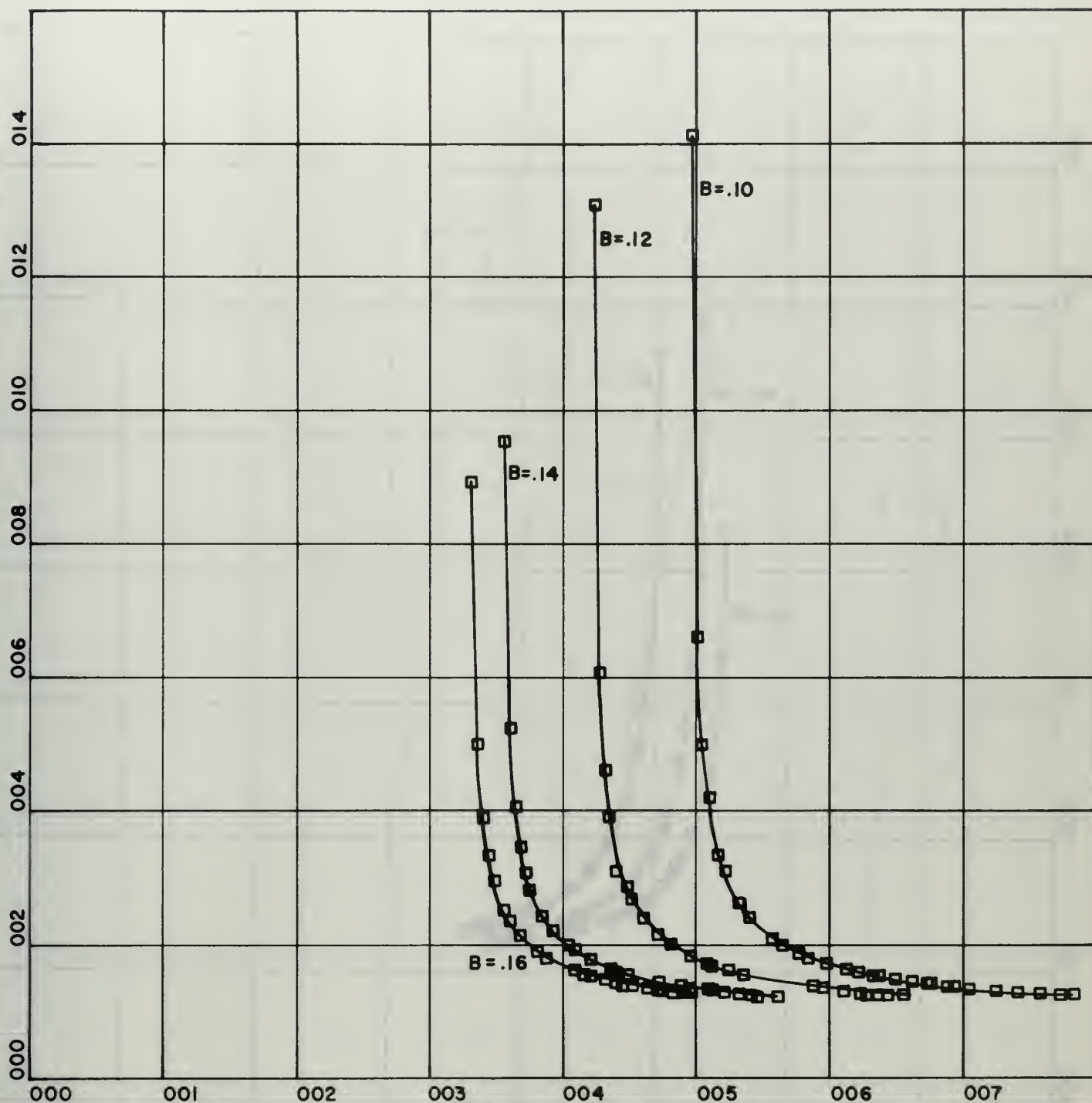
72

X-SCALE= 1.00E+00 UNITS/INCH.
Y-SCALE= 2.00E+00 UNITS/INCH.

PHASE VELOCITY VS FREQUENCY

B = .20

B=.16

B =.12

B =.08
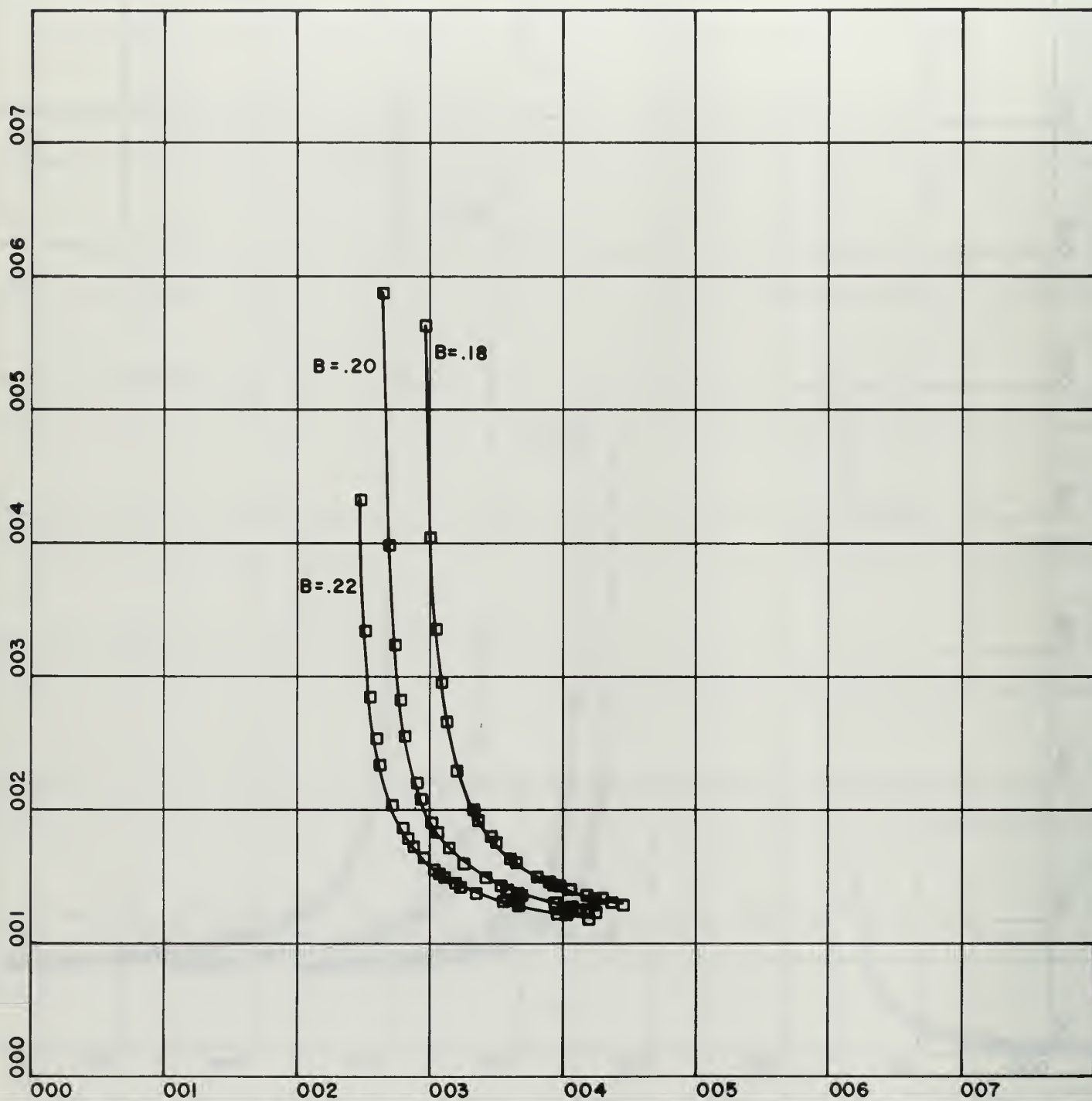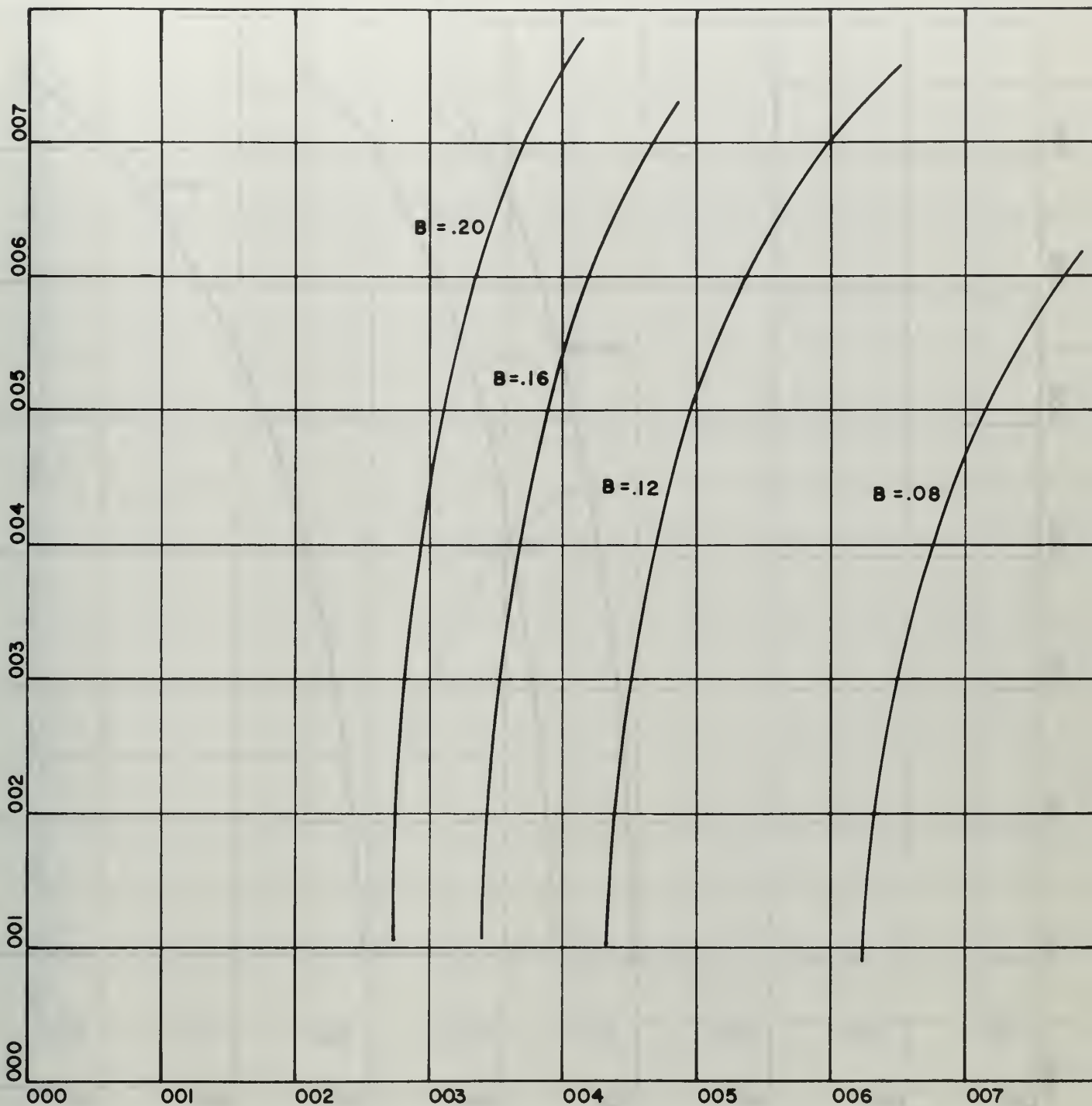
X-SCALE= 1.00E+00 UNITS/INCH.
Y-SCALE= 1.00E-01 UNITS/INCH.

GROUP VELOCITY VS FREQUENCY

X-SCALE= 1.00E+00 UNITS/INCH.
Y-SCALE= 1.00E-01 UNITS/INCH.

GROUP VELOCITY VS FREQUENCY

B = .22

X-SCALE= 1.00E+00 UNITS/INCH.
Y-SCALE= 2.00E-01 UNITS/INCH.

GROUP VELOCITY VS FREQUENCY

77

The last 4 curves represent the general behavior of the dispersion function throughout the first quadrant of $k$, $\omega$ space. Plots are presented for $y = \frac{\alpha c}{\Omega}$ vs. x, $z = \frac{\beta c}{\Omega}$ vs. x, $\frac{1}{c} \frac{\omega}{k}$ vs. x, and $\frac{1}{c} \frac{\partial \omega}{\partial k}$ vs. x. The 1000 gauss magnetic field setting was typical, and these plots represent the dispersion function with the 5 parameters having values appropriate to that setting. Since the 1000 gauss data points have already been presented in the previous curves, the data are omitted from these 4 curves.

The first 3 curves are for the complete quadrant, but the group velocity is depicted only for the regions in which the damping is small, that is where ion acoustic waves might be useful for communication purposes. These are also the regions where $\frac{\partial \omega}{\partial k} > 0$. In the regions of anomalous dispersion ($\frac{\partial \omega}{\partial k} < 0$) the concept of group velocity becomes vague, since it no longer necessarily represents the velocity of propagation of a signal. [18]

78

X-SCALE = 1.00E+00 UNITS/INCH.
Y-SCALE = 2.00E+00 UNITS/INCH.

PROPAGATION CONSTANT VS FREQUENCY
B=.10

79

X-SCALE = 1.00E+00 UNITS/INCH.
Y-SCALE = 2.00E+00 UNITS/INCH.
ATTENUATION CONSTANT VS FREQUENCY
B=.10

80
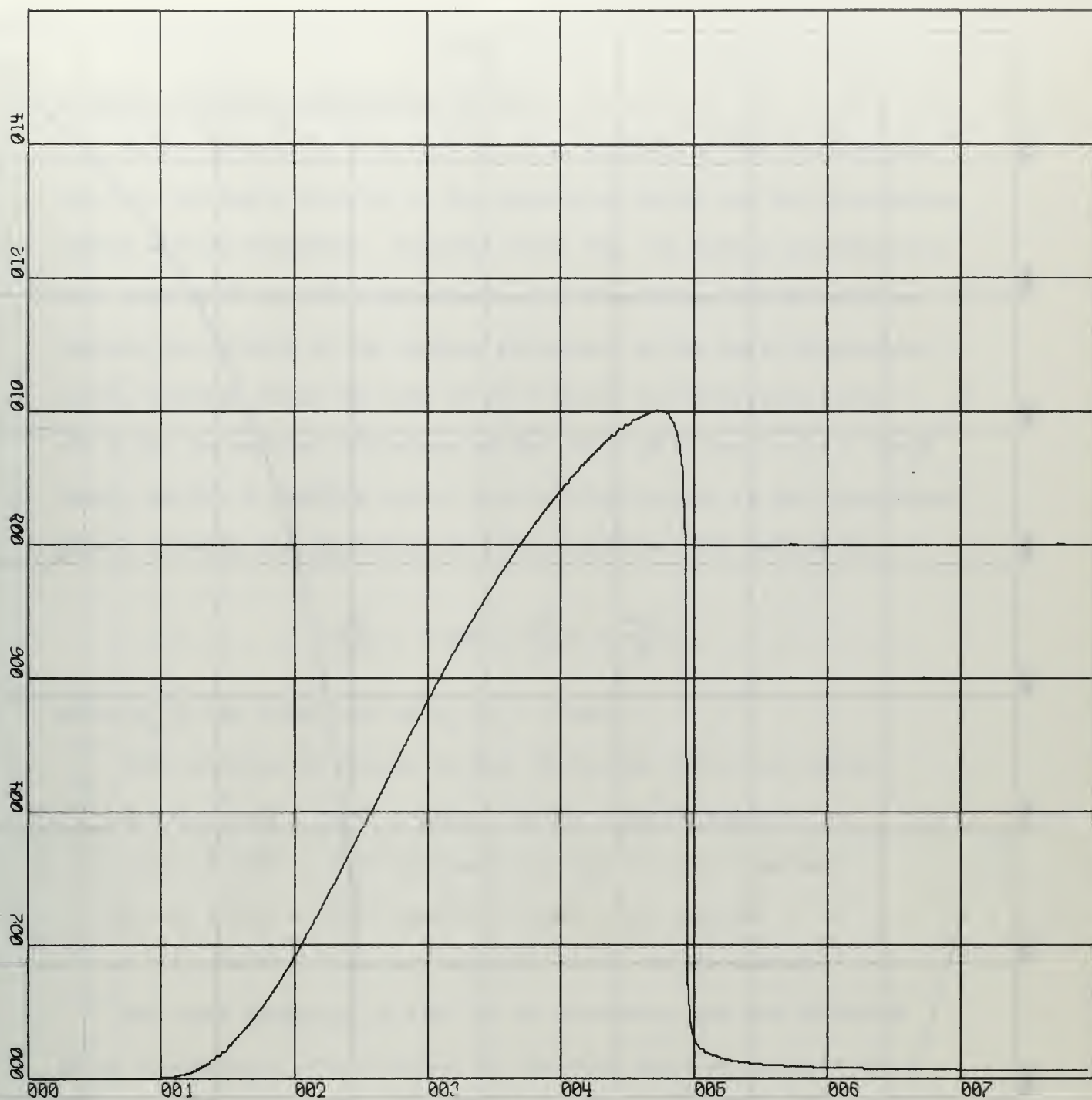
X-SCALE = 1.00E+00 UNITS/INCH.
Y-SCALE = 2.00E+01 UNITS/INCH.

PHASE VELOCITY VS FREQUENCY
B=.10
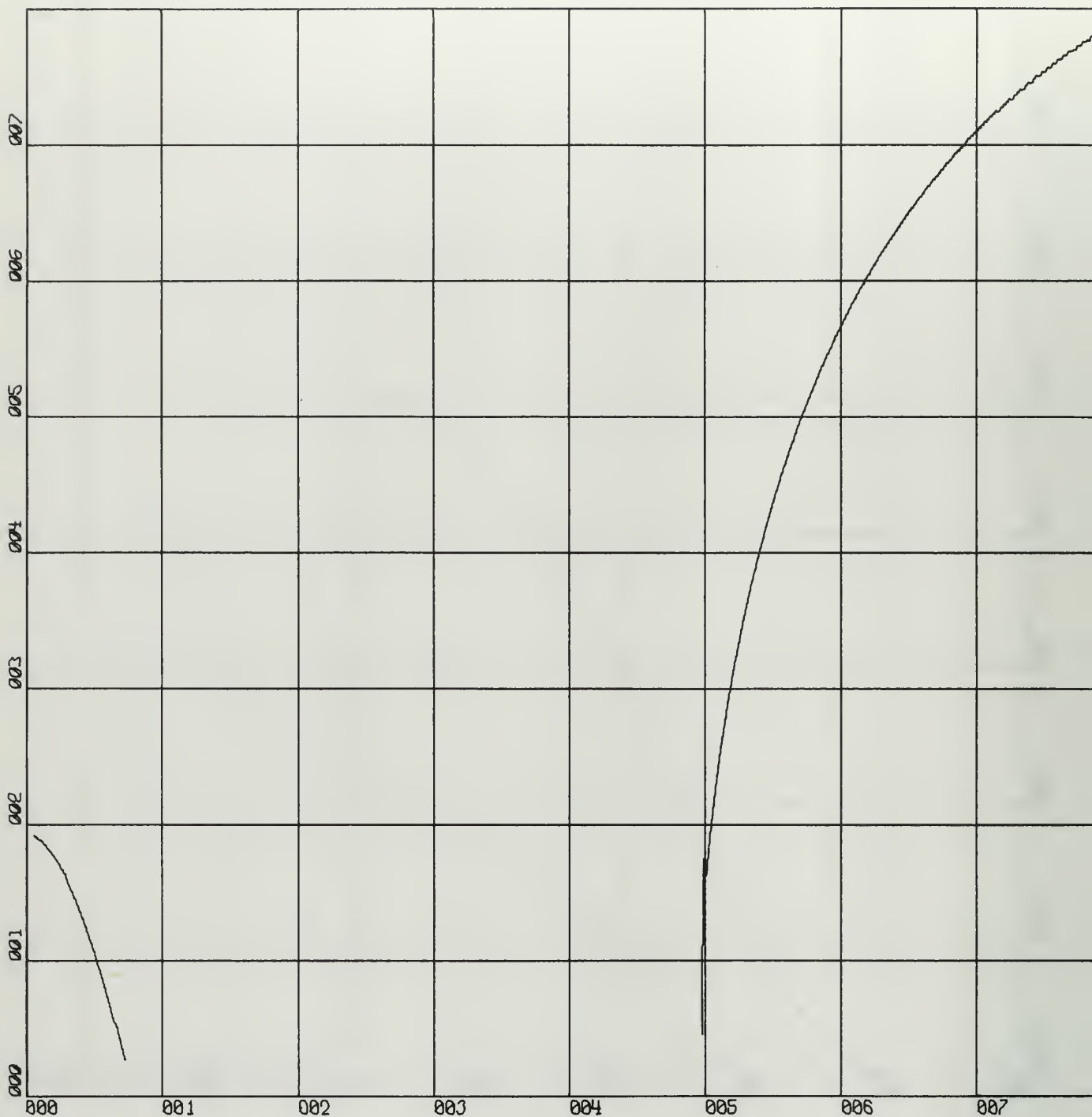
81

X-SCALE = 1.00E+00 UNITS/INCH.
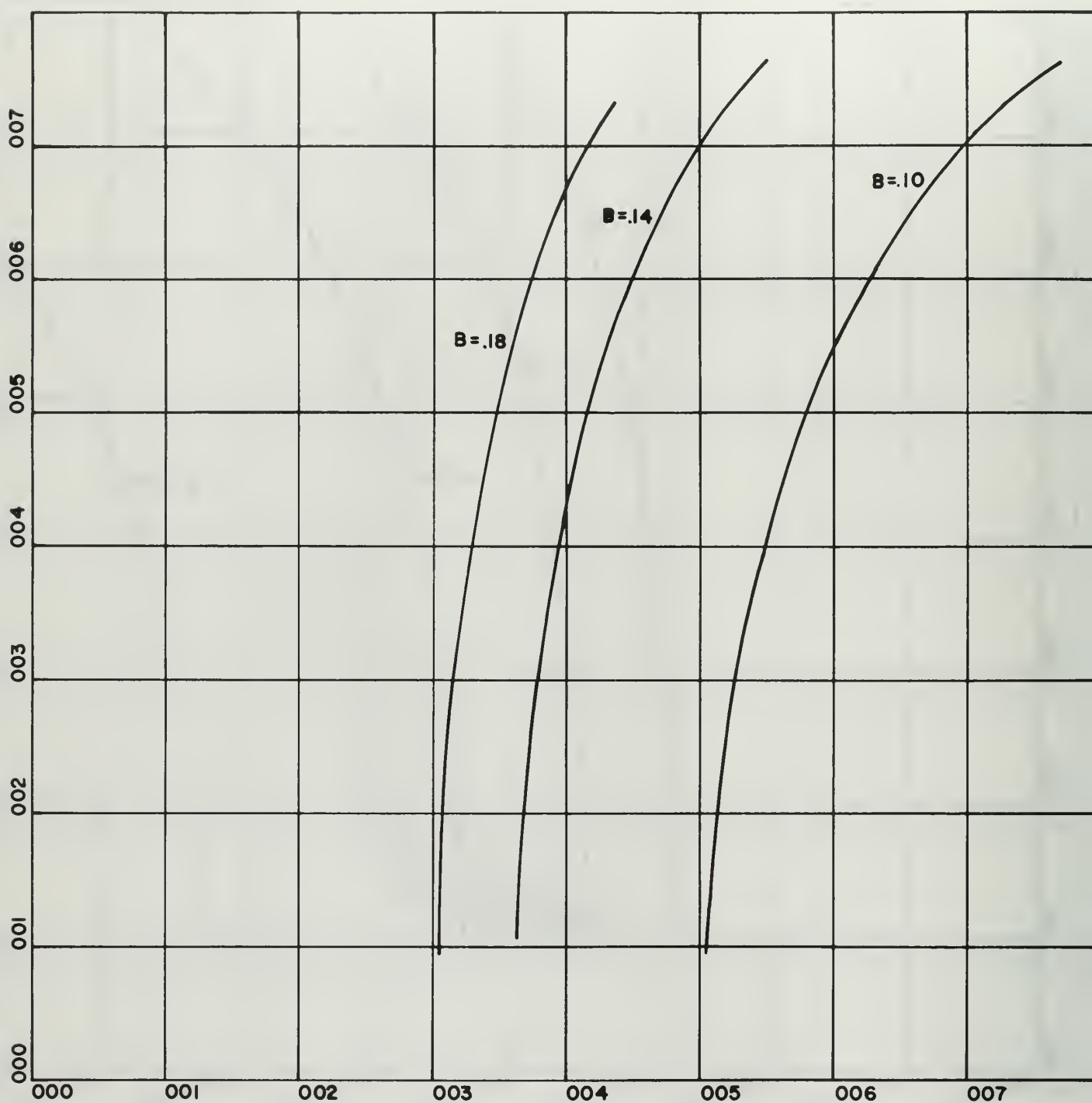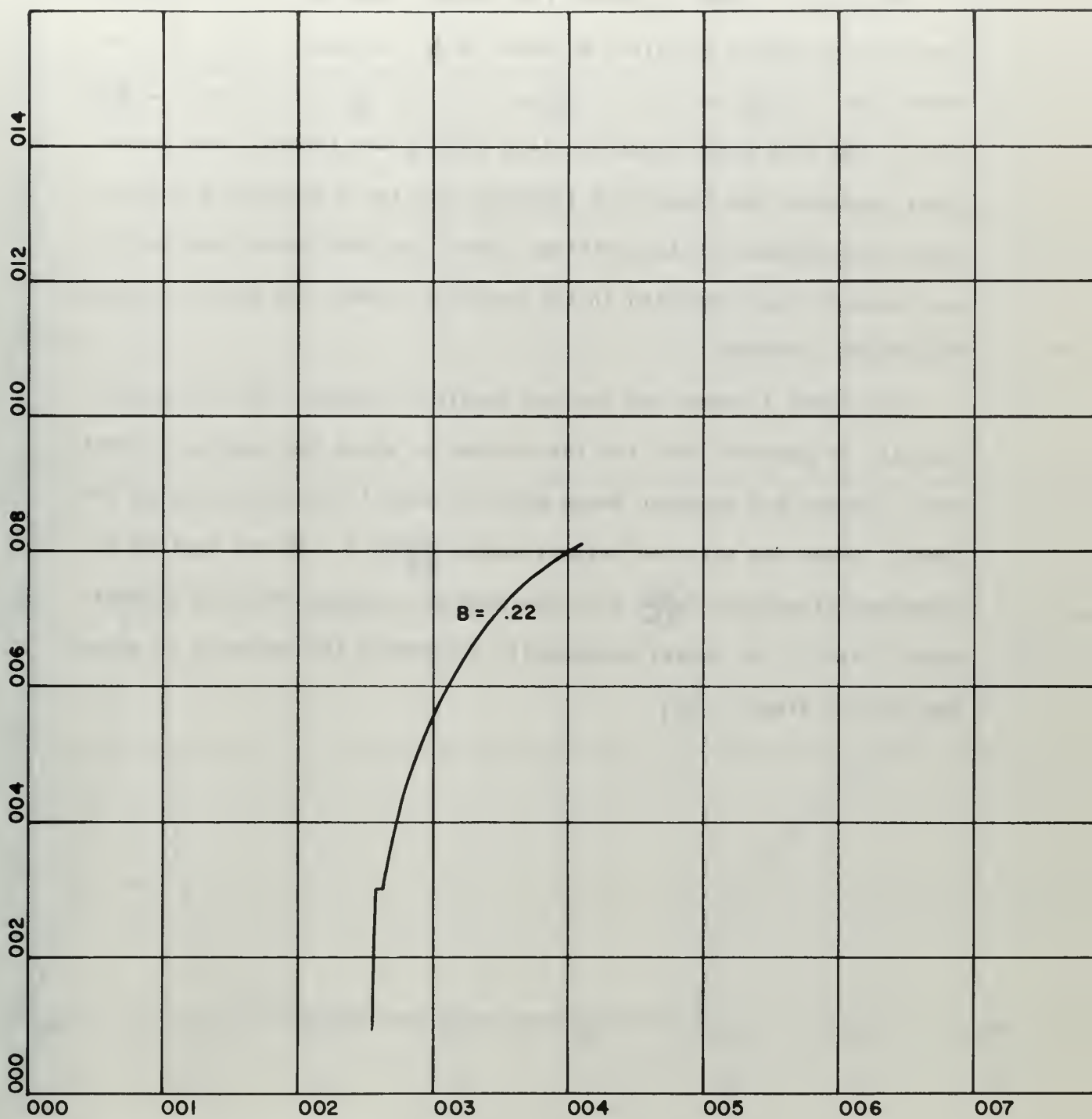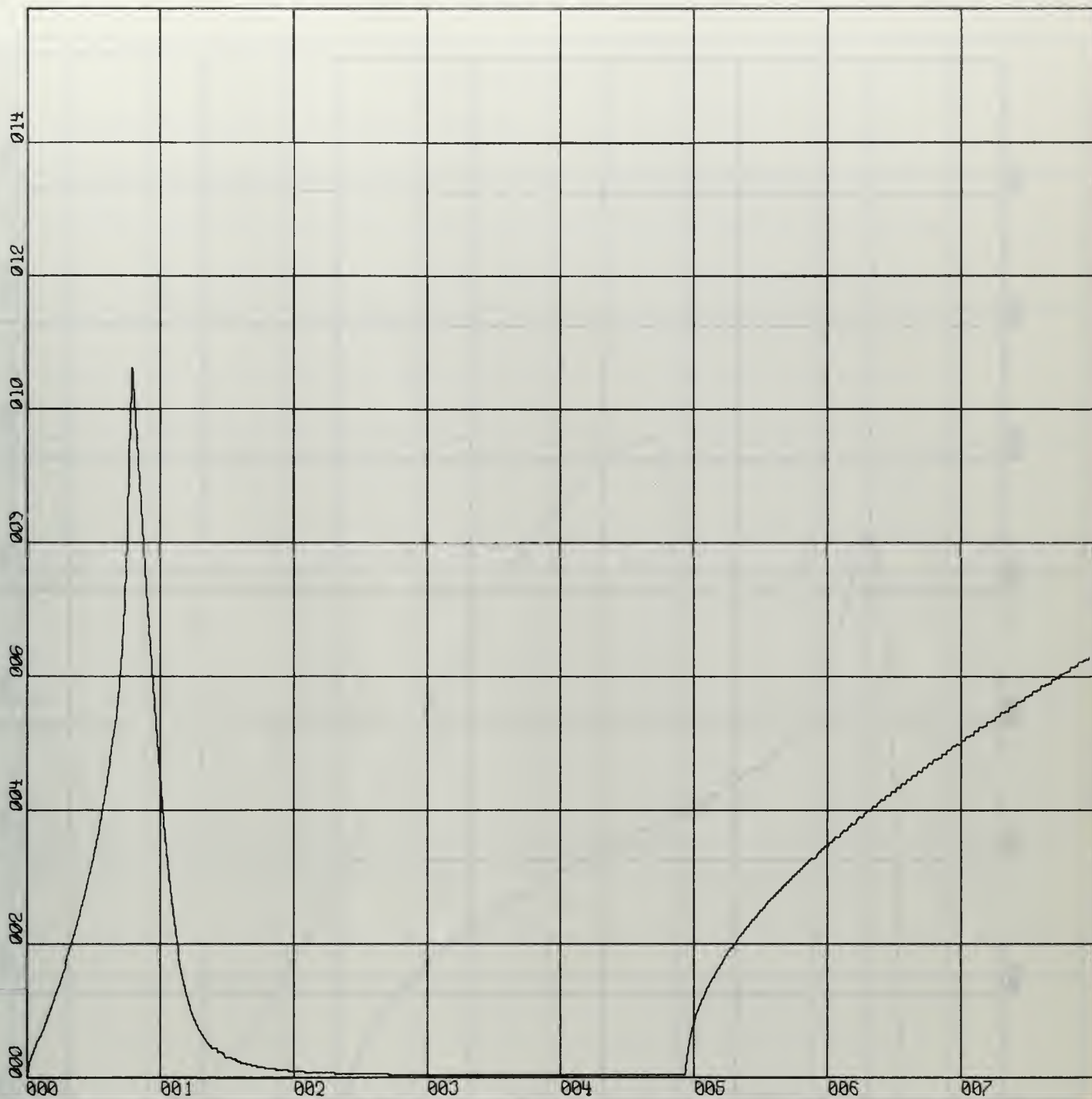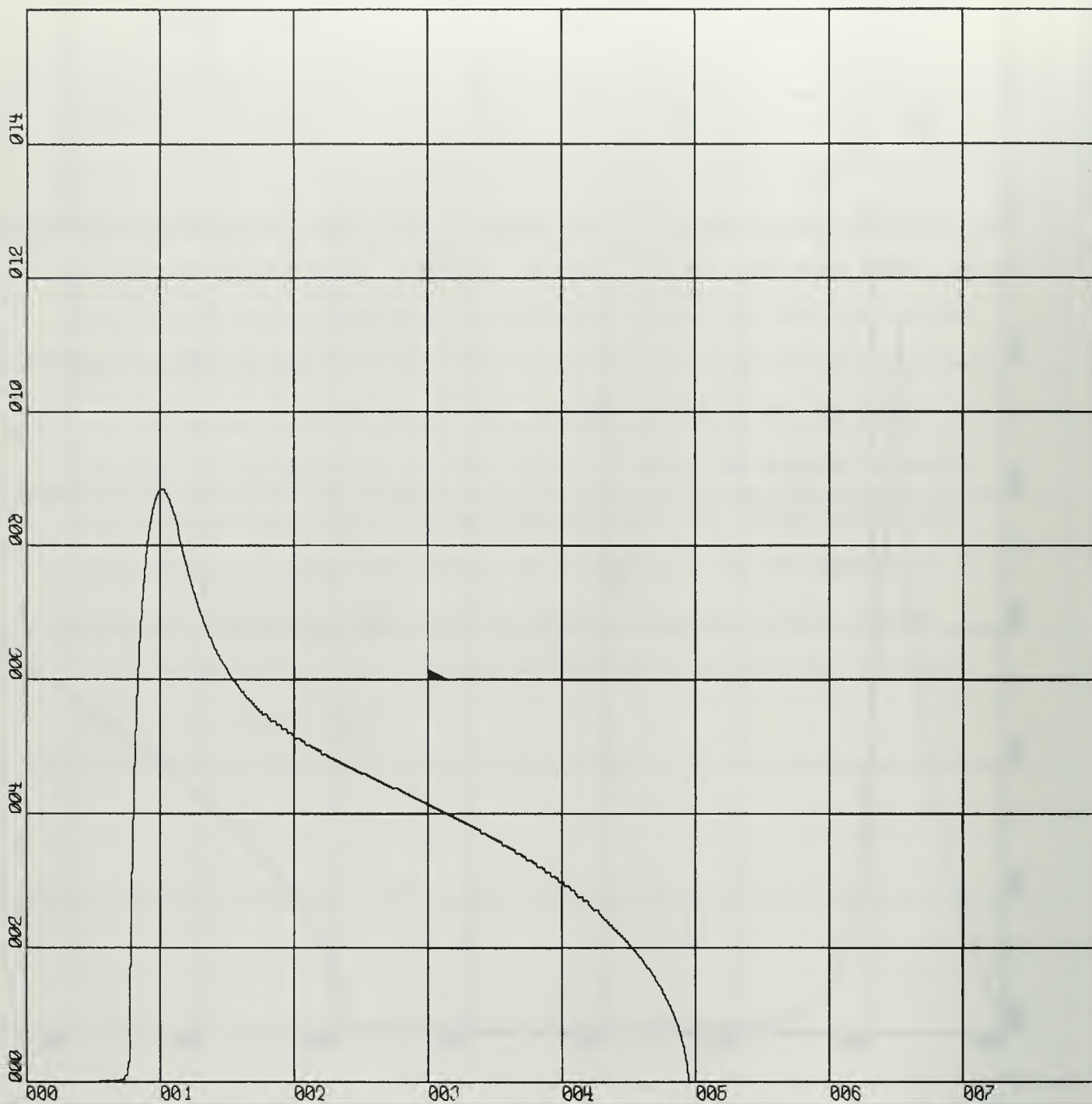Y-SCALE = 1.00E-01 UNITS/INCH.

GROUP VELOCITY VS FREQUENCY
B=.10

82

## Section 5

INTERPRETATION OF EXPERIMENTAL RESULTS

Before proceeding to a more detailed analysis of the experimental results, the basic behavior of the dispersion curves and the attenuation curves will be discussed. Consider first Fig. 13; here a non-dimensionless plot of $\alpha$ vs. $\omega$ is presented. For simplicity, and in order to isolate the effects of the various parameters on the basic dispersion curve, consider first the case of W = 0 (zero ion drift velocity); $\nu$ = 0 (no ion-neutral collisions and $k = \alpha + i\beta$ is real); C = 0 (cold ions); and $\delta$ = 0 (uniform radial density distribution in the unperturbed plasma column); the dispersion relation, equation (17) reduces to:

$$\left(\frac{\Omega^2}{\omega^2} - 1\right)\left(\alpha^2 - \frac{\omega^2}{c^2}\right) = \frac{\alpha_o^2}{\ell^2} ,$$

where $\alpha_o$ is the first root of $J_o$, $\alpha_o$ = 2.405...

This equation is plotted in Fig. 13 for the 4 distinct cases:

$\Omega = 0, \ell = \infty$     (zero magnetic field, infinite medium)

$\Omega \neq 0, \ell = \infty$     (non-zero magnetic field, infinite medium)

$\Omega = 0, \ell \neq \infty$     (zero magnetic field, finite medium)

$\Omega \neq 0, \ell \neq \infty$     (non-zero magnetic field, finite medium)

The cases presented in Fig. 13 are elementary and are presented as an introductory clarification for the more detailed analysis which follows.

From Fig. 13 it is evident that the presence or absence of a magnetic field has no effect on the dispersion in an infinite medium. The reason is that the perturbational velocities $V_\theta$ and $V_r$ are always zero for this case (see equations 4a and 4b). Only $V_z$ is non-zero, and since it is not a function of $\Omega$ (see equation 4c), there is no dispersion.
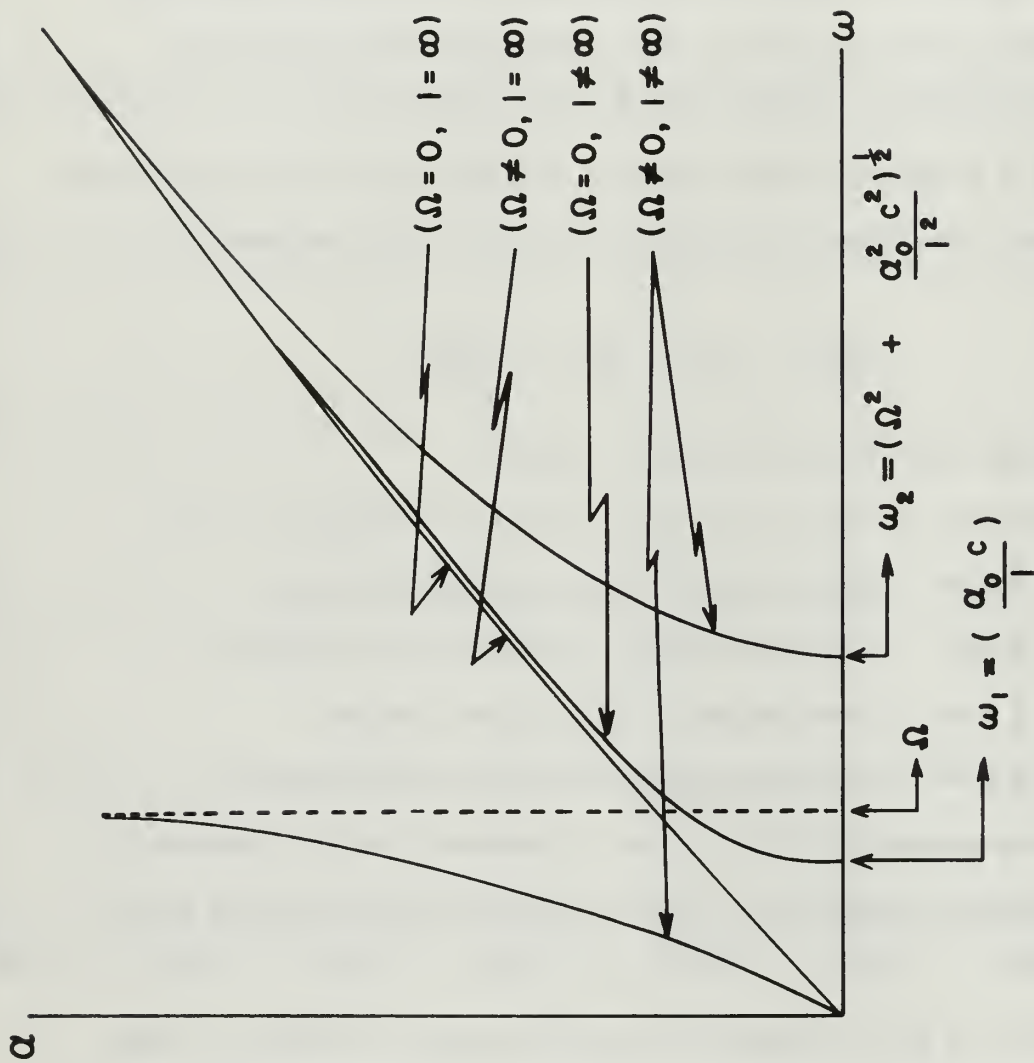
83

$\alpha$ (ARBITRARY UNITS) vs $\omega$ (ARBITRARY UNITS) FOR THE CASE OF $\vec{W}=0$, $\nu=0$, $c=0$, $\delta=0$.

FIG.13

$$\omega_2 = \left(\Omega^2 + \frac{\alpha_0^2 c^2}{1^2}\right)^{\frac{1}{2}}$$

$$\omega_1 = \left(\frac{\alpha_0 c}{1}\right)$$

$\Omega$

$(\Omega=0, 1=\infty)$

$(\Omega\neq0, 1=\infty)$

$(\Omega=0, 1\neq\infty)$

$(\Omega\neq0, 1\neq\infty)$

84

The term cutoff will be used to describe the propagation condition under which the phase velocity of the wave is infinite (or when the real part of the propagation constant, $\alpha$, is zero). The term resonance will be used to describe the condition under which the phase velocity is zero ($\alpha$ is infinite).

For a finite medium the high frequencies (and hence small wavelengths) can easily propagate down the plasma column. As the wavelength increases there is a point at which the plasma can no longer transmit the signal. This appears as a cutoff at frequency $\omega_1 = \frac{\alpha_o c}{\ell}$, and means that at frequencies less than $\omega_1$, $\alpha^2 < 0$ meaning propagation is impossible. This is a consequence of the location of the boundary surface (the cylinder of radius $\ell$).

Finally for the case of a finite medium with a non-zero magnetic field, there is a resonance at the ion cyclotron frequency. At this frequency all the ion momemtum appears as cyclotron motion. Again there is a cutoff, but this time at $\omega_2 = (\Omega^2 + \frac{\alpha_o^2 c^2}{\ell^2})^{\frac{1}{2}}$. At frequencies $\Omega < \omega < \omega_2$ the plasma beam cannot transmit the signals, and propagation is impossible since $\alpha^2 < 0$.

In the following discussion it will be assumed that the dispersion relation is exactly the Bessel function of order zero. This is equivalent to the assumption that the unperturbed plasma column has a uniform radial density profile. This will considerably simplify the discussion, since the infinite series for the dispersion relation need not be considered. For this case the relation $\lambda \ell = 2.405$ holds. In actual practice the perturbations differ from pure Bessel functions by no more than about 10%, so the approximation is justified for discussion purposes.

From this point on the assumption will be made that the plasma is

finite in the radial direction ($\ell \neq \infty$) and that there is a non-zero
magnetic field ($\Omega \neq 0$). Also all variables will be normalized (in-
cluding the 5 parameters) to the dimensionless values. These definitions
are repeated here for clarification.

$$x = \frac{\omega}{\Omega} \qquad y = \frac{\alpha c}{\Omega} \qquad z = \frac{\beta c}{\Omega} \qquad \eta = \frac{W}{c}$$

$$j = \frac{\gamma}{\Omega} \qquad \sigma = \frac{C}{c} \qquad \xi = \frac{c}{\Omega \ell} \qquad \epsilon = \frac{c \delta}{\Omega}$$

The effect of $\eta$ (ion drift) is easily understood, since it intro-
duces a Doppler shift due to the moving medium. In this experiment $\eta$
and $y$ were anti-parallel, so the phase velocities are slightly reduced
by the drift. This is illustrated in Fig. 14.

A set of measurements was made with $\eta$ and $y$ parallel at a field
strength of 1000 gauss. Direct measurement of the difference in phase
velocities for the parallel and anti-parallel cases (not the use of com-
puter data reduction) gave an entirely independent determination of the
value of the ion drift velocity. This value was within 12% of that ob-
tained by the computer data reduction process, and this agreement lends
strong confirmation to the values indirectly deduced from the measure-
ments.

The effect of ion temperature is also easily understood. Since ion
acoustic waves are density perturbations, they propagate at a velocity
proportional to $(\frac{\text{pressure term}}{\text{inertia term}})^{\frac{1}{2}}$. Passing from the case of cold ions
to warm ions will increase the pressure term by a small amount equal to
the ion pressure. Thus the phase velocity will be higher for a given
frequency; that is $y$ will be reduced. This effect is illustrated in
Fig. 15. The solid curve represents the case of cold ions, and the

$(\eta = 0 \quad ie. \ f(x))$

$(\eta < 0 \quad ie. \ f(x-\eta y))$

X

y
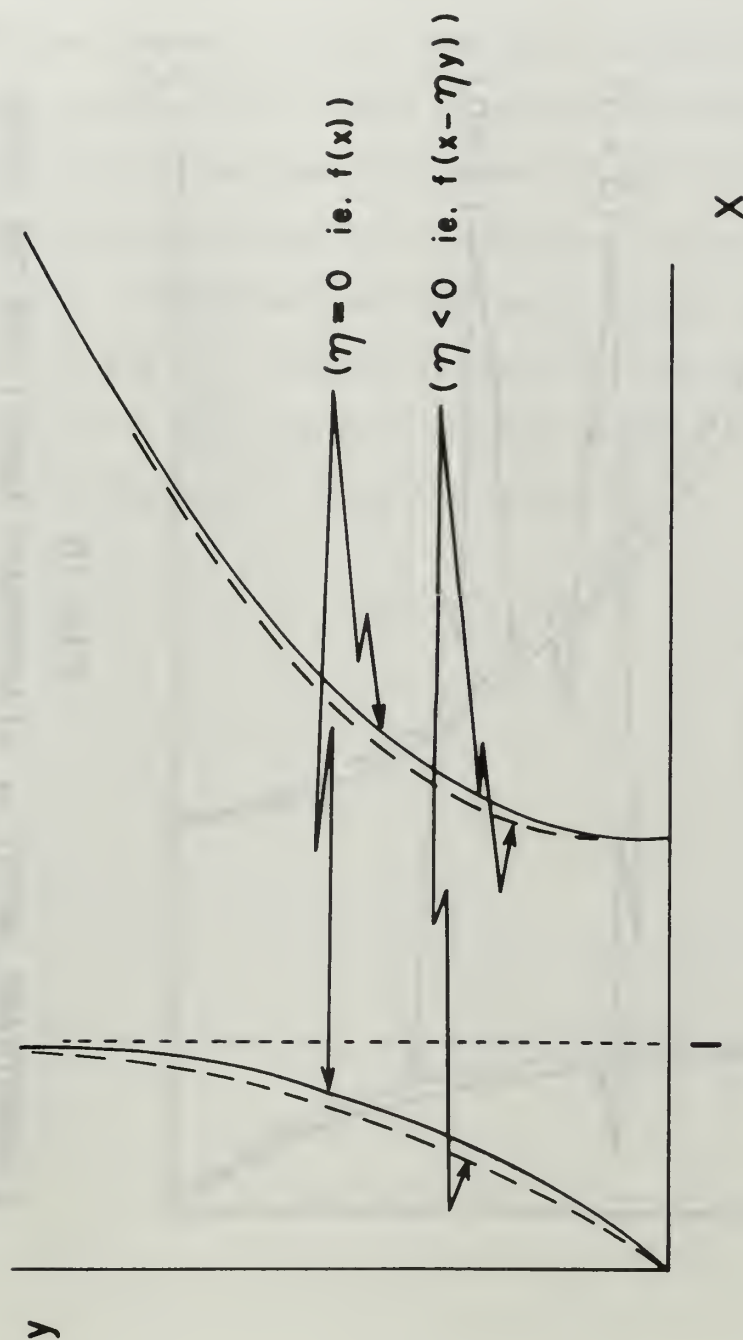
FIG. 14

y (ARBITRARY UNITS) vs x (ARBITRARY UNITS) FOR THE CASE
$\zeta = 0, \ \sigma = 0, \ \xi \neq 0, \ \epsilon = 0.$

87

($\sigma = 0$)

($\sigma > 0$)

X
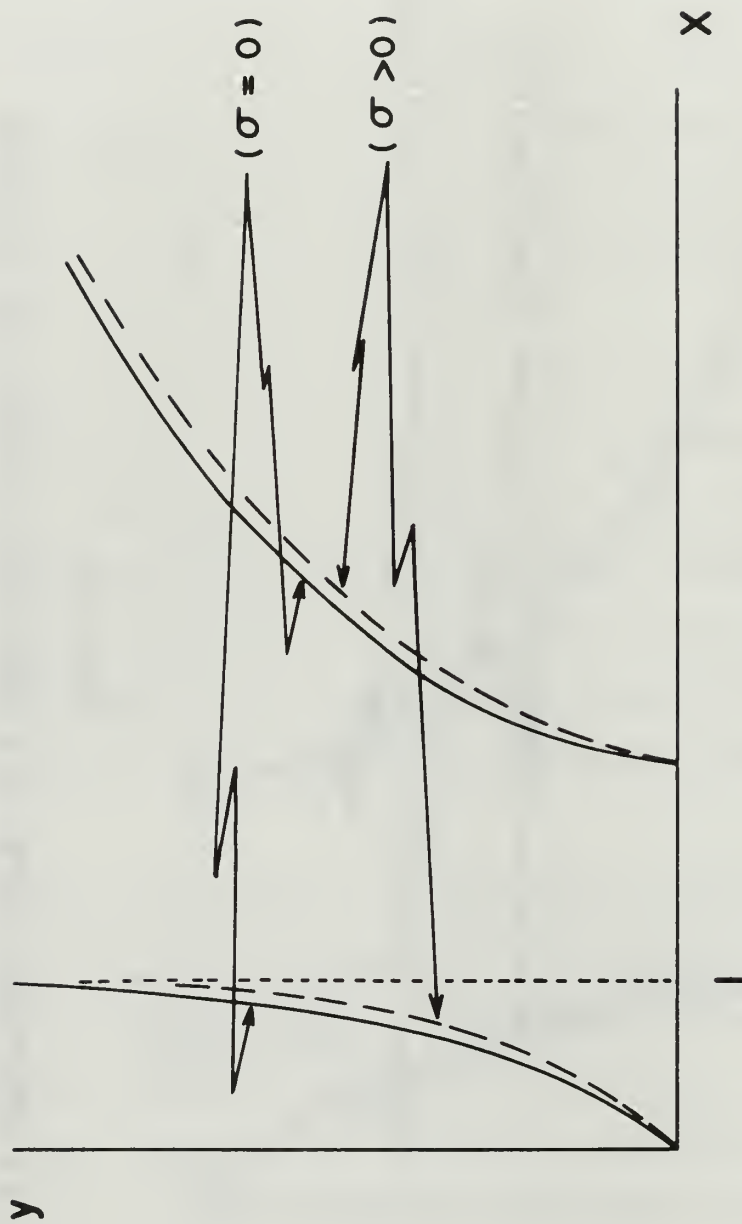
FIG. 15

y (ARBITRARY UNITS) vs x (ARBITRARY UNITS) FOR THE CASE
$\eta = 0, \zeta = 0, \xi \neq 0, \epsilon = 0.$

y

dashed curve represents the case of warm ions.

The effect of $\mathcal{J}$ is more involved. If ion-neutral collisions are considered, there will be a decrease in the wave phase velocity to a value smaller than in the collisionless case. [17] In the present investigation, however, this effect is of the second order. The more important effect of collisions, however, is that a damping mechanism has been introduced. This means that there is no longer an undamped resonance at $x = 1$. Rather the resonance is diffuse, and the maximum wavenumber is limited due to the damping. Waves can also exist in the previously forbidden region, $1 < x < \dfrac{\omega_2}{\Omega}$ , although here they are heavily damped. This effect is illustrated in Fig. 16. Although attempts to excite and detect waves in the region $1 < x \quad \dfrac{\omega_2}{\Omega}$ were made, the heavy damping plus the long wavelengths in this region precluded their detection.
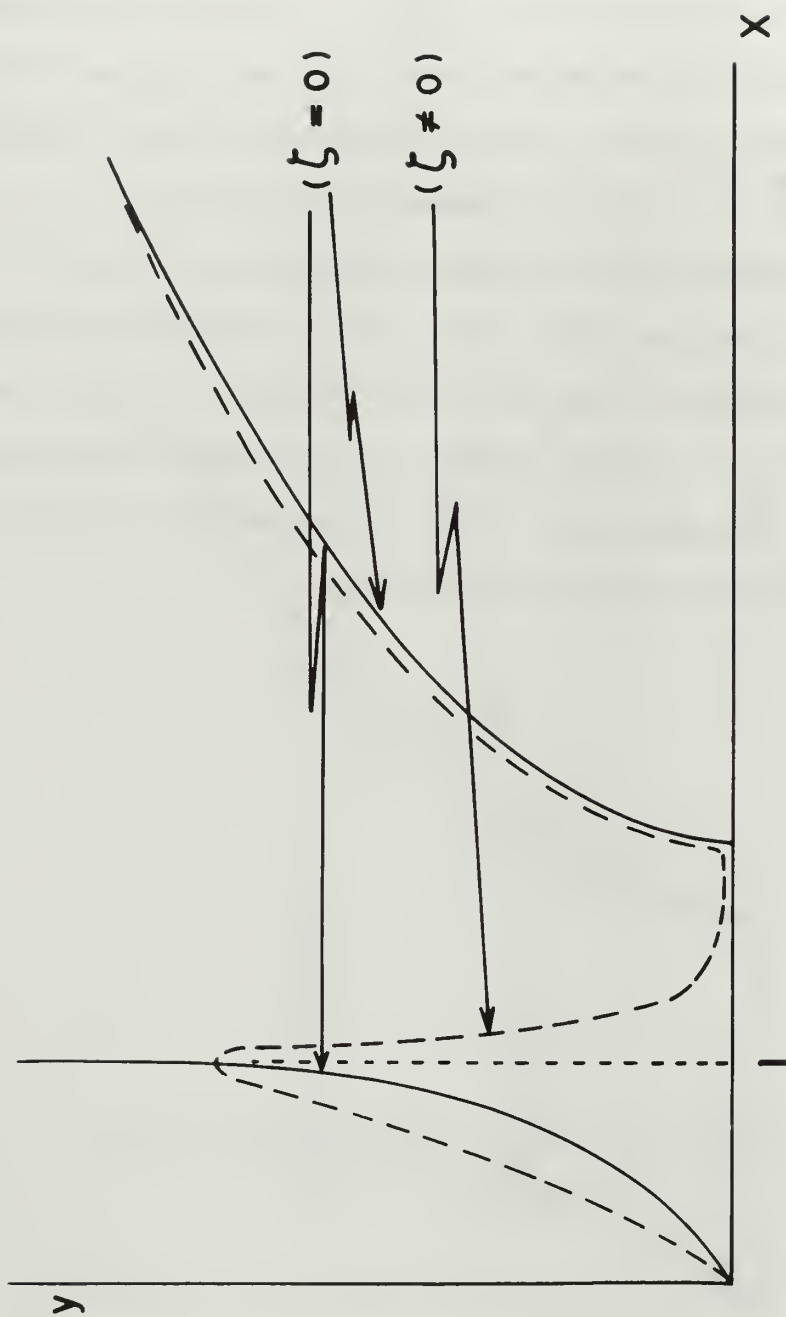
FIG. 16

y (ARBITRARY UNITS) vs x (ARBITRARY UNITS) FOR THE CASE $\eta = 0$, $\sigma = 0$, $\xi \neq 0$, $\epsilon = 0$.

Ion acoustic waves are produced by the Coulomb interaction (a long range interaction). Propagation is possible only when the ion-neutral collision frequency is small compared to the wave frequency. The few collisions present disrupt the long-range ordering, and damping increases with increasing collision frequency. Typical ion-neutral collision frequencies for this investigation were less than 500 $sec^{-1}$, so the contition of heavy damping would be encountered only at frequencies much less than those studied (plus the heavily damped waves in the region $1 < x \frac{\omega_2}{\Omega}$ ).

Due to the apparent invariance of $\eta$ with magnatic field, it is suspected that the mechanism producing the drift is an electric field in the interior of the plasma, rather than a fluid pressure differential between anodes. If the ion drift were due to the latter mechanism, its value would depend on the magnetic field strength, since the neutral gas injection pressure varied with the field strength. Unfortunately previous electric field measurements were not available, so a confirmation of the mechanism which produces the drift cannot be made.

For ion-neutral collisions, $\lambda_{ion} = \dfrac{1}{\sqrt{2} N_g \sigma_c} \dfrac{(\overline{v^2})^{\frac{1}{2}}}{\nu}$

where $\lambda_{ion}$ is the ion mean free path

$N_g$ is the neutral gas density

$\sigma_c$ is the collision cross section for the process

$(\overline{v^2})^{\frac{1}{2}}$ is the mean ion thermal speed

Knowing $\sigma_c$ and $N_g$ (which is manually adjusted for each magnetic field strength to give optimum machine operation), a straightforward calculation gives $\nu = \sigma P_g \times 246 \times 10^6$ where $P_g$ is the neutral gas pressure and $\sigma = \dfrac{C}{c}$ .

Thus $= 41.7 \times 10^{-8} \dfrac{\nu}{B_o}$ .

In the above calculation it is assumed that there is a 100% excess ion momentum loss per collision. This assumption is not strictly true, but it is certainly reasonable, since a large fraction of the directed momentum is lost in any collision. It is also assumed that the ion perturbation velocities are small compared to the mean ion thermal speed. Thus the collision frequencies will not depend on the strength of the perturbation.

The above equation appears as the theory on the ion temperature curves in Section 4. The value of $\sigma$ used was taken from the data reduction program appropriate to the magnetic field strength.

Since $\sigma \ll 1$ (the ions are much colder than the electrons), the dispersion equation is quite insensitive to changes in $\sigma$ . This can be seen by examining the data points of the $\sigma$ curves in Section 4. It is considered by the author that the deduced values of $\sigma$ (and hence the ion energies) should not be interpreted too literally. In the $\sigma$ vs. $B_o$ curve the deduced data points are rather widely scattered. This inaccuracy is reflected not only in the $\sigma$ vs. $B_o$ curves, but also in the $J$ vs. $B_o$ curves, since $J \propto \sigma$. But it can be seen, at least qualitatively, the observed damping results primarily from ion-neutral collisions.

Variations in $B_o$ affect the propagation characteristics (that is $\omega_2 = (\Omega^2 + \dfrac{\alpha_{oc}^2 c^2}{\ell^2})^{\frac{1}{2}}$, since $\Omega$ is of the same order of magnitude as $\dfrac{\alpha_o c}{\ell}$ . An analysis by Wong [19] concludes that the transverse boundary conditions are important only if the ion cyclotron radius, $\rho_i$, is comparable to the plasma beam radius. At 1000 gauss $\rho_i \doteq 3.2$ mm and $\ell \doteq 15$ mm, so this criterion is approximately met.

92

Neglecting $\delta$ (uniform unperturbed column) Wong has shown that

$$1 - \frac{4\pi^2}{k^2\lambda_D^2} Z'(\frac{\omega}{kV}) + 2\frac{T}{\tau} \cdot \frac{4\pi^2}{k^2\lambda_D^2} + \frac{\alpha_0^2}{k^2\ell^2} + \frac{4\pi^2\rho_i^2\alpha_0^2}{k^2\lambda_D^2\ell^2} \doteq 0$$

where $Z'$ is the derivative of the plasma dispersion function

$$Z(\chi) \equiv \exp(-\chi^2)\left[ i\sqrt{\pi} - 2\int_0^\chi \exp \gamma^2 \, d\gamma \right]$$

with respect to its argument.

In the present investigation, $\dfrac{k^2\lambda_D^2}{4\pi^2} << \dfrac{\alpha_0^2\lambda_D^2}{4\pi^2\ell^2} << \dfrac{2T}{\tau}$ .

Thus $Z'(\dfrac{\omega}{kV}) \doteq 2\dfrac{T}{\tau} + \dfrac{\alpha_0^2\rho_i^2}{\ell^2}$ , and the effect of the radial boundary

is important only if $2\dfrac{T}{\tau} \doteq \dfrac{\alpha_0^2\rho_i^2}{\ell^2}$ .   Since this is indeed the case,

it must be true that $T \doteq \dfrac{\alpha_0^2\rho_i^2\tau}{2\ell^2}$ , or $T \doteq 2$ ev.

This is a lower limit for the ion temperature, since any tempera-
ture appreciably lower would predict that $\omega_2$ is not a function of $B_0$.
This estimate is considerably higher than the results of the data re-
duction (.05 ev to .17 ev), and the spectroscopic measurements of Booth
and Kelly. [10] For that reason it must be stated that the ion energy
cannot be determined accurately by this experimental method.  It is
probable, however, that the ion energies lie somewhere between .05 ev
and 2 ev.  The ion temperature has been found to increase with distance
from the plasma source in a helium plasma, varying in value from about
1 ev at the first anode to about 8 ev several meters downstream. [20]

The increase of ion energy with increasing magnetic field is be-
lieved to be due to the increased electron-ion collision frequency in
the denser beams resulting from higher field strengths.

It should be noted that volume recombination and ionization would
increase the damping by producing hot neutrals and cold ions respectively.

Also, since most ion momentum is directed along the $\hat{z}$ axis, elastic scattering of an ion through anything other than a small angle would appear as a damping effect. Charge exchange would substitute a hot neutral and a cold ion for the original hot ion and cold neutral. Although the mean free paths for charge exchange and ion-neutral collisions are of the same order of magnitude, the actual collision rate for charge exchange would be somewhat less than that for elastic collisions, since not every ion-neutral collision would result in charge exchange. But charge exchange would certainly appear as another damping mechanism. All these processes probably contribute to the inaccuracies of the above theory.

It should be noted that the observed damping is much less than that observed by Little and Jones in a gaseous discharge where the percentage ionization is low and there are many more neutrals present. [5] Also in such a discharge collisions between the ions and the container walls would cause additional damping. Such an effect is not a factor in the present investigation.

The primary effect of $\epsilon$ is to alter the form of the radial perturbation from $J_o$ to a more rapidly decreasing function of r. The effect of $\epsilon$ on y and z is a complicated second order process; it will not be discussed further here.

Neglecting the second-order effects ($\eta$, $\sigma$, $\epsilon$), the equations 4a, 4b, and 4c become (for $\mu = 0$):

$$MNV_\theta = \frac{-\Omega \frac{\partial p}{\partial r}}{(i\omega - \gamma)^2 + \Omega^2}$$

$$MNV_r = \frac{\frac{\partial p}{\partial r}(i\omega - \gamma)}{(i\omega - \gamma)^2 + \Omega^2}$$

94

$$MNV_z = \frac{ik p}{(i\omega - \nu)} \quad .$$

In this form the equations clearly illustrate the damping effect of $\nu$.
If $\nu$ is now set to zero, these equations can be solved to give:

$$\left| \frac{V_\theta}{V_z} \right| = \left( \frac{1}{k p} \frac{\partial p}{\partial r} \right) \frac{\omega \Omega}{\Omega^2 - \omega^2}$$

$$\left| \frac{V_r}{V_z} \right| = \left( \frac{1}{k p} \frac{\partial p}{\partial r} \right) \frac{\omega^2}{\Omega^2 - \omega^2}$$

$$\left| V_z \right| = \frac{k p}{MN\omega}$$

Since $\frac{\partial p}{\partial r} \ll k p$ (except near cutoff), it is clear that most of the
perturbational momentum appears in the motion of the ions in the $\hat{z}$ direc-
tion. It is for this reason that the waves are called acoustic waves.

Theory for the $\xi$, $\ell$ curves is derived from the probe analysis
mentioned in Section 3. Those measurements (which confirmed the pre-
sence of only the $\mu = 0$ mode) showed that no density perturbation was
detectable beyond 15 mm from the plasma beam axis. This distance was
also found to be independent of the magnetic field strength up to 2200
gauss. This was a remarkably strong confirmation of the values of
deduced from the data reduction. It also demonstrates the validity of
the basic dispersion relation, since this relation is far more sensitive
to small changes in $\ell$ than for any other parameter.

Fig. 17 is reproduced from the work of Gall and Oleson [15]; it can
be seen that a value of $\ell$ = 10 mm would be a more reasonable estimate,
at least from the point of view of electron temperature alone. However
the value of $\ell$ = 15 mm taken from the probe analysis gave a much better
fit to the data and was used as the theoretical value, since it was

FIG.17
Radial Temperature
Profile of Argon Plasma
For Various Magnetic fields

600 Gauss ≤ B ≤ 4000 Gauss

5000 Gauss ≤ B ≤ 6000 Gauss

7000 Gauss ≤ B ≤ 8000 Gauss

$T_e$
(electron
volts)

DISTANCE (mm)
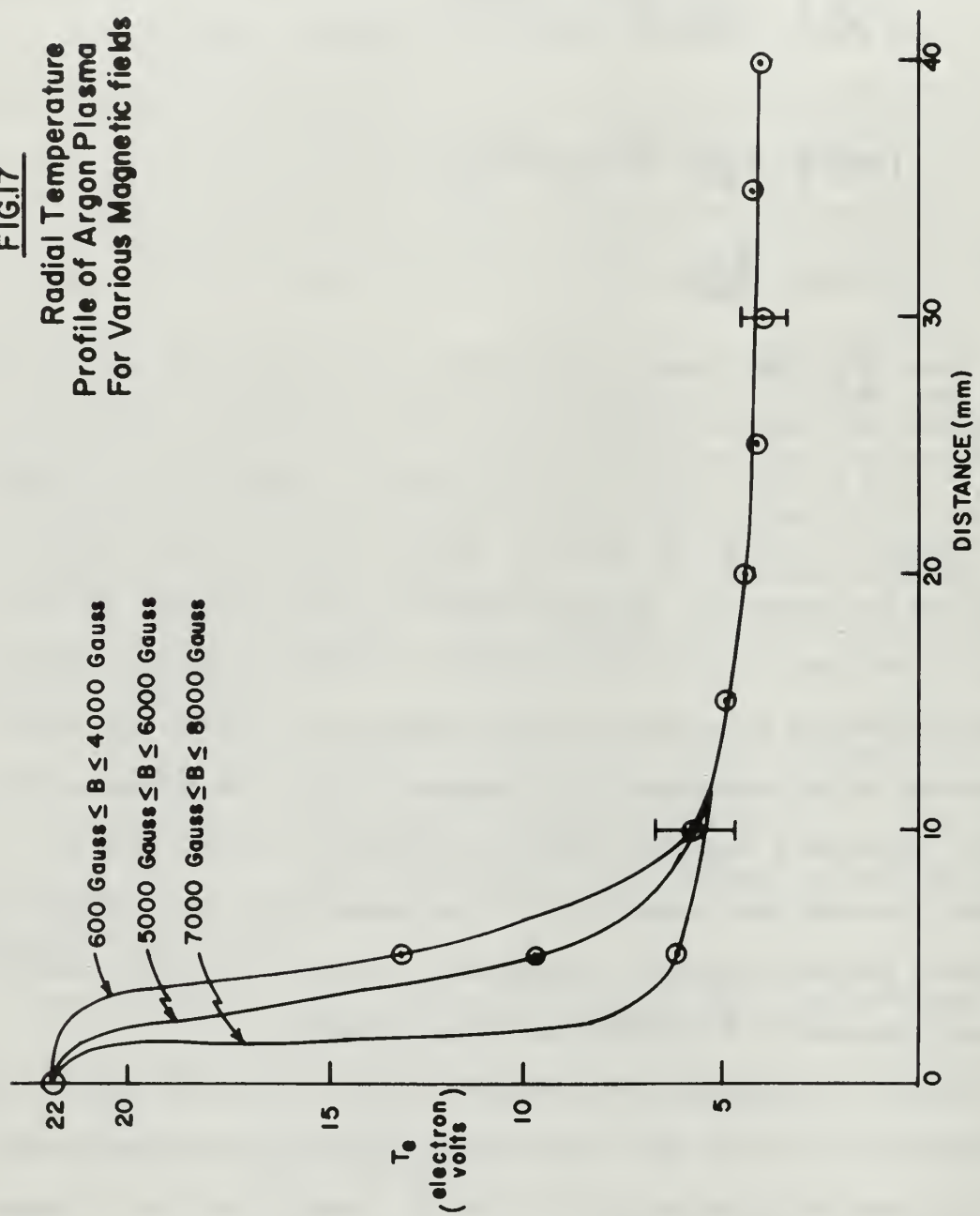
independently confirmed.

Theory for the $\epsilon$, $\delta$ curves was taken from the work of Gall and Oleson. [15] Although their work did not directly yield values of $\delta$ as a function of the magnetic field strength, it did indicate that this quantity is not a sensitive function of the magnetic field strength in the range used in the present investigation (800 to 2200 gauss). Fig. 18 is reproduced to illustrate this point. From Fig. 18 $\delta$ is seen to be equal to 100 $m^{-1}$ at $B_O$ = 600 gauss. Assuming $\delta$ is not a function of $B_O$, $\epsilon = \dfrac{.303}{B_O}$ .

Table 2 summarizes the results of the present investigation for the low, medium, and high field strengths used.

### Table 2

| quantity | 800 gauss | 1600 gauss | 2200 gauss |
|---|---|---|---|
| wavelength (m) | .0458 to 1.19 | .0314 to .341 | .0248 to .145 |
| i/e attenuation dist. (m) | 20 to 500 | 133 to 1110 | 455 to 2500 |
| phase velocity/c | 1.25 to 26 | 1.25 to 9.0 | 1.2 to 4.4 |
| group velocity/c | .09 to .62 | .1 to .73 | .1 to .8 |
| ion drift velocity $(ms^{-1})$ | 90.8 | 89.4 | 87.1 |
| effective ion collision frequency for momentum loss $(s^{-1})$ | 342 | 510 | 431 |
| ion energy (ev) | .05 | .13 | .16 |
| radial cutoff distance (m) | .0152 | .0147 | .0152 |
| radial 1/e profile parameter $(m^{-1})$ | .0100 | .0105 | .0105 |

FIG.18
ION DENSITY PROFILE FOR
AN ARGON PLASMA
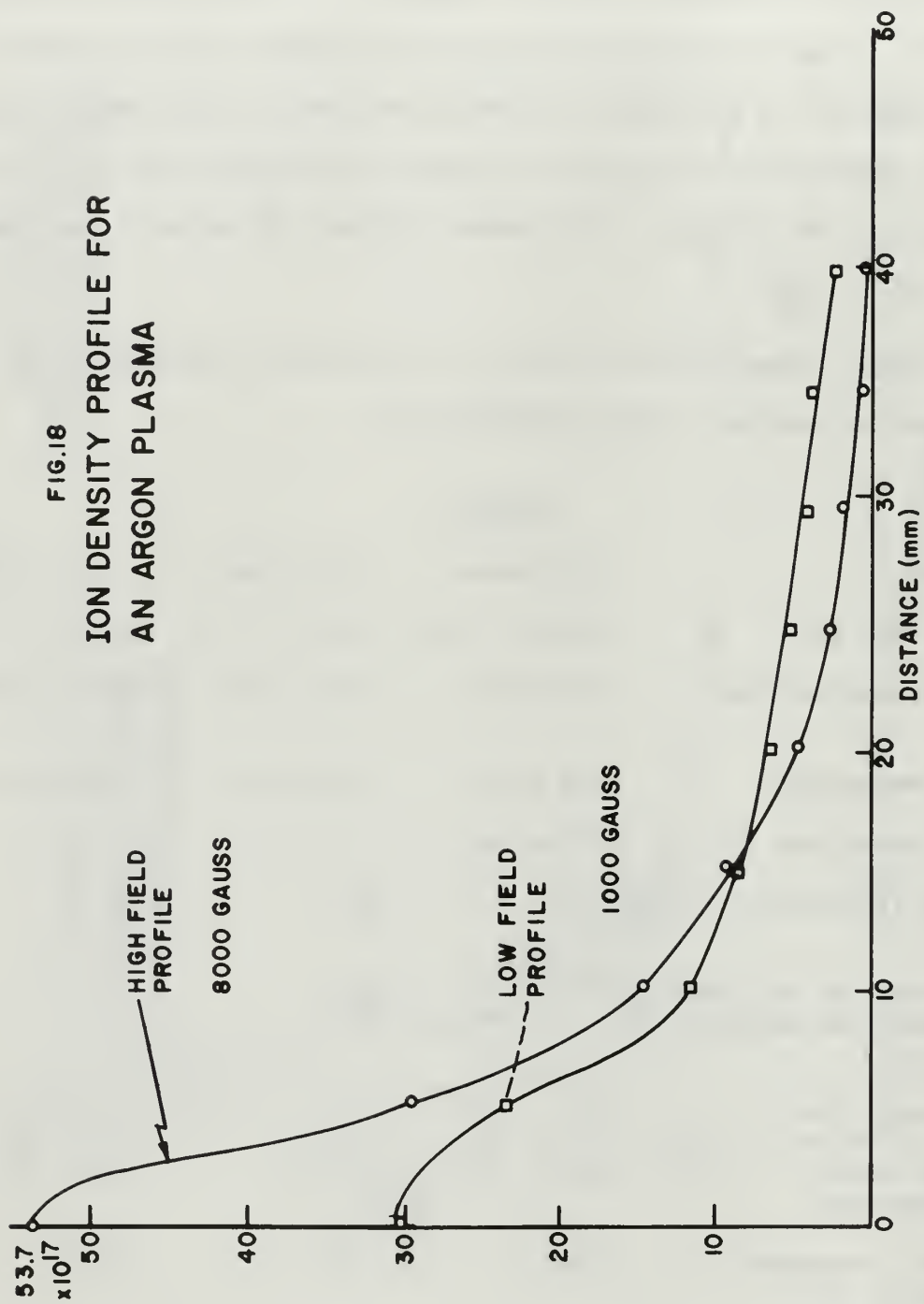
Since the values of y and z vs. x cover such wide ranges, a tabula-
tion of these quantities vs. x is not included at this point. Represen-
tative values can be read from the curves presented in Section 4.

## Table 3

| Parameter | Measured Value | Deduced Value |
|-----------|----------------|---------------|
| $|\bar{w}|$ | 95.2 m/s | 85.0 m/s |
| $\nu$ | 421 s$^{-1}$ | 480 s$^{-1}$ |
| T | none | .092 ev |
| $\ell$ | 15 mm | 15.5 mm |
| $\delta$ | 100 m$^{-1}$ | 102 m$^{-1}$ |

CONCLUSIONS

In conclusion it may be stated that for the propagation of ion acoustic waves where Landau damping is not present the new dispersion relation derived in Section 2 is capable of predicting the propagation characteristics of these waves quite accurately. The greatest error present in the dispersion and attenuation curves (that is the greatest departure between data and theory) is 6%. It was, however, much more difficult to arrive at satisfactory theories for the 5 adjustable parameters. The close agreement in the dispersion and attenuation curves, however, is believed to result from the unambiguous boundary condition specified and from the use of photomultiplier detection (rather than probe detection with its inherent errors).

Where damping processes other than ion-neutral collisions occur, the effective ion collision rate for momentum loss may be redefined to include all such processes (such as the collision rate of ions with the walls of the container). For this case $\gamma$ would be the sum of the individual collision rates for all processes. Since negligible momentum is carried by the electrons, electron momentum loss mechanisms may be ignored without appreciable error.

The externally accomplished excitation and dispersion measurements described have been a valuable diagnostic tool for the investigation of the plasma characteristics. It was by this method that the values of $W, \nu, \sigma, \ell$ and $\delta$ were deduced from the data. This method could be even more valuable where internal measurements (such as probe diagnostics) are impractical.

It is recommended that future investigations be made to test the

theory at very low frequencies (1 kc to 100 kc). Due to the frequency limitations of the TAB-7 transmitter employed, measurements in this lower frequency region were not possible. Future investigations in this region would provide an additional test of the theory and additional confirmation of the deduced values of the 5 parameters considered.

It is also recommended that the noise spectrum of the plasma be analyzed. This would provide additional information on the naturally occurring interior phenomena.

Investigation of ion acoustic wave propagation in other rare gases (helium and neon for example) would also provide additional checks of the theory.

## BIBLIOGRAPHY

1. D. Rose and M. Clark, *Plasmas and Controlled Fusion*, Wiley, New York, 1961

2. J. Denisse and J. Delcroix, *Plasma Waves*, Interscience, New York, 1963

3. L. Tonks and I. Langmuir, Phys. Rev., 33, 195 (1929A)

4. I. Alexeff and R. Neidigh, Phys. Rev., 129, 516 (1963)

5. P. Little and H. Jones, Proc. Phys. Soc., 85, 979 (1965)

6. A. Wong, R. Motley, and N. D'Angelo, Phys. Rev., 133, A436 (1964)

7. I. Alexeff and W. Jones, Thermonuclear Division Semi-Annual Progress Report, 30 April 1965

8. B. Fried and R. Gould, Phys. Fluids, 4, 139 (1961)

9. L. Landau, J. Phys. (USSR), 10, 25 (1946)

10. R. Booth and R. L. Kelly, unpublished results, personal communication

11. D. M. Gall, unpublished results

12. W. Kunkel (ed.), *Plasma Physics in Theory and Application*, McGraw-Hill, New York, 1966

13. W. Newcomb, Ion Oscillations in a Magnetic Field, UCRL Livermore Site, 4941 (1957)

14. D. Pfirsch and L. Biermann, Z. Naturf., 15A, 14 (1960)

15. D. M. Gall and N. L. Oleson, Langmuir Probe Studies of a Steady State Argon Plasma in a Magnetic Field, Proc. of the 7th Int. Conf. of Phen. of Ionization in Gases, Belgrade, 1966

16. L. Lidsky et. al., J. Appl. Phys., 33, 2490 (1962)

17. I. Alexeff and W. Jones, Thermonuclear Division Semi-Annual Progress Report, 30 April 1964

18. J. A. Stratton, *Electromagnetic Theory*, McGraw-Hill, New York, 1941

19. A. Wong, Phys. Fluids, 9, 1261 (1966)

20. A. Gardner, W. Barr, R. Kelly and N. Oleson, Phys. Fluids, 5, 794 (1962)

INITIAL DISTRIBUTION LIST

<table>
<tr><td></td><td></td><td>No. Copies</td></tr>
<tr><td>1.</td><td>Defense Documentation Center<br>Cameron Station<br>Alexandria, Virginia 22314</td><td>20</td></tr>
<tr><td>2.</td><td>Library<br>Naval Postgraduate School<br>Monterey, California 93940</td><td>2</td></tr>
<tr><td>3.</td><td>Office of Naval Research<br>Department of the Navy<br>Washington, D. C.</td><td>1</td></tr>
<tr><td>4.</td><td>Prof. Norman L. Oleson<br>Department of Physics<br>Naval Postgraduate School<br>Monterey, California 93940</td><td>5</td></tr>
<tr><td>5.</td><td>LCDR Richard R. Levin, USN<br>Naval Postgraduate School<br>Monterey, California 93940</td><td>6</td></tr>
</table>

## DOCUMENT CONTROL DATA - R&D

*(Security classification of title, body of abstract and indexing annotation muet be entered when the ovsrell report is classified)*

| 1. ORIGINATING ACTIVITY *(Corporate euthor)* | 2a. REPORT SECURITY CLASSIFICATION |
|---|---|
| Naval Postgraduate School<br>Monterey, California 93940 | UNCLASSIFIED |
| | 2b. GROUP |

**3. REPORT TITLE**

A THEORETICAL AND EXPERIMENTAL INVESTIGATION OF ION ACOUSTIC
WAVE DISPERSION IN A NON-UNIFORM HIGHLY IONIZED ARGON PLASMA

**4. DESCRIPTIVE NOTES** *(Type of report and inclusive dates)*

Thesis, Doctor of Philosophy in Physics, December 1966

**5. AUTHOR(S)** *(Last name, first name, initial)*

LEVIN, Richard Robert

| 6. REPORT DATE | 7a. TOTAL NO. OF PAGES | 7b. NO. OF REFS |
|---|---|---|
| December 1966 | 104 | 20 |

| 8a. CONTRACT OR GRANT NO. | 9a. ORIGINATOR'S REPORT NUMBER(S) |
|---|---|
| b. PROJECT NO. | |
| c. | 9b. OTHER REPORT NO(S) *(Any other numbers that may be assigned this report)* |
| d. | |

**10. AVAILABILITY/LIMITATION NOTICES**

| 11. SUPPLEMENTARY NOTES | 12. SPONSORING MILITARY ACTIVITY |
|---|---|

**13. ABSTRACT**

Ion acoustic waves have been artificially excited and detected in the Steady State Plasma Facility at the Naval Post-graduate School by a magnetic excitation device and an optical detection system. The dispersion of these waves has been studied as a function of the exciting frequency and the confining static magnetic field.

Dispersion curves are presented which compare the experimental data to a new dispersion equation which is derived in the present thesis. After the validity of this dispersion relation is demonstrated, the measurements are used as a diagnostic tool, and five operating parameters of the plasma facility are deduced from the measurements.

Theories are presented to explain the behavior of the dispersion curves and three of the five operating parameters.

**DD** FORM 1 JAN 64 **1473**

| 14. KEY WORDS | LINK A | | LINK B | | LINK C | |
|---|---|---|---|---|---|---|
| | ROLE | WT | ROLE | WT | ROLE | WT |
| ion acoustic waves:<br><br>excitation<br>detection<br>dispersion | | | | | | |

## INSTRUCTIONS

1. ORIGINATING ACTIVITY: Enter the name and address of the contractor, subcontractor, grantee, Department of Defense activity or other organization *(corporate author)* issuing the report.

2a. REPORT SECURITY CLASSIFICATION: Enter the overall security classification of the report. Indicate whether "Restricted Data" is included. Marking is to be in accordance with appropriate security regulations.

2b. GROUP: Automatic downgrading is specified in DoD Directive 5200.10 and Armed Forces Industrial Manual. Enter the group number. Also, when applicable, show that optional markings have been used for Group 3 and Group 4 as authorized.

3. REPORT TITLE: Enter the complete report title in all capital letters. Titles in all cases should be unclassified. If a meaningful title cannot be selected without classification, show title classification in all capitals in parenthesis immediately following the title.

4. DESCRIPTIVE NOTES: If appropriate, enter the type of report, e.g., interim, progress, summary, annual, or final. Give the inclusive dates when a specific reporting period is covered.

5. AUTHOR(S): Enter the name(s) of author(s) as shown on or in the report. Enter last name, first name, middle initial. If military, show rank and branch of service. The name of the principal author is an absolute minimum requirement.

6. REPORT DATE: Enter the date of the report as day, month, year; or month, year. If more than one date appears on the report, use date of publication.

7a. TOTAL NUMBER OF PAGES: The total page count should follow normal pagination procedures, i.e., enter the number of pages containing information.

7b. NUMBER OF REFERENCES: Enter the total number of references cited in the report.

8a. CONTRACT OR GRANT NUMBER: If appropriate, enter the applicable number of the contract or grant under which the report was written.

8b, 8c, & 8d. PROJECT NUMBER: Enter the appropriate military department identification, such as project number, subproject number, system numbers, task number, etc.

9a. ORIGINATOR'S REPORT NUMBER(S): Enter the official report number by which the document will be identified and controlled by the originating activity. This number must be unique to this report.

9b. OTHER REPORT NUMBER(S): If the report has been assigned any other report numbers *(either by the originator or by the sponsor)*, also enter this number(s).

10. AVAILABILITY/LIMITATION NOTICES: Enter any limitations on further dissemination of the report, other than those imposed by security classification, using standard statements such as:

  (1)  "Qualified requesters may obtain copies of this report from DDC."

  (2)  "Foreign announcement and dissemination of this report by DDC is not authorized."

  (3)  "U. S. Government agencies may obtain copies of this report directly from DDC. Other qualified DDC users shall request through

                                                         ."

  (4)  "U. S. military agencies may obtain copies of this report directly from DDC. Other qualified users shall request through

                                                         ."

  (5)  "All distribution of this report is controlled. Qualified DDC users shall request through

                                                          ."

If the report has been furnished to the Office of Technical Services, Department of Commerce, for sale to the public, indicate this fact and enter the price, if known.

11. SUPPLEMENTARY NOTES: Use for additional explanatory notes.

12. SPONSORING MILITARY ACTIVITY: Enter the name of the departmental project office or laboratory sponsoring *(paying for)* the research and development. Include address.

13. ABSTRACT: Enter an abstract giving a brief and factual summary of the document indicative of the report, even though it may also appear elsewhere in the body of the technical report. If additional space is required, a continuation sheet shall be attached.

It is highly desirable that the abstract of classified reports be unclassified. Each paragraph of the abstract shall end with an indication of the military security classification of the information in the paragraph, represented as *(TS)*, *(S)*, *(C)*, or *(U)*.

There is no limitation on the length of the abstract. However, the suggested length is from 150 to 225 words.

14. KEY WORDS: Key words are technically meaningful terms or short phrases that characterize a report and may be used as index entries for cataloging the report. Key words must be selected so that no security classification is required. Identifiers, such as equipment model designation, trade name, military project code name, geographic location, may be used as key words but will be followed by an indication of technical context. The assignment of links, roles, and weights is optional.

DD FORM 1 JAN 64 1473 (BACK)